AD-A107 948 ARMY ARMAMENT RESEARCH AND DEVELOPMENT COMMAND ABERD--ETC F/6 20/4
AN EXPERIMENTAL STUDY OF FORCED ASYMMETRIC OSCILLATIONS IN A RO--ETC(U)
OCT 81 R D WHITING
UNCLASSIFIED ARBRL-TR-02376 NL

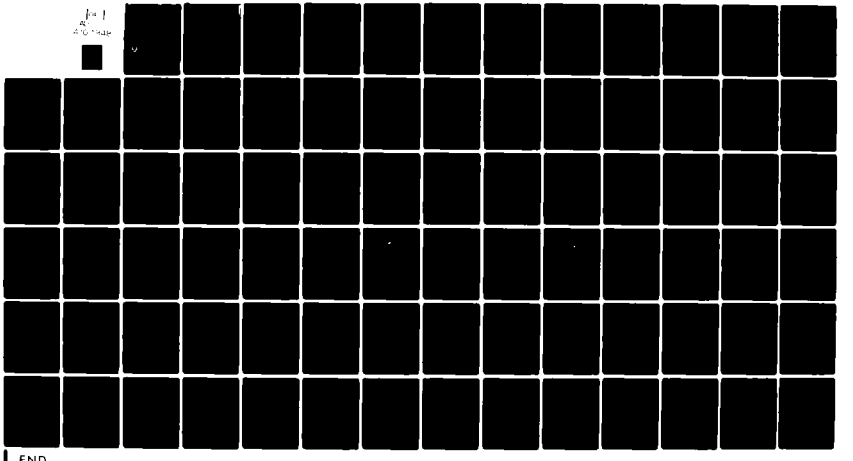

END
DATE FILMED
82
DTIC

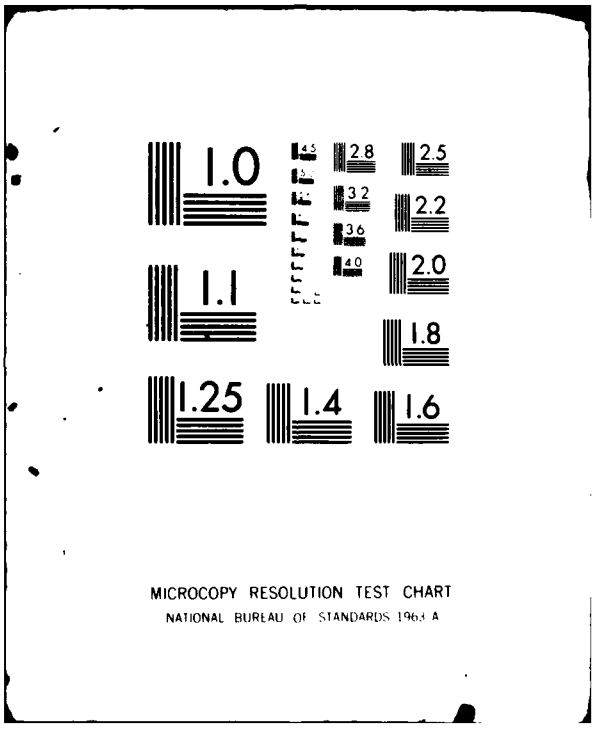
1.0
1.1
1.25
1.4
1.6
1.8
2.0
2.2
2.5
2.8
3.2
3.6
4.0
MICROCOPY RESOLUTION TEST CHART
NATIONAL BUREAU OF STANDARDS 1963 A

AD

TECHNICAL REPORT ARBRL-TR-02376

AN EXPERIMENTAL STUDY OF FORCED ASYMMETRIC OSCILLATIONS IN A ROTATING LIQUID-FILLED CYLINDER

Richard D. Whiting

October 1981

US ARMY ARMAMENT RESEARCH AND DEVELOPMENT COMMAND
BALLISTIC RESEARCH LABORATORY
ABERDEEN PROVING GROUND, MARYLAND

Destroy this report when it is no longer needed.
Do not return it to the originator.

Secondary distribution of this report by originating or sponsoring activity is prohibited.

Additional copies of this report may be obtained from the National Technical Information Service, U.S. Department of Commerce, Springfield, Virginia 22151.

The findings in this report are not to be construed as an official Department of the Army position, unless so designated by other authorized documents.

The use of trade names or manufacturers' names in this report does not constitute indorsement of any commercial product.

UNCLASSIFIED

SECURITY CLASSIFICATION OF THIS PAGE (When Data Entered)

REPORT DOCUMENTATION PAGE		READ INSTRUCTIONS BEFORE COMPLETING FORM
1. REPORT NUMBER TECHNICAL REPORT ARBRL-TR-02376	2. GOVT ACCESSION NO. AD-A107948	3. RECIPIENT'S CATALOG NUMBER
4. TITLE (and Subtitle) AN EXPERIMENTAL STUDY OF FORCED ASYMMETRIC OSCILLATIONS IN A ROTATING LIQUID-FILLED CYLINDER		5. TYPE OF REPORT & PERIOD COVERED Final 6. PERFORMING ORG. REPORT NUMBER
7. AUTHOR(s) Richard D. Whiting		8. CONTRACT OR GRANT NUMBER(s)
9. PERFORMING ORGANIZATION NAME AND ADDRESS U.S. Army Ballistic Research Laboratory (ATTN: DRDAR-BLL) Aberdeen Proving Ground, MD 21005		10. PROGRAM ELEMENT, PROJECT, TASK AREA & WORK UNIT NUMBERS RDT&E 1L161102AH43
11. CONTROLLING OFFICE NAME AND ADDRESS US Army Armament Research & Development Command US Army Ballistic Research Laboratory (DRDAR-BL) Aberdeen Proving Ground, MD 21005		12. REPORT DATE October 1981 13. NUMBER OF PAGES 82
14. MONITORING AGENCY NAME & ADDRESS(if different from Controlling Office)		15. SECURITY CLASS. (of this report) Unclassified 15a. DECLASSIFICATION/DOWNGRADING SCHEDULE

16. DISTRIBUTION STATEMENT (of this Report)

Approved for public release; distribution unlimited.

17. DISTRIBUTION STATEMENT (of the abstract entered in Block 20, if different from Report)

18. SUPPLEMENTARY NOTES

19. KEY WORDS (Continue on reverse side if necessary and identify by block number)

Gyroscope Experiments	Liquid-Filled Gyroscopes
Solid-Body Rotation	Perturbation Pressure
Coning Frequencies	Stewartson-Wedemeyer Theory
Nutating Spinning Cylinder	Eigenfrequencies
Non-symmetric Azimuthal Mode	

20. ABSTRACT (Continue on reverse side if necessary and identify by block number)

An experimental study was made of forced asymmetric oscillations in a liquid-filled, rapidly-rotating, right circular cylinder. Oscillations were forced by causing the cylinder to cone about an axis passing through the center of the cylinder but offset by a small angle from the axis of rotation; the motion is similar to precession of a gyrostat but constrained to fixed frequency and amplitude. The fluctuating pressure response of the liquid in the cylinder was measured using pressure transducers mounted in an end wall. Fluctuating pressure was measured for non-dimensional coning frequencies of

DD FORM 1 JAN 73 1473 EDITION OF 1 NOV 65 IS OBSOLETE

UNCLASSIFIED

SECURITY CLASSIFICATION OF THIS PAGE (When Data Entered)

.030 to .075, for coning angles of 1.8×10^{-4} to 3.5×10^{-2} radians, and for Reynolds numbers of 5×10^{3} to 5×10^{5}. Comparisons were made to existing linear theories of the liquid response. The results agreed with theoretical predictions at the highest Reynolds number and smallest angles. At the smallest Reynolds number, the data agreed better with the solution of a forced oscillation problem than with the solution of a free oscillation problem. At coning angles as small as 5×10^{-4}, the data showed significant departure from the predictions of linear theory, and at coning angles as small as 8×10^{-4}, the liquid exhibited nonstationary behavior suggestive of a flow instability.

TABLE OF CONTENTS

		Page
	LIST OF ILLUSTRATIONS	5
I.	INTRODUCTION	9
	A. Background	9
	B. Purpose	14
II.	EXPERIMENTAL METHOD	14
	A. Diagnostic Variable	14
	B. Independent Variables	15
	C. Instrumentation	16
	D. Procedure	19
III.	RESULTS	20
	A. Comments on the Measurements	20
	B. General Results	20
	C. The Linear Regime	21
	D. The Nonlinear Regime	23
IV.	DISCUSSION AND CONCLUSIONS	23
	A. Validity of Linear Theory	23
	B. Applicability of Linear Theory	24
	C. Nonlinear Behavior	24
V.	RECOMMENDATIONS FOR FUTURE WORK	24
	REFERENCES	26
	LIST OF SYMBOLS	69
	APPENDIX A. PROPERTIES OF LIQUIDS	71
	APPENDIX B. CALIBRATIONS	73
	DISTRIBUTION LIST	77

LIST OF ILLUSTRATIONS

Figure		Page
1	The Cylinder	28
2	Gimbal Case	29
3	Adjustable Cam	30
4	Placement of Pressure Transducers	31
5	Telemetry Link	32
6	Typical Display of Spectrum Analyzer	33
7	Overlaid Spectra Taken at Different Coning Frequencies	34
8	Estimated Uncertainty of Pressure Coefficient	35
9	Variation of C_p with Coning Frequency, c/a = 3.1481, f = 0.92, Re = 4×10^5 Δ -- $\varepsilon = 1.85 \times 10^{-4}$; $\square$ -- $\varepsilon = 3.51 \times 10^{-4}$; X -- $\varepsilon = 7.78 \times 10^{-4}$; $\diamond$ -- $\varepsilon = 1.97 \times 10^{-3}$; $\bigcirc$ -- $\varepsilon = 3.91 \times 10^{-3}$	36
10	Variation of Pressure Coefficient with Coning Frequency in the Linear Regime. Transducer at r/a = 0.668. Dashed vertical line is eigenfrequency at nominal c/a (Refs. 5, 6 and 9); dotted vertical lines show the effect on eigenfrequency of experimental error in c/a. Solid curve is prediction of Ref. 7	37
	a. c/a = 3.1481, f = 1.00, Re = 5×10^5	37
	b. c/a = 3.1481, f = 1.00, Re = 1×10^5	38
	c. c/a = 3.1481, f = 1.00, Re = 5×10^3	39
	d. c/a = 1.0509, f = 1.00, Re = 5×10^5	40
	e. c/a = 1.0509, f = 1.00, Re = 1×10^5	41
	f. c/a = 3.1481, f = 0.92, Re = 4×10^5	42
	g. c/a = 3.1481, f = 0.92, Re = 8×10^4	43
11	Variation of Frequency of Peak Response with Reynolds Number. Transducer at r/a = 0.668. Solid lines are Stewartson-Wedemeyer eigenfrequency; dashed lines are Gerber frequency of peak response	44
	a. c/a = 3.1481 $\bigcirc$ - f = 1.00; Δ - f = 0.92	44
	b. c/a = 1.0509, f = 1.00	45

LIST OF ILLUSTRATIONS
(Continued)

Figure		Page
12	Variation of Amplitude of Peak Response with Reynolds Number. Transducers at 0.668. Solid lines are Gerber peak response. f = 1.00; ○ - c/a = 3.1481; Δ - c/a = 1.0509.....	46
13	Ratio of Amplitude at r/a = 0.436 to Amplitude at r/a = 0.668. Solid line is Gerber theory.....	47
	a. c/a = 3.1481, f = 1.00, Re = 5×10^5 Δ -- $\varepsilon = 1.66 \times 10^{-4}$; □ -- $\varepsilon = 3.79 \times 10^{-4}$; X -- $\varepsilon = 5.93 \times 10^{-4}$; ◇ -- $\varepsilon = 8.17 \times 10^{-4}$; ∇ -- $\varepsilon = 3.84 \times 10^{-3}$	47
	b. c/a = 3.1481, f = 1.00, Re = 1×10^5 Δ -- $\varepsilon = 1.75 \times 10^{-4}$; □ -- $\varepsilon = 3.79 \times 10^{-4}$	48
	c. c/a = 1.0509, f = 1.00, Re = 5×10^5 □ -- $\varepsilon = 3.70 \times 10^{-4}$; ◇ -- $\varepsilon = 7.30 \times 10^{-4}$	49
	d. c/a = 3.1481, f = 0.92, Re = 4×10^5 Δ -- $\varepsilon = 1.85 \times 10^{-4}$; □ -- $\varepsilon = 3.51 \times 10^{-4}$; X -- $\varepsilon = 7.78 \times 10^{-4}$; ○ -- $\varepsilon = 1.97 \times 10^{-3}$	50
	e. c/a = 3.1481, f = 0.92, Re = 8×10^4 □ -- $\varepsilon = 3.79 \times 10^{-4}$; X -- $\varepsilon = 8.95 \times 10^{-4}$; ◇ -- $\varepsilon = 1.85 \times 10^{-3}$; ○ -- $\varepsilon = 3.78 \times 10^{-3}$; ∇ -- $\varepsilon = 8.70 \times 10^{-3}$	51
14	Variation of Pressure Coefficient with Coning Frequency in the Linear/Nonlinear/Nonstationary Regimes Transducer at r/a = 0.668. Symbols connected by vertical lines represent nonstationary behavior.....	52
	a. c/a = 3.1481, f = 1.00, Re = 5×10^5 Δ -- $\varepsilon = 2 \times 10^{-4}$; □ -- $\varepsilon = 3.79 \times 10^{-4}$; X -- $\varepsilon = 6 \times 10^{-4}$; ◇ -- $\varepsilon = 8.17 \times 10^{-4}$; ○ -- $\varepsilon = 1.85 \times 10^{-3}$; ∇ -- $\varepsilon = 3.84 \times 10^{-3}$	52
	b. c/a = 3.1481, f = 1.00, Re = 1×10^5 Δ -- $\varepsilon = 1.75 \times 10^{-4}$; □ -- $\varepsilon = 4 \times 10^{-4}$; X -- $\varepsilon = 9.23 \times 10^{-4}$; ◇ -- $\varepsilon = 3.68 \times 10^{-3}$; ○ -- $\varepsilon = 8.70 \times 10^{-3}$	53
	c. c/a = 3.1481, f = 1.00, Re = 5×10^3 Δ -- $\varepsilon = 4 \times 10^{-4}$; □ -- $\varepsilon = 1.90 \times 10^{-3}$; X -- $\varepsilon = 3.75 \times 10^{-3}$; ◇ -- $\varepsilon = 6.93 \times 10^{-3}$; ○ -- $\varepsilon = 1.74 \times 10^{-2}$; ∇ -- $\varepsilon = 3.48 \times 10^{-2}$	54
	d. c/a = 1.0509, f = 1.00, Re = 5×10^5 Δ -- $\varepsilon = 2 \times 10^{-4}$; □ -- $\varepsilon = 3.70 \times 10^{-4}$; X -- $\varepsilon = 5.64 \times 10^{-4}$; ◇ -- $\varepsilon = 7 \times 10^{-4}$; o -- $\varepsilon = 1.86 \times 10^{-4}$	55

LIST OF ILLUSTRATIONS
(Continued)

Figure		Page
14	e. c/a = 1.0509, f = 1.00, Re = 1×10^5 Δ -- $\varepsilon = 1.66 \times 10^{-4}$; $\square$ -- $\varepsilon = 3.70 \times 10^{-4}$; X -- $\varepsilon = 9 \times 10^{-4}$; $\diamond$ -- $\varepsilon = 3.70 \times 10^{-4}$	56
	f. c/a = 3.1481, f = 0.92, Re = 4×10^5 Δ -- $\varepsilon = 1.85 \times 10^{-4}$; $\square$ -- $\varepsilon = 3.51 \times 10^{-4}$; X -- $\varepsilon = 7.78 \times 10^{-4}$; $\diamond$ -- $\varepsilon = 1.97 \times 10^{-3}$; O -- $\varepsilon = 3.91 \times 10^{-3}$	57
	g. c/a = 3.1481, f = 0.92, Re = 8×10^4 Δ -- $\varepsilon = 3.79 \times 10^{-4}$; $\square$ -- $\varepsilon = 8.95 \times 10^{-4}$; X -- $\varepsilon = 1.85 \times 10^{-3}$; $\diamond$ -- $\varepsilon = 3.78 \times 10^{-3}$ O -- $\varepsilon = 8.70 \times 10^{-3}$	58
15	Dependence of Peak Amplitude on Coning Angle. Symbols Connected by Vertical Arrows Represent Nonstationary Behavior. Error bars indicate uncertainty.....	59
	a. c/a = 3.1481, f = 1.00, Re = 5×10^5	59
	b. c/a = 3.1481, f = 1.00, Re = 1×10^5	60
	c. c/a = 3.1481, f = 1.00, Re = 5×10^3	61
	d. c/a = 1.0509, f = 1.00, Re = 5×10^5	62
	e. c/a = 1.0509, f = 1.00, Re = 1×10^5	63
	f. c/a = 3.1481, f = 0.92, Re = 4×10^5	64
	g. c/a = 3.1481, f = 0.92, Re = 8×10^4	65
16	Coning Angle at Which Transition to Nonlinear Behavior Occurred O -- c/a = 1.0509, f = 1.00; Δ -- c/a = 3.1481, f = 1.00; $\square$ -- c/a = 3.1481, f = 0.92.....	66
17	Coning Angle at Which Transition to Nonstationary Behavior Occurred O -- c/a = 1.0509, f = 1.00; Δ -- c/a = 3.1481, f = 1.00; $\square$ -- c/a = 3.1481, f = 0.92.....	67

LIST OF APPENDIX ILLUSTRATIONS

B.1	Setup for Measuring Transfer Function of Telemetry Link.....	75

I. INTRODUCTION

A. Background

It has been known for some time that spin-stabilized projectiles with liquid payloads can suffer flight instabilities related to the presence of the liquid[1]. It has also been known that a rotating fluid can sustain inertial oscillations[2], and that these oscillations are constrained to certain discrete natural frequencies if the fluid is contained. In 1959, Stewartson[3] demonstrated that a rotating rigid body having a right circular cylindrical cavity filled with liquid can suffer an instability of its fast precessional motion, if the frequency of the body is sufficiently close to one of the natural frequencies of a nonsymmetric mode of inertial oscillation of the liquid. Stewartson and, independently, Phillips[4], calculated the eigenfrequencies for an inviscid liquid, and Stewartson presented a linear theory giving the frequency of precession of the rotating body-liquid system, and the rate at which the angle of precession grows or decays with time. Wedemeyer[5,6] used boundary layer-type corrections to determine the change in eigenfrequencies from inviscid values caused by small viscosity, and proposed that the change in the frequency and growth rate of system precession due to small viscosity could be entirely explained (to first order accuracy in the Ekman number) by the change in liquid eigenfrequencies. Stewartson's theory with Wedemeyer's extension, hereafter referred to as the Stewartson-Wedemeyer theory, comprises the theoretical basis for the principal tool[1] now available for the design of stable liquid-filled projectiles. Important assumptions made in the derivation of the theory which limit its range of applicability are that (i) the angle of precession is small, (ii) the viscosity of the liquid is small (the Reynolds number is large), (iii) the ratio of the mass of the liquid to the mass of the solid parts of the system is small, and (iv) the

---

1. *Engineering Design Handbook, Liquid-Filled Projectile Design, AMC Pamphlet No. 706-165, U.S. Army Materiel Development and Readiness Command, Washington, DC, April 1969. AD 853719*

2. *Greenspan, H.P., The Theory of Rotating Fluids, Cambridge Univ. Press, NY, 1969, pp. 81 ff.*

3. *Stewartson, K., "On the Stability of a Spinning Top Containing Liquid", J. Fluid Mech., Vol. 5, No. 4, September 1959, pp. 577-592.*

4. *Phillips, O.M., "Centrifugal Waves", J. Fluid Mech., Vol. 7, 1960, pp. 340-352.*

5. *Wedemeyer, E.H., "Viscous Corrections to Stewartson's Stability Criterion", U.S. Army Ballistic Research Laboratory/ARRADCOM Report No.1325, Aberdeen Proving Ground, Maryland, June 1966. AD 489687.*

6. *Wedemeyer, E.H., "Viscous Corrections to Stewartson's Stability Criterion", AGARD Conference Proceedings No. 10, NATO Advisory Group for Aerospace Research and Development, Paris, pp. 99-116, September 1966.*

the liquid is in a basic state of rigid rotation, the only departure being the small motion due to the inertial oscillations. In addition, the influence of the liquid on the system frequency and growth rate is approximated as being entirely due to one of the inertial modes, which requires that the system frequency be very near the eigenfrequency of that mode, i.e., that the system be very near resonance.

Gerber[7] has produced a linear theory in which the contributions of several eigenmodes are summed, and which is therefore valid away from resonance. He also makes no assumptions about the relative masses of the liquid and solid parts of the system. The assumptions of small precession angle, small viscosity, and a basic state of rigid rotation of the liquid remain, and there is the important new requirement that the liquid fill the cavity completely. For those cases which have been examined, Gerber's predicted growth rates agree with the Stewartson-Wedemeyer theory in the regions where both theories should be valid[7].

The author is unaware of any theory predicting the motion of the system when the liquid is not in a basic state of rigid rotation, for example, when it is being spun up. However, two theories have been presented predicting the eigenmodes of oscillation for this case. Lynn[8] has calculated eigenfrequencies of axisymmetric (i.e., azimuthally-constant) inertial modes, using an inviscid formulation. Kitchens, Gerber, and Sedney[9] have calculated eigenvalues for both axisymmetric and nonaxisymmetric modes, with a viscous formulation valid for large Reynolds number.

All of the theories mentioned above are linear in the angle of precession, ε. Scott[10] used a formal expansion of the cavity length in powers of ε to obtain a first-order finite amplitude correction to the inviscid eigenfrequencies. Although the applicability of his model to real fluids seems somewhat doubtful, since he included no viscous effects, his predicted

---

7. *Gerber, N., "Moment on a Liquid-Filled Projectile: Solid-Body Rotation", U.S. Army Ballistic Research Laboratory/ARRADCOM Report (to be published).*

8. *Lynn, Y.M., "Free Oscillations of a Liquid During Spin-Up", U.S. Army Ballistic Research Laboratory/ARRADCOM Report No. 1663, Aberdeen Proving Ground, Maryland, August 1973. AD 769710.*

9. *Kitchens, Jr., C.W., Gerber, N., and Sedney, R., "Oscillations of a Liquid in a Rotating Cylinder: Part I. Solid Body Rotation", U.S. Army Ballistic Research Laboratory/ARRADCOM Report ARBRL-TR-02081, Aberdeen Proving Ground, Maryland, June 1978. AD A057759.*

10. *Scott, W.E., "The Large Amplitude Motion of a Liquid-Filled Gyroscope and the Non-interaction of Inertial and Rossby Waves", J. Fluid Mech., Vol. 72, Part 4, pp. 649-660, 1975.*

frequency corrections did seem to match the observed shift in system frequency at maximum growth rate observed by Scott and D'Amico[11].

Relevant experimental investigations fall into two broad classes: (1) studies of the behavior of the solid-liquid systems; and (2) studies of the motion of the liquid only. Ward[12] conducted the first reported experiment of the first class, in which he crudely measured the growth rate of the precession angle of a liquid-filled gyrostat, finding one of Stewartson's predicted resonances. Karpov[1] conducted a series of experiments using liquid-filled projectiles, demonstrating the existence of instabilities and showing qualitatively the effects of viscosity and of the ratio of liquid mass to solid mass. Karpov and others conducted gyrostat experiments, recently reviewed by Whiting and Gerber[13], the results of which, for a very limited set of conditions, agreed moderately well with the predictions of the Stewartson-Wedemeyer theory. In all of these experiments the liquid was in a basic state of rigid rotation.

Karpov[1] and more recently Mark[14] have found evidence in tests with liquid-filled projectiles strongly suggesting that system instabilities can occur when the liquid payload is being spun up. D'Amico and Miller[15] have observed an instability of a projectile filled with a highly-viscous liquid (Reynolds number about 1); it seems unlikely that the mechanism of resonance of inertial oscillations with projectile precession had anything to do with this instability, but the observations make the practical point that instabilities at smaller viscosities cannot necessarily be made to go away by simply increasing the viscosity.

In all of the experiments using liquid-filled gyrostats, it was found that the growth rates of instabilities deviated from linear dependence on ε at rather small angles. Scott and D'Amico[11] found, for example, that growth

---

11. *Scott, W.E., and D'Amico, W.P., "Amplitude-Dependent Behavior of a Liquid-Filled Gyroscope", J. Fluid Mech., Vol. 60, Part 4, pp. 751-758, 1973.*

12. *Ward, B.N., Appendix to Reference 3.*

13. *Whiting, R.D., and Gerber, N., "Dynamics of a Liquid-Filled Gyroscope: Update of Theory and Experiment", U.S. Army Ballistic Research Laboratory/ARRADCOM Technical Report ARBRL-TR-02221, Aberdeen Proving Ground, Maryland, March 1980. AD A083886.*

14. *Mark, A., "Measurements of Angular Momentum Transfer in Liquid-Filled Projectiles", U.S. Army Ballistic Research Laboratory/ARRADCOM Report ARBRL-TR-2029, Aberdeen Proving Ground, Maryland, November 1977. AD A051342.*

15. *D'Amico, W.P., and Miller, M., "Flight Instability Produced by a Rapidly-Spinning, Highly-Viscous Liquid", J. Spacecraft and Rockets, Vol. 16, No. 1, pp. 62-64, January 1979.*

rates of instabilities, and the system frequency at which maximum growth rate occurred, changed at precession angles as small as 9×10^{-3} radians.

The first quantitative investigation of the second class (studies of the motion of the liquid only) was by Fultz[16], who excited axisymmetric modes in a cylinder by means of axial oscillations of a disk in the liquid. He measured the frequencies of forcing which produced the greatest response, as observed by means of dye injected into the liquid. For Reynolds numbers around 5×10^3, he found agreement to within one percent with eigenvalues computed using inviscid theory.

Thompson[17] used gravitational forcing of the free surface of the liquid in a tilted cylinder to drive a nonsymmetric mode of frequency zero (in the laboratory frame of reference). He found that nonlinear effects produced an azimuthally-constant, radially-varying secondary flow, which could suffer a shear instability if the liquid depth were such that an inertial mode had natural frequency near zero.

McEwan[18] forced nonsymmetric oscillations by causing the rotation axis of a tilted, rigid lid to cone about the rotation axis of the cylinder, at a speed different from that of the cylinder rotation. Using flow visualization, he demonstrated the presence of a number of nonsymmetric modes near the critical aspect ratios predicted by linear, inviscid theory. He was not able to show viscous effects on the natural modes directly. He did show the presence of a mean secondary flow apparently qualitatively similar to that seen by Thompson. Although he did not resolve the radial structure of this flow, some of his measurements roughly indicated the change, caused by the secondary flow, in the critical cavity dimensions required for resonance of a natural mode.

Both Thompson and McEwan observed flow instabilities whenever the disturbance angle (in McEwan's case the tilt of the lid, in Thompson's case the tilt of the cylinder) was sufficiently large. Thompson found that the flow became unstable at a disturbance angle of about 10^{-3} radians, when the fundamental mode was in resonance, and about 0.015 radians when the next higher mode was in resonance. The only value of Reynolds number he used was 6.6×10^4.

McEwan found flow instability at a tilt angle of .018 radians, for Reynolds number greater than 9×10^4. He presents data indicating that higher viscosity inhibits the instability. He remarked that "Collapse [instability]

---

16. *Fultz, D., "A Note on Overstability and the Elastoid-Inertia Oscillations of Kelvin, Solberg, and Bjerkness", J. Meteorology, Vol. 16, pp. 199-208, April 1969.*

17. *Thompson, R., "Diurnal Tides and Shear Instabilities in a Rotating Cylinder", J. Fluid Mech., Vol. 40, Part 4, pp. 737-751, 1970.*

18. *McEwan, A.D., "Inertial Oscillations in a Rotating Fluid Cylinder", J. Fluid Mech., Vol. 40, Part 3, pp. 603-640, 1970.*

would also be avoided in all other configurations for sufficiently weak excitation rate or low rotation rate [low Reynolds number]...", but he did not report what angles or rotation rates were "sufficiently weak".

Aldridge[19,20] forced axisymmetric oscillations in a cylinder during spin-up of the liquid by causing the rotational speed of the cylinder to vary periodically. He determined the response of the liquid by measuring the fluctuating pressure in the cylinder, and found that as time progressed, that is, as the liquid spun-up, the amplitude of the pressure fluctuations came to a peak value, then decayed. The time at which the peak occurred was usually later than the time at which Lynn[8] predicted that the liquid eigenfrequency would match the forcing frequency, being about fifteen percent later at most. Subsequently, Gerber and Sedney (personal communication) have used the solution of Reference 9 to make predictions analogous to those of Lynn. Their results lie between Lynn's predictions and Aldridge's data. Stergiopoulos and Aldridge[21] have studied nonsymmetric oscillations during spin-up of a liquid in a slightly tilted cylinder with the upper end open, the same type set-up used by Thompson [17]. They were able to determine the time evolution of resonant height as the liquid progressed to rigid rotation, a result not yet available in theory. When the liquid was in rigid rotation, they found nonlinear effects at the smallest tilt angle studied (.005 radians), and instability of the flow at any angle above .01 radians, when the depth of the liquid was such that the second lowest mode was in resonance (the same mode for which Thompson found instability above .015 radians).

It is useful to summarize the "state-of-the-art" as represented by the theories and experiments described above. In regard to the motion of the liquid, it can be said that the existence of discrete frequencies of oscillation in the liquid[1,2,4] is amply confirmed[16-18]. For liquids of small viscosity, the spectrum of allowed frequencies seems to have nearly the dependence on geometry predicted by linear, inviscid theory, for the lower wave number modes of oscillation[16-19,21]. The effects of viscosity[5,6,9] on the oscillations have not been quantitatively confirmed, though it is clear that there are effects [18], and that in some respects they scale with viscosity more-or-less as viscous theory predicts. The amplitude attained by forced nonsymmetric oscillations has not been accurately measured, except for the mode with frequency zero[21]. The existence of nonlinear effects on the

---

19. *Aldridge, K., "Experimental Verification of the Inertial Oscillations of a Fluid in a Cylinder During Spin-Up", U.S. Army Ballistic Research Laboratory/ARRADCOM Contract Report No. 273, Aberdeen Proving Ground, Maryland, November 1975.* AD #A018797

20. *Aldridge, K., "Axisymmetric Inertial Oscillations of a Fluid in a Cylindrical Cavity During Spin-Up from Rest", Geophysical and Astrophysical Fluid Dynamics, Vol. 8, No. 4, pp. 279-301, 1977.*

21. *Stergiopoulos, S., and Aldridge, K., "Inertial Waves in a Partially-Filled Cylindrical Container during Spin-Up from Rest", submitted to Geophysical and Astrophysical Fluid Dynamics.*

response of a nonsymmetric mode and a change in the mean motion of the liquid due to these nonlinearities have been well demonstrated at angles as small as .001 radians[17,18]. It has been established that the flow may become unstable, possibly due to shear instability of the secondary flow, at angles of the order of .001 radians[17,18]. It has been shown that inertial oscillations can be driven during spin-up[19-21], and that for several axisymmetric modes, and some nonsymmetric modes of zero frequency, the trajectories of eigenfrequency in time are smooth. For the nonsymmetric modes, nonlinear effects have been found during spin-up[21]. For the axisymmetric modes, the predicted trajectories of eigenfrequency are reasonably close to the measured trajectories of peak response[19,20], though no demonstration has been made that the eigenfrequency calculated by the theories[8,9] should be identified with the peak response.

With respect to system response, there has been only one complete check of the predicted versus measured precession frequency and growth rate of a liquid-filled gyrostat[13]. Several partial checks are available, including cases where the liquid does not completely fill the cavity. These experiments match the theoretical predictions to within ten to twenty-five percent[13]. There is clear evidence in gyrostats of an effect of finite amplitude of precession angle on the growth rate at angles as small as .009 radians[11], but it cannot be said whether the effect is due primarily to nonlinear processes in the liquid or in the gyrostat response. The point that liquid motions seem to become unstable[17,18] at smaller angles than those at which the growth rates of gyrostats change has not been addressed. System instabilities can occur while the liquid is being spun-up[1,14], but such instabilities cannot be predicted.

B. Purpose

The objective of this experiment was to measure the flow due to forced nonsymmetric oscillations when the liquid was in a basic state of rigid rotation, by measuring pressure fluctuations, using a modified version of Aldridge's technique. The effects of viscosity, fill ratio, and geometry were examined, for a range of coning frequencies in the region applicable to liquid-filled projectiles. For each combination of these parameters, the limiting precession angle at which linear theory could be used was determined, as were the nature of the nonlinear effects when this angle was exceeded.

In addition, apparatus and techniques were developed which could be used to conduct similar studies of the flow while the liquid is being spun-up from rest, these studies to form a separate, follow-on effort.

II. EXPERIMENTAL METHOD

A. Diagnostic Variable

Fluctuating pressure was chosen as the quantity to be measured. It is a primitive flow variable, and is the quantity whose value is required for computing overturning moments on a container. It was decided to measure the

pressure at an end wall, so that the measuring device need not intrude into the flow. The inference of interior pressure from measurements at a wall requires that the boundary layer approximation be valid, so that the normal derivative of pressure near the wall is small. This in turn requires that the Reynolds number be large.

The choice of an end wall in preference to the side wall was based purely on convenience. One might argue that the pressure on the side wall contributes more to the overturning moment exerted on the container and is therefore more relevant than pressure on the end wall. However, the pressure measured anywhere in the liquid should be equally useful as a flow diagnostic. The only new information to be gained from sidewall pressure is spatial structure, which is, of course, important. If it is later decided that measurements at the sidewall are desirable, they can be made with minor changes in the apparatus.

B. Independent Variables

The quantities varied during the experiment, and the apparatus to implement the variations, were:

1. Cylinder Geometry. The cylinder (Figure 1) was constructed of Lucite, with a mean inner radius, a, of 31.761± .012mm. Aluminum top and bottom inserts of several different lengths were made, so that the interior length, 2c, could be changed by changing inserts. Two lengths were used in this experiment: 199.972± .010mm, and 66.756± .011mm. The aspect ratios, c/a, were thus 3.1481 and 1.0509 at 22° C. The total uncertainty in c/a, including the effect of temperature fluctuations, is estimated to be .0012 for c/a = 3.1481, and .0004 for c/a = 1.0509.

2. Coning Angle. The cylinder was mounted in a gimbal case (Figure 2) which contained a motor to maintain the rotational speed Ω. The case had a shaft extending from its lower end, which mated with a bushing gripped by an adjustable cam (Figure 3). The cam was rotated by a second electric motor; as it rotated, it caused the cage, hence the axis of rotation of the cylinder, to cone about a line passing through the center of the cam and the pivot point of the cylinder (the "coning axis" in Figures 2 and 3). The pivot point, that is, the intersection of the axes of the inner and outer gimbal bearings, was coincident with the center of the cylinder. The coning angle ε was adjusted by adjusting the offset screw in the cam. The angle was measured (after the locking screw was tightened) in one of two ways: (1) if the coning angle was less than 3.5×10^{-3} rad., the displacement of a point on the motor mount was measured with a dial indicator; (2) if the coning angle was greater than 3.5×10^{-3} rad., the number of turns of the offset screw used to set the angle was recorded. Either measurement could be turned into horizontal displacement of a known point on the gimbal cage; with the previously-measured distance of that point from the pivot point, ε could then be determined. Geometric relations accurate to first order in ε were used, so that ε was measured to $\pm 1.3 \times 10^{-4}$ rad. when it was less than 3.5×10^{-3} rad., or $\pm 9.7 \times 10^{-6}$ rad., when it was greater than 3.5×10^{-3} rad.

The smallest coning angle used was about 1.7×10^{-4} rad.; the largest was about 3.5×10^{-2} rad.

3. Viscosity Three different liquids were used: Dow Corning 200 Silicon Fluids with nominal kinematic viscosities ν of 1, 5, and 100 centistokes. Details of the variation of viscosity and density of the liquids with temperature are described in Appendix A. Two cylinder rotational speeds were used: 523.6 rad./s, and 433.3 rad./s*. Two non-dimensional numbers involving ν are commonly used: the Reynolds number, $Re \equiv \Omega a^2/\nu$, and the Ekman number, $E \equiv \nu/\Omega c^2$. In this experiment, Re was varied from about 5×10^3 to 5×10^5; E varied from about 2×10^{-7} to 2×10^{-5}.

4. Fill Ratio In addition to the filled case, data were taken with about 50 ml (about eight percent of the cavity volume) of liquid removed from the cylinder with aspect ratio 3.1481. This gave a fill ratio, f ($\equiv$ liquid volume/cavity volume) of about 0.92. If the axial acceleration of the liquid (e.g., gravity) were zero, then the interface between the liquid and the air would be cylindrical (neglecting distortions due to oscillations). In this case, the air core radius, b, would be $a(1-f)^{1/2}$, or about 8.9mm. The appropriate measure of the axial acceleration is the Froude number, $F \equiv \Omega^2 b/g$, which was about 172 for this experiment. This caused the air-liquid interface to be a truncated paraboloid, with the radius at the upper and lower ends respectively 6.3% greater and 6.7% less than the value of b computed above. F was not varied during the experiment.

5. History of Cylinder Spin. In this experiment, Ω was held constant to within about one percent for at least five minutes before data were recorded, ensuring that the liquid had come to a basic state of rigid rotation. While data were actually being recorded, Ω was kept constant to within .05%.

6. History of Coning Frequency. The coning frequency was kept constant to within about 0.1% long enough for transients to die away (see paragraph D6 below).

C. Instrumentation

The principal instrumentation included the following:

1. Pressure Transducers. Kulite XT-39-190-25A absolute transducers were used. These transducers were specially built with metal stops behind the sensing diaphram. Large deflections which would ordinarily damage the transducers are not permitted due to the metal stop. Over pressure ratios of 40/1 are permitted without a loss in calibration. Two transducers were flush mounted in the bottom end face of the cavity, as shown in Figure 4. One transducer was at a non-dimensional radius r/a = 0.436, the other at r/a = 0.668; the transducers differed in azimuthal location by about $\pi/2$. The sensing area of each transducer had a diameter of about 2.16mm, or 0.068a. The transducer signals were fed into amplifiers

*The lower speed was used in the cases of partial fill, to avoid a resonance with the supporting structure.

which provided a gain of about 700 in the range 70-90 Hz (the range of concern in this experiment); the amplifier cut off frequencies were slightly below 10 Hz. Details of the calibration of the transducers and amplifiers are in Appendix B.

2. Telemetry. The pressure signals were transferred from the rotating cylinder frame of reference to the laboratory frame by a telemetry link, shown schematically in Figure 5. The outputs of the transducer amplifiers were input to two Omnitek Model 22A1E voltage controlled oscillators (VCOs) with 40 kHz and 52.5 kHz center frequencies, whose outputs were combined and sent to an Optimax Model 4001 FM transmitter. The transmitted signal was received, amplified by a Mu-Del Electronics, Inc., Model MDA-2132 RF preamplifier, and sent to a Defense Electronics, Inc., Model TMR-511 receiver. The video output from the receiver passed to two EMR Model 4142 tunable discriminators, set for 40 kHz and 52.5kHz, whose outputs were then equal to the VCO inputs (less an adjustable offset). The overall transfer function of all of this equipment, including the transducer amplifiers, was determined using a Hewlett-Packard HP 3582A spectrum analyzer. Details of the equipment settings and calibration procedures are shown in Appendix B.

3. Signal Analyzer. The same HP 3582A spectrum analyzer was used to analyze the pressure signals. This device computed discrete Fourier transforms of two 512-point time samples of data gathered simultaneously, enabling data to be taken on two channels at once. The instrument was set to take evenly-spaced samples over a 12.5-second interval; low-pass filters within the instrument prevented aliasing. The instrument performed complex multiplications of the signals by a sinusoid of 80 Hz frequency, which enabled the 128-point discrete transforms to cover a span from 75 Hz to 85 Hz. Details of the procedure are in the manufacturer's literature[22].

The spectrum analyzer presented both magnitude and phase of the transform, and both were recorded. The manufacturer cites accuracy of about $\pm 6\%$ in magnitude and $\pm 10°$ in phase over the entire operating range of the instrument; tests with controlled sources in only the range used in the experiment showed the actual worst case error in magnitude to be about 1.5%. The instrument offers three choices of data windowing. The "flat top" window was selected, since it offers the best amplitude accuracy for signals which differ in frequency from any Fourier frequency[22].

The spectra obtained during the experiments had, in general, two dominant peaks, as shown in Figure 6. One was at the spin frequency, and was only slightly affected in its amplitude by the coning frequency. Its amplitude was reduced by a factor of two or three when there was no liquid in the cylinder, and was increased if the cylinder was poorly balanced. The phases of the transforms of the two pressure signals at this frequency were equal, indicating that there was no azimuthal variation of this component in the rotating frame of reference. This peak was taken to be due to disturbances caused by

---

22. *"Operating Manual, Model 3582A Spectrum Analyzer", HP Manual 03582-90000, Hewlett Packard Co., Loveland, Colorado, 1978.*

vibration due to residual imbalance and bearing imperfections, plus some electrical interference or other effect due to azimuthal variations in the pattern of the transmitting antenna.

The second peak was at a frequency equal to the spin frequency minus the coning frequency, which is what is expected from a transducer sweeping at the spin frequency through a wave travelling at the coning frequency (spin and coning were always in the same directions). This peak was taken to be the response of the liquid to the coning. Its amplitude was the amplitude datum recorded, and its variation with coning frequency and coning angle is the subject of the discussion in Section III of this report. The phases of the two signals at this frequency differed by approximately $\pi/2$, indicating that there was azimuthal variation in the rotating frame of reference. Figure 7 shows the amplitude spectra taken on one channel at ten different coning frequencies, overlaid on the same scale. This figure clearly illustrates the large variation of the forced response, and the much smaller variation of the peak at the spin frequency.

4. Interval Timers. Magnetic sensors and associated signal conditioners were used to produce electrical pulses on three circuits: one when the cylinder completed one revolution; one when the coning cam completed one revolution (hence when the cylinder axis completed one cycle of coning); and one whenever the other two pulses happened to occur within about 800 μs of each other. This last pulse thus occurred when the transducers were within .0175 radians of a known position relative to the plane defined by the cylinder rotation axis and the axis about which it was coning, that is, when the phases of the transducers with respect to the coning were known. This pulse was used to trigger the spectrum analyzer to begin gathering a sample of data, and in principle allowed the computed phase of the pressure signals to be related to the phase of the coning.

The pulses produced by cylinder rotation were fed to a Tektronix model DC503 counter set to time the interval between pulses; the counter displayed the period of cylinder rotation to the nearest microsecond. This signal was observed continuously during the time a data sample was being gathered, and the constancy of cylinder speed cited earlier comes from observations of the variation of the rotation period. In every case, the actual period was recorded to the nearest 10 μs.

The pulses produced by rotation of the coning cam were fed to the BRL Yaw Processor, which stored each period of revolution in a digital memory. After each sample of data was gathered by the spectrum analyzer, a HP 9830A calculator recovered the stored periods, and calculated the mean, minimum, and maximum periods for the interval (typically 48 periods), as well as the standard deviation of the periods. The mean period was recorded to the nearest 10 μs. The other information was used to determine the extent of fluctuations in coning period, which was used to compute the constancy of coning frequency cited previously.

5. Computer. A Hewlett-Packard 9845B computer was connected to the spectrum analyzer, and the amplitudes and phases of the two pressure signals at the frequency of the forced oscillation were transmitted directly from the analyzer to the computer. Cylinder rotation period and mean coning period

were entered into the computer by hand. The computer collected all of the data from one "run", that is, one value of all parameters except coning period, and a sequence of values of coning period, into a file. All subsequent manipulation of the data was performed on this computer.

Although it was not done in this experiment, the HP 9830A calculator which computed the coning period could also have been connected to the HP 9845B computer. The addition of a counter with the appropriate interface (IEE-488) and two digital-to-analog converters would in the future allow completely automated control of cylinder and coning speed plus data gathering.

D. Procedure

The procedure for one run was as follows:

1. The cylinder and inserts were assembled, and the cavity was filled with liquid. The cavity was connected to a vacuum pump for (typically) an hour, to deaerate the liquid. Since this caused substantial cooling of the liquid, the apparatus was allowed to settle, usually overnight, to allow the liquid to come to room temperature.

2. The coning angle was set and measured, as discussed previously.

3. The electronic instruments were turned on and allowed to warm up for at least 30 minutes. The discriminators were adjusted to obtain unity gain in the telemetry link (the procedure is detailed in Appendix B).

4. Room temperature was measured and recorded. It was assumed that the liquid thereafter remained at room temperature, and this value was used later to determine the density and viscosity of the liquid.

5. The cylinder was inserted in the gimbal cage, and brought up to speed. At least five minutes elapsed before any data were taken. Since the longest linear spin-up time $(c/(\Omega\nu)^{1/2})$ for this experiment was 4.8 seconds, this delay ensured that the liquid was fully spun up.

6. The coning cam was brought to its selected speed. The spectral display was monitored to determine when the amplitude of the forced oscillations had stabilized, or for at least 30 seconds. In every case in which the display did stabilize, that occurred within 30 seconds; therefore in practice the time limit governed.

7. If the display stabilized, a data sample was taken. In many earlier cases in which the display did not stabilize (the significance of which is discussed in Section III), several data samples were taken. In later cases, if the display did not stabilize, the spectrum analyzer was switched to a 2.5-second sampling time, and the maximum and minimum values attained over some period of time, typically 30 seconds, were recorded.

Steps 6 and 7 were repeated for all selected coning frequencies.

Because the data were immediately available in the computer, plots of suitably non-dimensionalized quantities could be viewed within a few minutes of the completion of a run, either singly or overlaid with plots from previous runs. This facility proved invaluable in guiding the choice of conditions of future runs.

III. RESULTS

A. Comments on the Measurements

1. Measurement of Phase. The effort to measure phase was not successful. For reasons associated with the characteristics of the data window employed by the spectrum analyzer, errors in the measurement of Ω and ω caused much larger relative errors in the measured phase. The estimated errors of .05% in Ω and .1% in ω can be shown to produce errors of about $\pi/2$ radians in phase, and the scatter of the actual data, as much as π radians, more typically $2\pi/3$ radians, in nominally identical cases, is consistent with the cited errors in Ω and ω.

2. Measurements of Amplitude. The results of the pressure measurements were much better than had been expected. This proved extremely fortunate, as it became necessary to make measurements at much smaller coning angles than had been anticipated when the equipment was designed.

The results of the measurements will be presented in the form of a dimensionless pressure coefficient,

$$C_p \equiv \hat{p}/\varepsilon\rho\omega^2 a^2,$$

where $\hat{p}$ is the amplitude of the fluctuating part of the pressure: p = constant + $\hat{p}$ sin $(\omega\Omega t + \phi)$. The accuracy with which C_p could be determined depended on the level of the signal and on the coning angle ε. Using the values of C_p presented later, the previously-cited uncertainties in ε, Ω, a, and the electronic signals, the relative uncertainty in C_p was determined, and is presented in Figure 8 for several values of ε. For a few points in the plots of C_p presented in the following sections, error bars are indicated. These reflect the relationship shown in Figure 8.

B. General Results

For the purpose of discussing the data, four definitions are helpful:

1. "Linear behavior": linear variation of $\hat{p}$ with ε, so that C_p does not depend on ε;

2. "Nonlinear behavior": nonlinear variation of $\hat{p}$ with ε, so that C_p varies with ε;

3. "Nonstationary behavior": variation of $\hat{p}$ with time, hence of C_p with time (thus included in nonlinear behavior); and

4. "Regime": a part of parameter space, e.g., "linear regime", in which some specified behavior occurs.

The major result of this experiment is that linear, nonlinear, and nonstationary regimes were all seen. This is illustrated in Figure 9, which presents C_p plotted against ω for one choice of aspect ratio, Reynolds number, and fill ratio. The different symbols represent data taken at different coning angles. Symbols connected by a vertical line represent measurements for which the amplitude of the spectral peak of the forced oscillation did not settle to a constant value, i.e., nonstationary behavior. The locations of the symbols at the ends of the line are C_p computed from the extreme values of the spectral peak. They must not be interpreted as extremes of C_p, however, since the spectrum analyzer operates on a finite-length sample, thus averaging over the sample time (up to 12.5 seconds, depending on the frequency span) and since no particular effort was made in every case to follow the fluctuations in time. The proper interpretation is that these points simply indicate nonstationary behavior.

Where different symbols lie along the same curve, linear behavior is indicated. In Figure 9, this can be seen to occur for $\varepsilon < 3.51 \times 10^{-4}$. For $\varepsilon = 7.78 \times 10^{-4}$, C_p has a constant value (in time), but near its peak it diverges from C_p at smaller ε. This indicates nonlinear but not nonstationary behavior.

In every case studied in this experiment, C_p attained a peak value for some ω. Comparisons of the ω's of peak C_p with their theoretical values for the various cases are presented later, but as a general comment, there was never sufficient disagreement between measured and theoretical values to cloud the identity, that is, the mode numbers, of the dominant inertial mode near the peak.

C. The Linear Regime

All of the theories mentioned in Section I of this report, except that of Scott[10], are linear in ε. The question of the of the theories is properly addressed by comparing their predictions with data which show linear behavior. Nonlinear behavior then provides the limits of . In this section, except where otherwise noted, only data in the linear regime are presented. Differences between points at the same aspect ratio, Reynolds number, and fill ratio are felt to represent scatter.

Representative error estimates are indicated for a few points. In most cases, the apparent scatter of the data is consistent with the error estimates. For the case $c/a = 1.0509$, $Re = 5 \times 10^5$, $f = 1.00$, shown in Figure 10(d), the scatter between runs considerably exceeds the error estimates. The reason for this is unknown.

The theories chosen for comparison are those of Stewartson-Wedemeyer[1], Kitchens, et al.[9], and Gerber[7]. The first two yield only eigenvalues for the comparison. A basic assumption of the Stewartson-Wedemeyer theory is that

near resonance of an eigenmode, the response of this mode dominates the response of the liquid. This implies that if the liquid is forced by steady coning, the peak of C_p should occur when ω is equal to an eigenfrequency. Thus, the proper comparison is between the computed eigenfrequency and the value of ω at which the peak of C_p occurs. The Gerber theory yields C_p as a function of ω, and should properly be compared at all frequencies.

The comparisons are presented in Figure 10(a) to 10(g). In each case, the vertical dashed line indicates the eigenfrequency; on the scale of the plots, the Stewartson-Wedemeyer and Kitchens, et al., predictions do not differ visibly. The two vertical dotted lines show the eigenfrequencies computed for cylinders with c/a incremented and decremented by its estimated error. For the partially-filled cases, the dotted lines also incorporate the estimated error in fill ratio. The solid curve in each figure is the Gerber prediction; no curve is shown for the partially-filled cases, since the theory does not apply there.

The dependence of the predicted and observed frequencies of peak response on Reynolds number is shown in Figures 11(a) and (b). In these figures the size of the symbols roughly corresponds to the effect of aspect ratio error. In each ease, Stewartson-Wedemeyer prediction seems to fall away from the data at lower Reynolds number; for $Re = 5 \times 10^3$, $c/a = 3.1481$, the error is about eight percent. The Gerber prediction matches the data much better, the worst error being about two percent.

Figure 12 shows the value of C_p at its peak, plotted against Re. Again, the size of the symbols indicates the error. The solid lines are the Gerber prediction. The data indicate a less rapid decrease of peak C_p with decreasing Re than does the theory.

All of the data presented so far were taken using a transducer at $r/a = 0.668$. A second transducer was also mounted in the end wall, at $r/a = 0.436$. For various reasons, data were taken using both transducers only about one-third of the time. The data taken with the second transducer showed the same behavior as those taken at $r/a = .668$, as to linear and nonlinear behavior and location of peak response. However, C_p at $r/a = .436$ was consistently less than at .668, which is an indication of the form of the radial structure of the fluctuating pressure field. A measure of the variation between radial locations is the ratio C_p $(r/a = .436)/C_p$ $(r/a = .668)$. This ratio is plotted against ω in Figures 13(a) to (e) for those cases in which data are available. Note that in these figures all available data are plotted, including those in the nonlinear regime. The vertical dashed line shows the observed frequency of peak C_p for the linear regime. The solid line indicates the prediction of the Gerber theory.

D. The Nonlinear Regime

The location and nature of this regime depended on Re, c/a, and fill ratio. Figures 14(a) to (g) show C_p plotted against ω for all available data, at r/a = .668. The different symbols indicate different coning angles.

Away from the peak of C_p, most of the data in each plot seem to lie along the same curve, showing linear behavior. For sufficiently large ϵ, the curve seems to be chopped off near the location of the linear peak. This effect would not be well-modeled by a simple shift in location of the peak response, so the theory of Scott[10] is not supported. For still larger ϵ, the behavior becomes nonstationary, indicated as before by vertical lines connecting data points.

A measure of nonlinearity is the change in C_p at the frequency at which Cp peaks in the linear regime -- call this value C_p^*. There is some arbitrariness in this measure, since the nonlinear regime C_p sometimes peaks at a different frequency, but it serves to show the onset of different types of behavior. Figures 15(a) to (g) show C_p^* plotted against ϵ. The error bars now indicate uncertainty in estimating C_p^*, and are based on the observed scatter of the data rather than the estimated uncertainty of the measurement of C_p. The symbols connected by vertical arrows indicate nonstationary behavior.

The onsets of nonlinear and nonstationary behavior can be seen to be strongly influenced by Re; for Re = 5×10^3, nonstationary behavior was not observed even at the maximum coning angle attained, ϵ = 0.035. Figure 16 shows the values of ϵ at which transitions to nonlinear behavior occurred, as functions of Re. Figure 17 shows a similar plot of the transitions to nonstationary behavior. Note that in Figure 17, only a lower bound is indicated for c/a = 3.1481, Re = 5×10^3, since nonstationary behavior was not observed for this case.

IV. DISCUSSION AND CONCLUSIONS

A. Validity of Linear Theory

The Stewartson-Wedemeyer[5] and Kitchens, et al.[9] eigenfrequencies approach the Gerber[7] frequency of peak response as Re becomes large (Figures 11(a) and (b)). The data agree with all of these theoretical results, to within 1.5% in the worst case.

As Re becomes small, however, the location of the peak of the Gerber theoretical curve diverges from the eigenfrequency. The data agree better with the Gerber theory (within 1.5%) than with the eigenfrequencies (greatest difference of 9%). This divergence of the frequency of peak response from the location of the S-W eigenfrequency probably reflects the increasing response of the other inertial modes. Since the Gerber theory computes the response

of these other modes, better agreement occurs. At low Re, the response of the liquid may be controlled by several modes.

The predictions of the Gerber theory of the maximum response (Figure 12) differ from the data by, at most, 13%. The maximum difference occurs at the largest value of Re, which is not consistent with an error due to improperly modeled viscous effects. The trend with decreasing Re also differs from the data, with the predicted peak C_p varying approximately with $Re^{1/2}$, and the data varying approximately with $Re^{.43}$ for c/a = 3.1481, and with $Re^{.36}$ for c/a = 1.0509.

The limited data available indicate some difference between the predicted and observed radial structure of the two modes observed. There is no indication that this is the cause of the observed differences in peak C_p, however, since the discrepancies in radial structure at the frequency of peak C_p have no apparent relation to the discrepancies of C_p itself. The differences do serve to qualify the remark made in Section IIA of this report regarding the location of the pressure transducers. If the observed spatial structure differs from the predicted structure, then it is conceivable that the extent of agreement found here is not representative of the whole flow. Only measurements at a large number of points would resolve this issue.

B. Applicability of Linear Theory

The onset of noticeably nonlinear behavior occurs at larger ε for smaller Re, but even at $Re = 5 \times 10^3$, the smallest value of Re used in this experiment, the transition occurred at $\varepsilon = 4 \times 10^{-3}$ rad., which is much smaller than precession angles typical of artillery projectiles. Since the existing theories are not applicable for small Re (less than, say, 10^3), their direct applicability to any artillery projectiles is questionable. This does not mean that they are useless, however, since they may serve as the basis for theories (perhaps semi-empirical) which can account for nonlinear effects.

C. Nonlinear Behavior

Based on work cited in the Introduction [17,18], it is reasonable to hypothesize that the onset of nonstationary behavior is associated with an instability of a secondary flow induced by the forced inertial mode. If this is so, then there is some time scale associated with growth of the mode to a point of instability. Since free gyrostat experiments are inherently time-dependent, this may account for the fact that in free gyrostat experiments departure from linear behavior was observed at larger ε than in the present experiment.

V. RECOMMENDATIONS FOR FUTURE WORK

The most obvious question raised by this experiment concerns the predictability of the nonlinear and nonstationary behavior. If the time scale of the fluid instability mentioned in the previous section is longer than the flight time of a typical projectile, then the proper theoretical approach is to model

the non-steady nonlinear evolution of the flow before it becomes unstable. If the time scale is shorter than the flight time, then the details of the approach to instability are irrelevant, and instead some attempt must be made to model the flow after the instability occurs, and the flow becomes (probably) turbulent. Thus, the first experimental task is to determine the time scale.

If it turns out that the time scale is long, and that the evolution of the flow before it becomes unstable is important to the question of projectile stability, then two issues must be addressed: first, whether the spatial variation of the flow field is essentially as described by linear theory, with perhaps small departures, and second, whether the Kitchens, et al., theory correctly describes the effect of non-rigid rotation on the resonant frequencies. If, on the other hand, the post-instability flow is of greatest importance, then it must be determined whether the flow is amenable to some statistical or other description which allow the moment exerted on the cylinder to be specified sufficiently well to predict system response.

The present experiment, and the ones suggested for the future, are felt to be relevant to projectiles and gyrostats, despite the fact that ε is held constant. However, this should be demonstrated directly by measuring unsteady pressure in a free gyrostat or in projectiles.

REFERENCES

1. Engineering Design Handbook, Liquid-Filled Projectile Design, AMC Pamphlet No. 706-165, U.S. Army Materiel Development and Readiness Command, Washington, DC, April 1969. AD 853719.

2. Greenspan, H.P., The Theory of Rotating Fluids, Cambridge University Press, New York, 1969, pp. 81 ff.

3. Stewartson, K., "On the Stability of a Spinning Top Containing Liquid", J. Fluid Mech., Vol. 5, No. 4, September 1959, pp. 577-592.

4. Phillips, O.M., "Centrifugal Waves", J. Fluid Mech., Vol. 7, 1960, pp. 340-352.

5. Wedemeyer, E.H., "Viscous Corrections to Stewartson's Stability Criterion", U.S. Army Ballistic Research Laboratory/ARRADCOM Report No. 1325, Aberdeen Proving Ground, Maryland, June 1966. AD 489687.

6. Wedemeyer, E.H., "Viscous Corrections to Stewartson's Stability Criterion", AGARD Conference Proceedings No. 10, NATO Advisory Group for Aerospace Research and Development, Paris, France, September 1966, pp. 99-116.

7. Gerber, N., "Moment on a Liquid-Filled Projectile: Solid-Body Rotation", U.S. Army Ballistic Research Laboratory/ARRADCOM Report (to be published).

8. Lynn, Y.M., "Free Oscillations of a Liquid During Spin-Up", U.S. Army Ballistic Research Laboratory/ARRADCOM Report No. 1663, Aberdeen Proving Ground, Maryland, August 1973. AD 769710.

9. Kitchens, Jr., C.W., Gerber, N., and Sedney, R., "Oscillations of a Liquid in a Rotating Cylinder: Part I. Solid Body Rotation", U.S. Army Ballistic Research Laboratory/ARRADCOM Technical Report ARBRL-TR-02081, Aberdeen Proving Ground, Maryland, June 1978. AD A057759.

10. Scott, W.E., "The Large Amplitude Motion of a Liquid-Filled Gyroscope and the Non-Interaction of Inertial and Rossby Waves", J. Fluid Mech., Vol. 72, Part 4, 1975, pp. 649-660.

11. Scott, W.E., and D'Amico, W.P., "Amplitude-Dependent Behavior of a Liquid-Filled Gyroscope", J. Fluid Mech., Vol. 60, Part 4, 1973, pp. 751-758.

12. Ward, B.N., Appendix to Reference 3.

13. Whiting, R.D., and Gerber, N., "Dynamics of a Liquid-Filled Gyroscope: Update of Theory and Experiment", U.S. Army Ballistic Research Laboratory/ARRADCOM Technical Report ARBRL-TR-02221, Aberdeen Proving Ground, Maryland, March 1980. AD A083886.

14. Mark, A., "Measurements of Angular Momentum Transfer in Liquid-Filled Projectiles", U.S. Army Ballistic Research Laboratory/ARRADCOM Technical Report No. 2029, Aberdeen Proving Ground, Maryland, November 1977. AD A051342.

15. D'Amico, W.P., and Miller, M., "Flight Instability Produced by a Rapidly-Spinning, Highly-Viscous Liquid", J. Spacecraft and Rockets, Vol. 16, No. 1, pp. 62-64, January 1979.

16. Fultz, D., "A Note on Overstability and the Elastoid-Inertia Oscillations of Kelvin, Solberg, and Bjerkness", J. Meteorology, Vol. 16, pp. 199-208, April 1969.

17. Thompson, R., "Diurnal Tides and Shear Instabilities in a Rotating Cylinder", J. Fluid Mech., Vol. 40, Part 4, pp. 737-751, 1970.

18. McEwan, A.D., "Inertial Oscillations in a Rotating Fluid Cylinder", J. Fluid Mech., Vol. 40, Part 3, pp. 603-640, 1970.

19. Aldridge, K., "Experimental Verification of the Inertial Oscillations of a Fluid in a Cylinder During Spin-Up", U.S. Army Ballistic Research Laboratory/ARRADCOM Contract Report No. 273, Aberdeen Proving Ground, Maryland, November 1975. AD #A018797

20. Aldridge, K., "Axisymmetric Inertial Oscillations of a Fluid in a Cylindrical Cavity During Spin-Up from Rest", Geophysical and Astrophysical Fluid Dynamics, Vol. 8, No. 4, pp. 279-301, 1977.

21. Stergiopoulos, S., and Aldridge, K., "Inertial Waves in a Partially-Filled Cylindrical Container during Spin-Up from Rest", submitted to Geophysical and Astrophysical Fluid Dynamics.

22. "Operating Manual, Model 3582A Spectrum Analyzer", HP Manual 03582-90000, Hewlett-Packard Company, Loveland, Colorado, 1978.

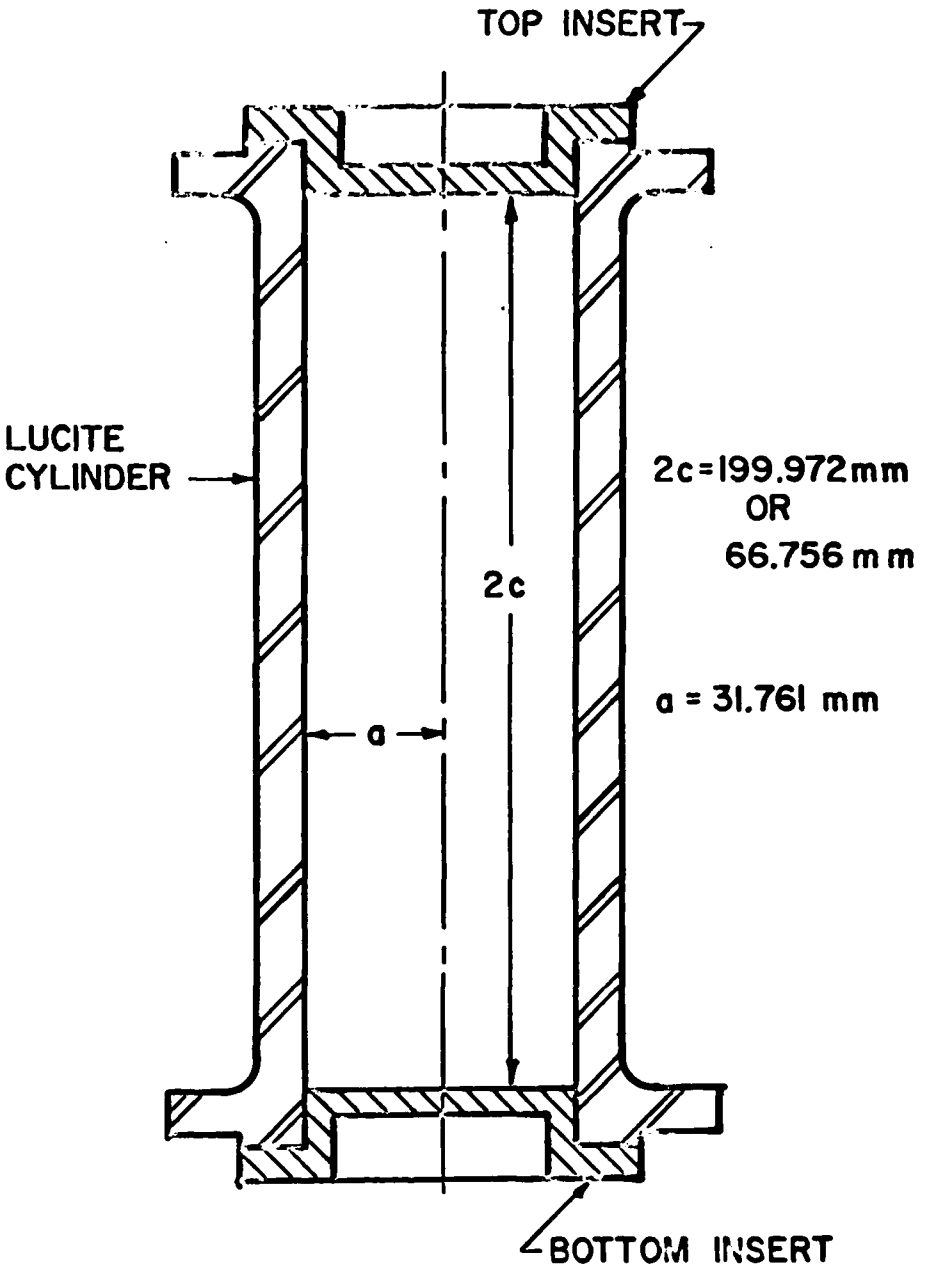

Figure 1. The Cylinder.

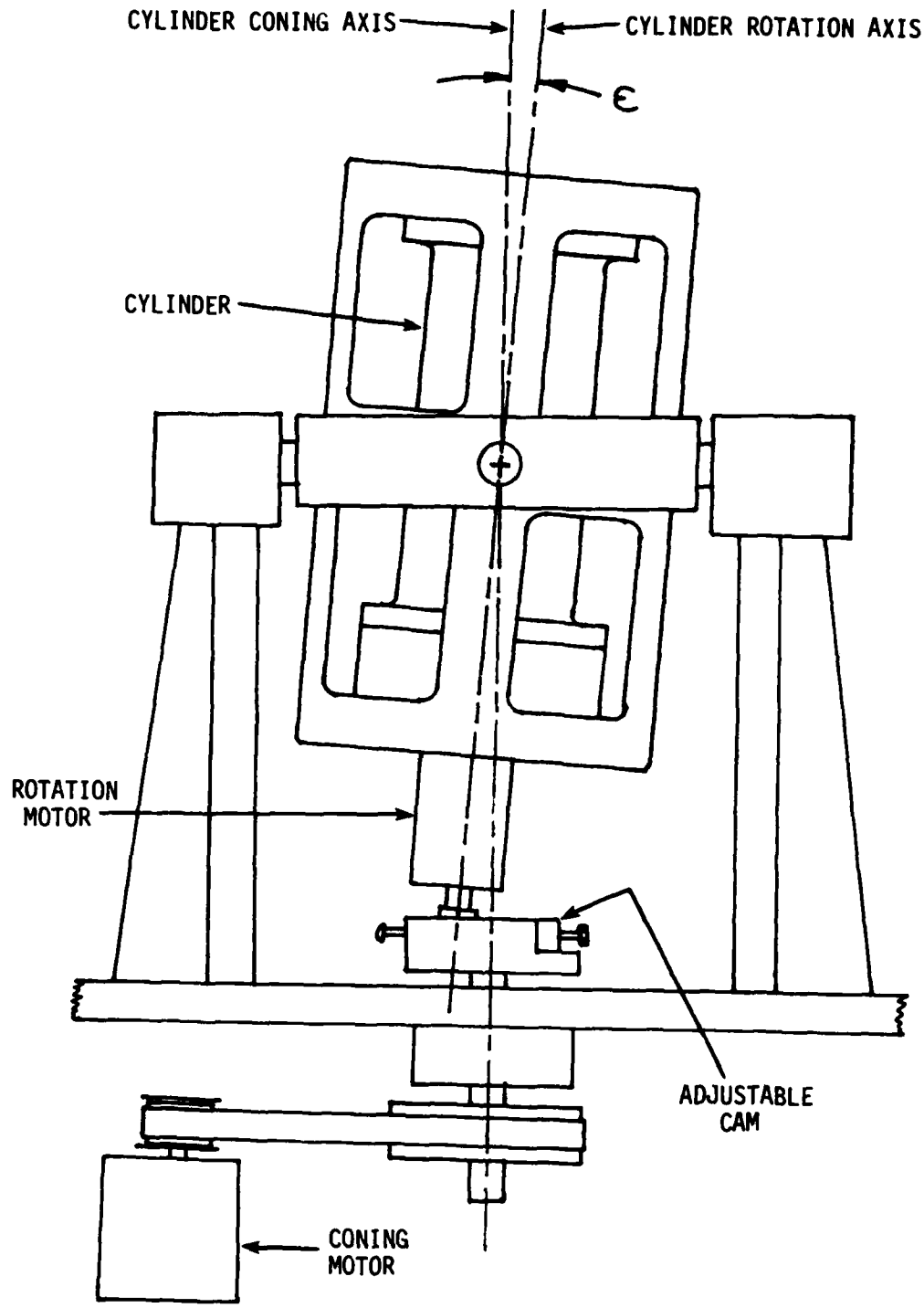

Figure 2. Gimbal Case

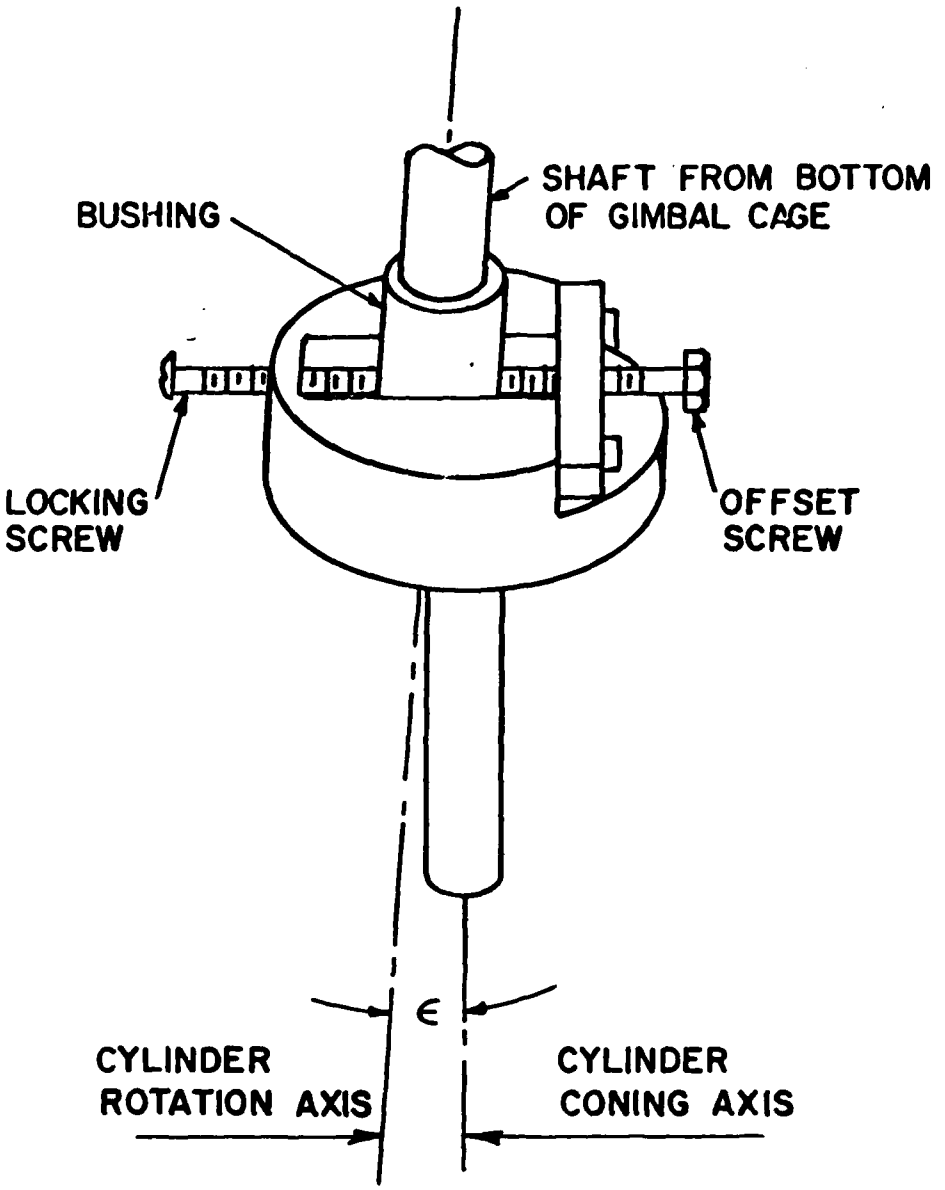

Figure 3. Adjustable Cam.

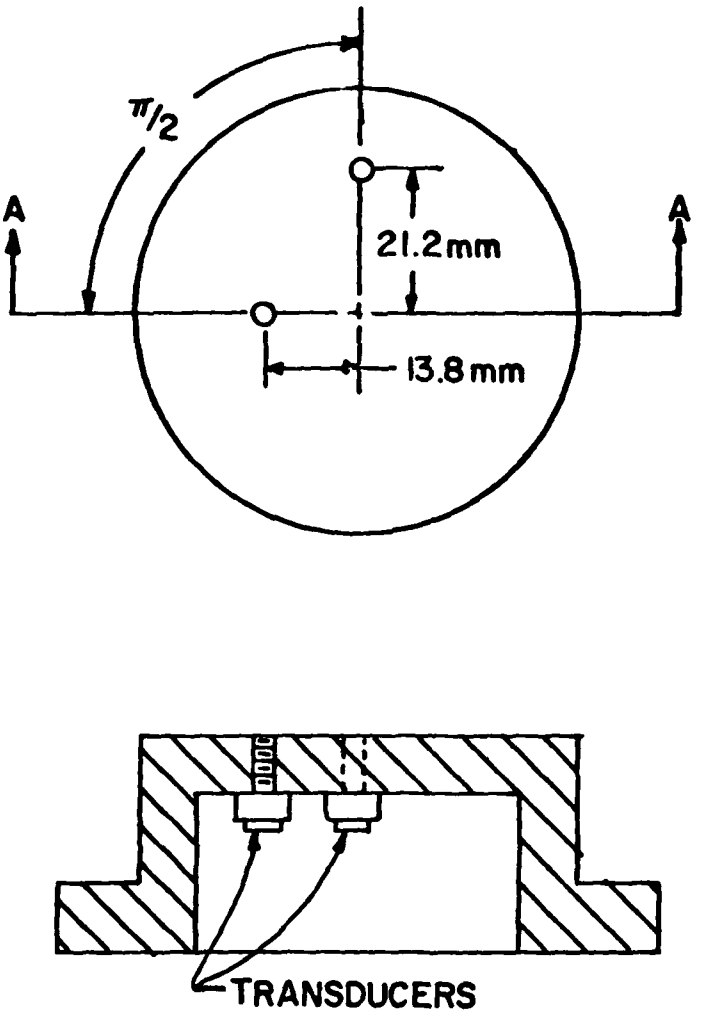

Figure 4. Placement of Pressure Transducers.

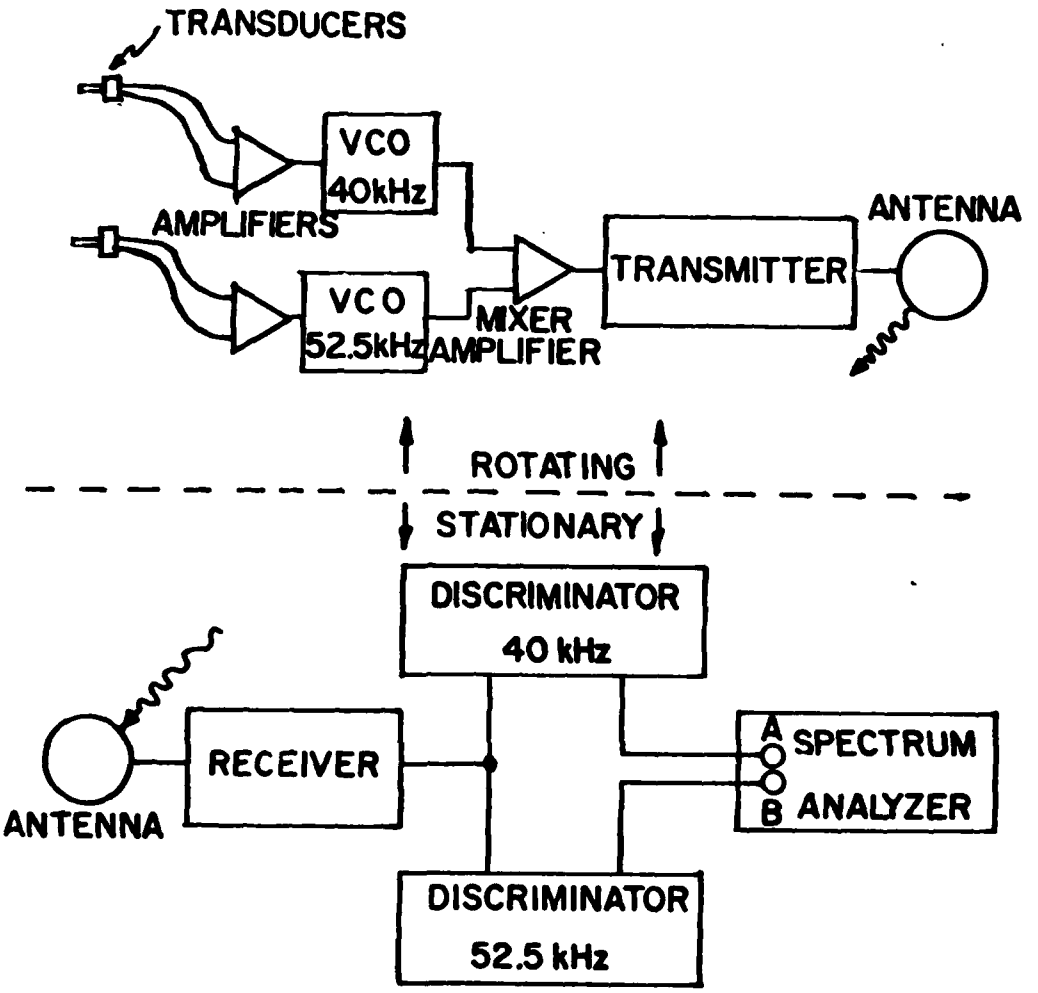

Figure 5. Telemetry Link.

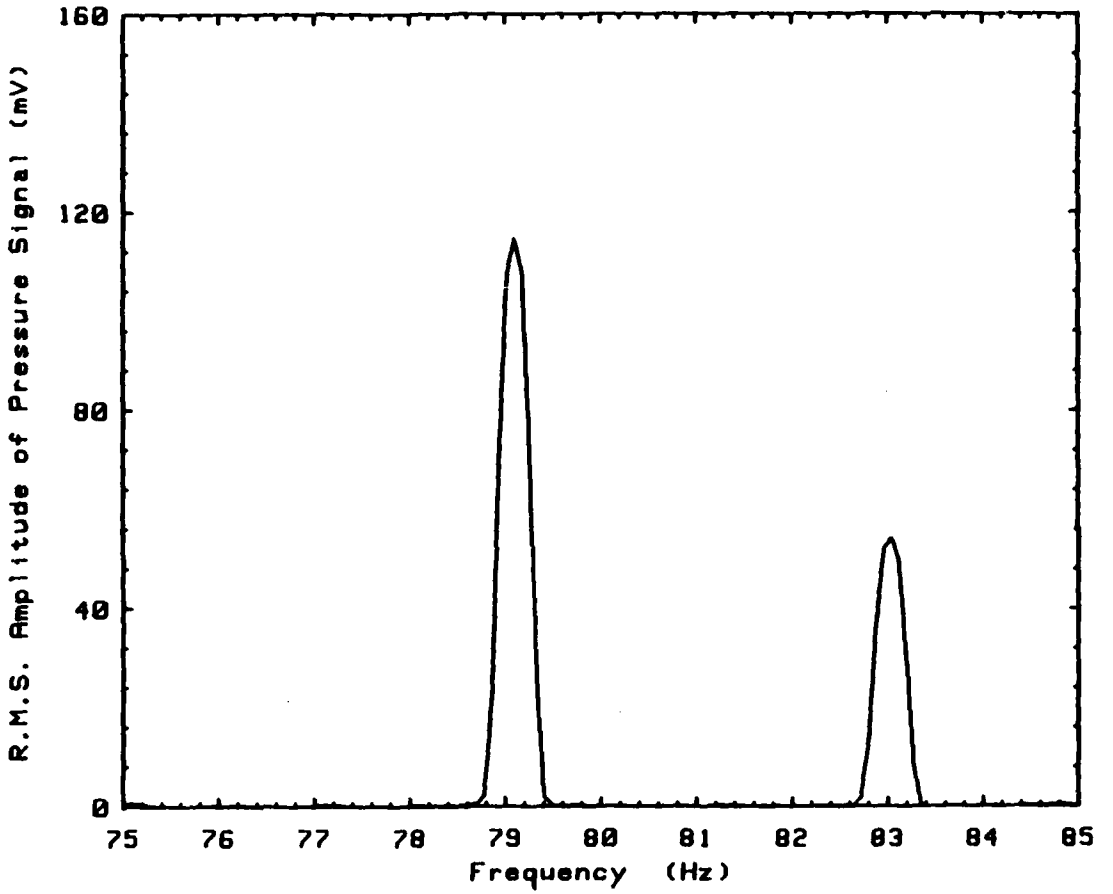

Figure 6. Typical Display of Spectrum Analyzer.

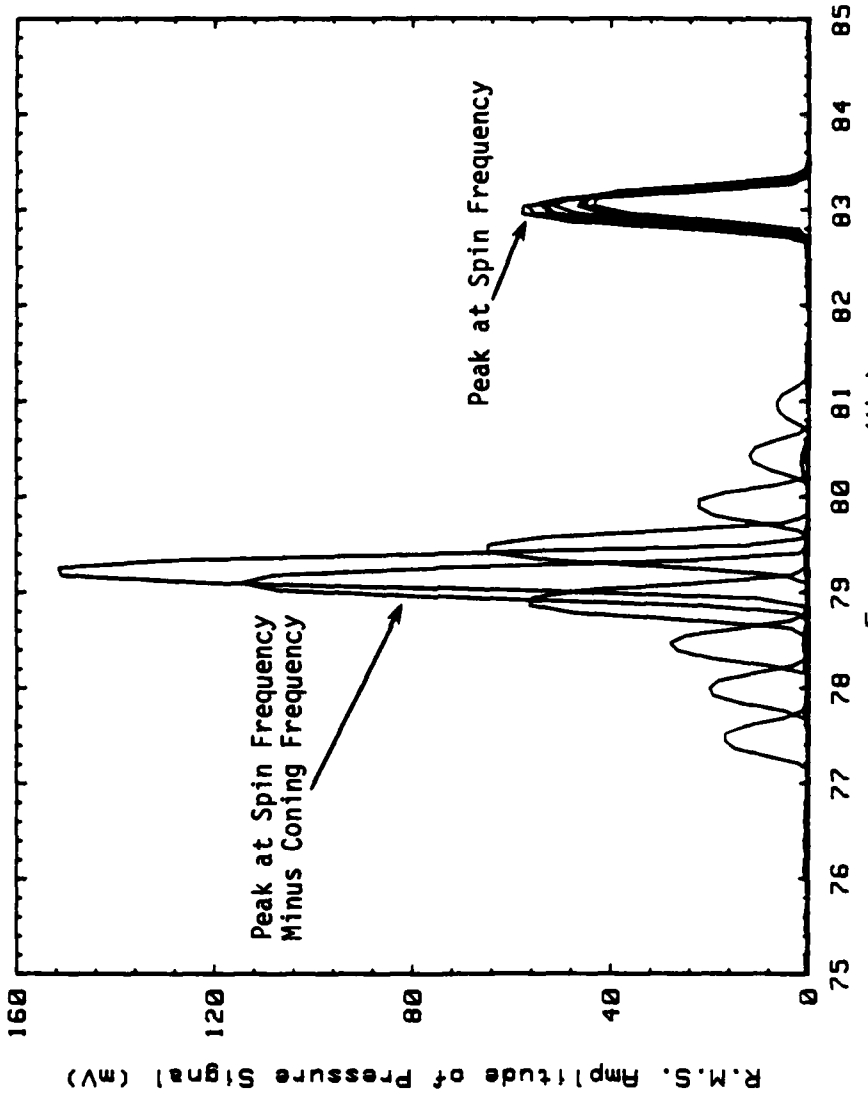

Figure 7. Overlaid Spectra Taken at Different Coning Frequencies.

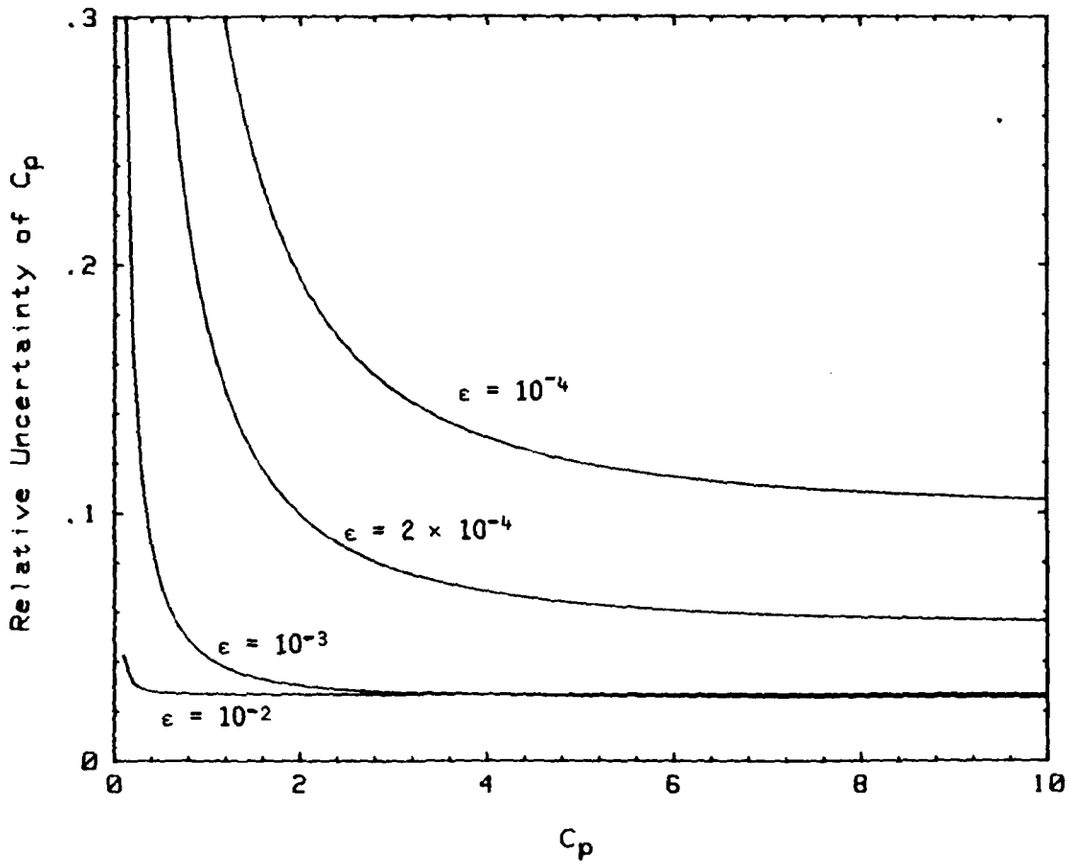

Figure 8. Estimated Uncertainty of Pressure Coefficient.

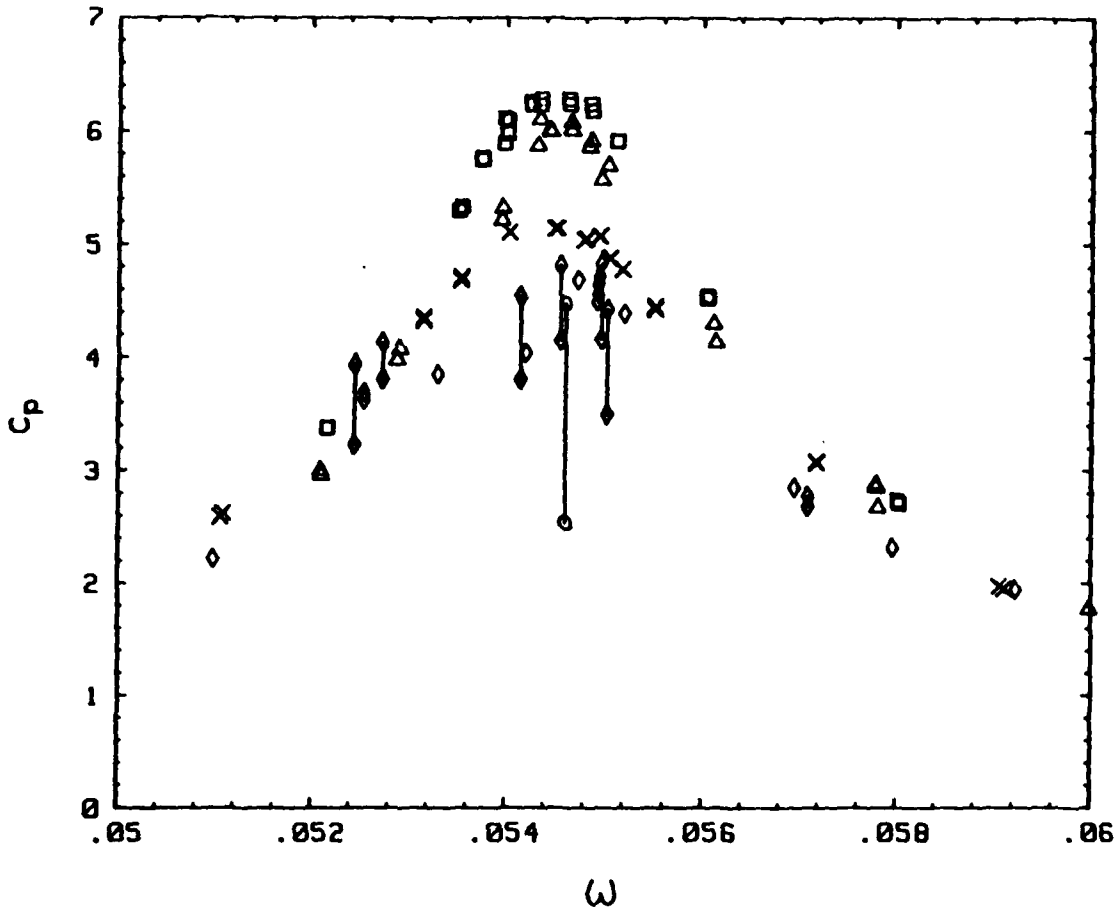

Figure 9. Variation of C_p with Coning Frequency,

c/a = 3.1481, f = 0.92, Re = 4×10^5

Δ - $\varepsilon = 1.85 \times 10^{-4}$; □ - $\varepsilon = 3.51 \times 10^{-4}$;

× - $\varepsilon = 7.78 \times 10^{-4}$; ◊ - $\varepsilon = 1.97 \times 10^{-3}$;

○ - $\varepsilon = 3.91 \times 10^{-3}$.

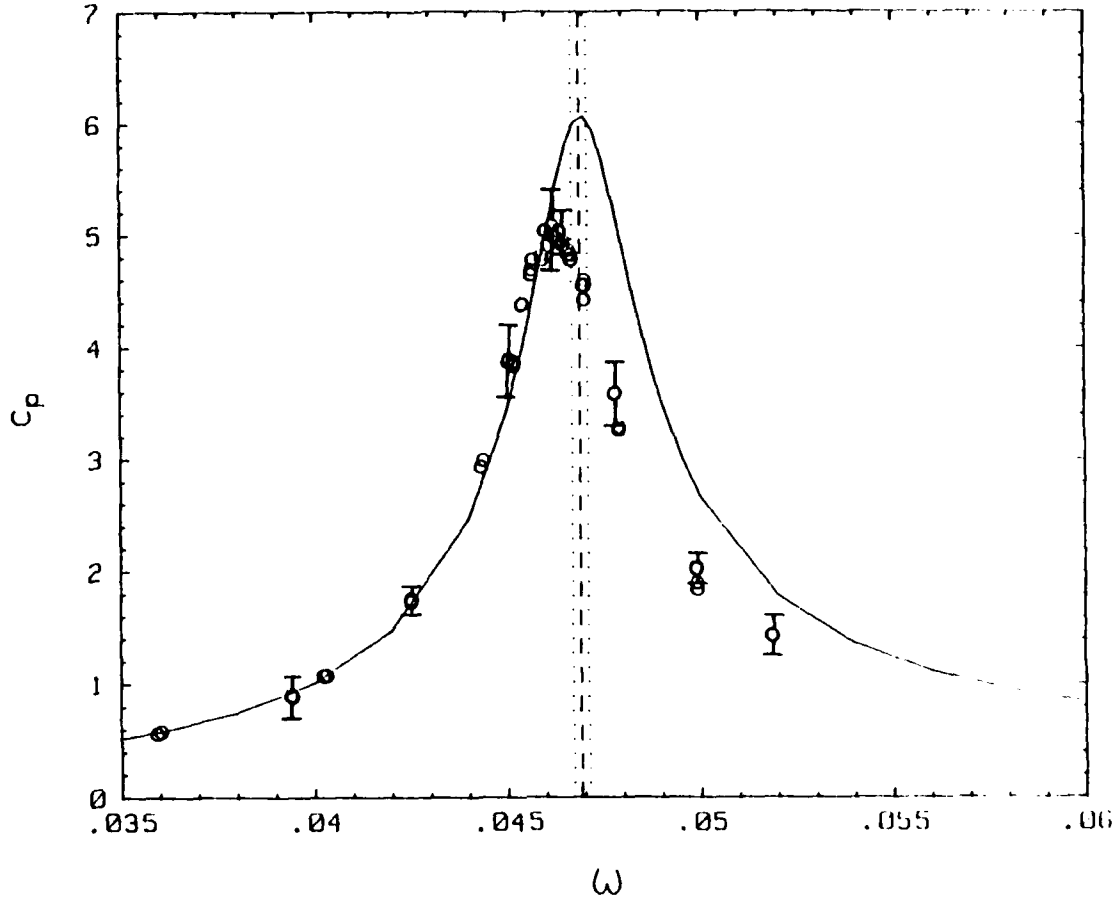

Figure 10. Variation of Pressure Coefficient with Coning Frequency in the Linear Regime. Transducer at r/a = 0.668. Dashed vertical line is eigenfrequency at nominal c/a, Ref. 5, 6, and 9; dotted vertical lines show the effect on eigenfrequency of experimental error in c/a. Solid curve is prediction of Ref. 7.

a. c/a = 3.1481, f = 1.00, Re = 5×10^5.

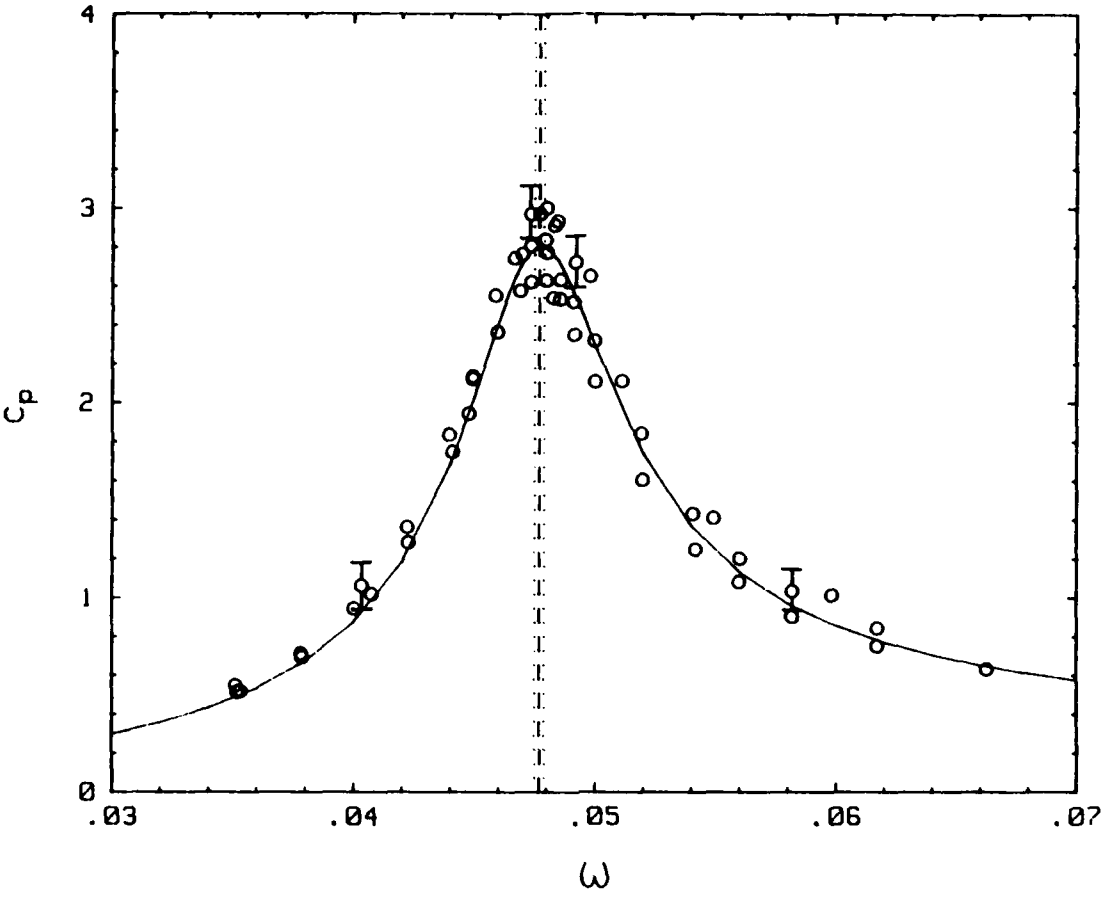

Figure 10b. c/a = 3.1481, f = 1.00, Re = 1 × 10^5.

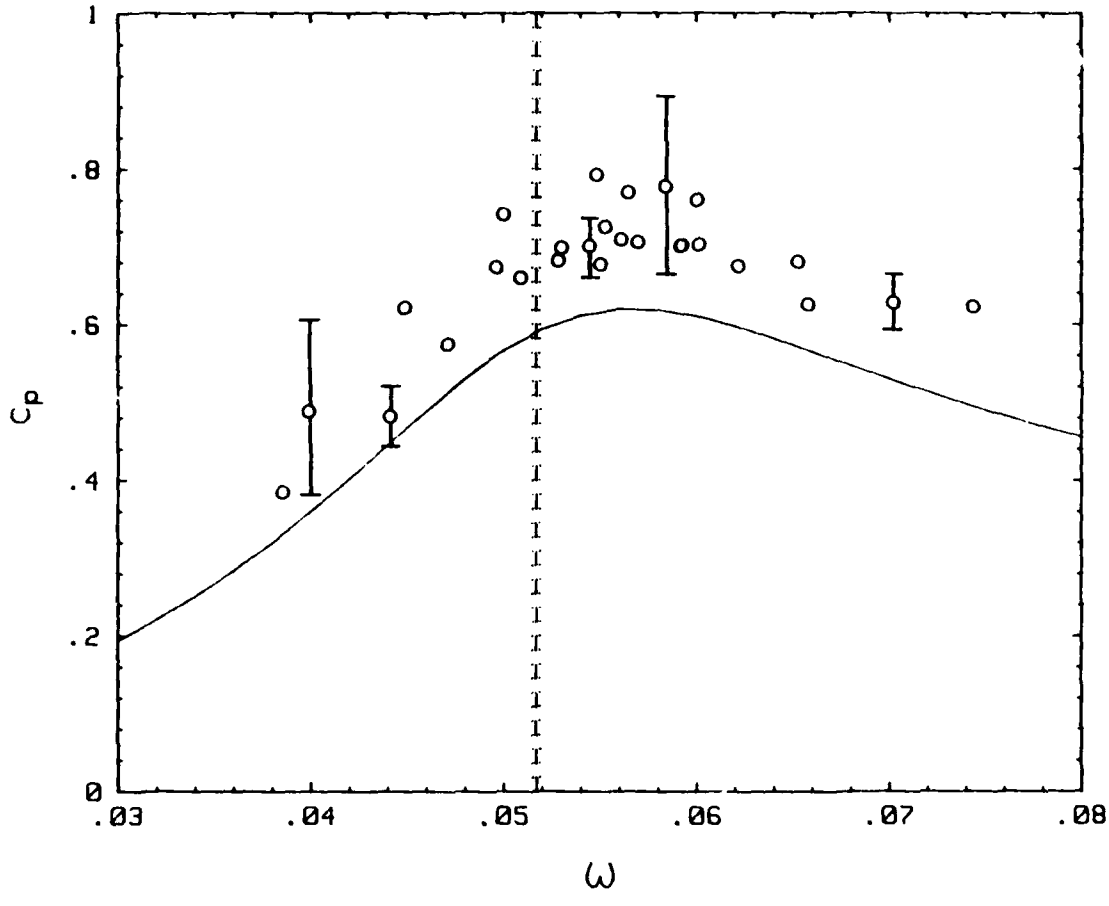

Figure 10c. c/a = 3.1481, f = 1.00, Re = 5×10^3.

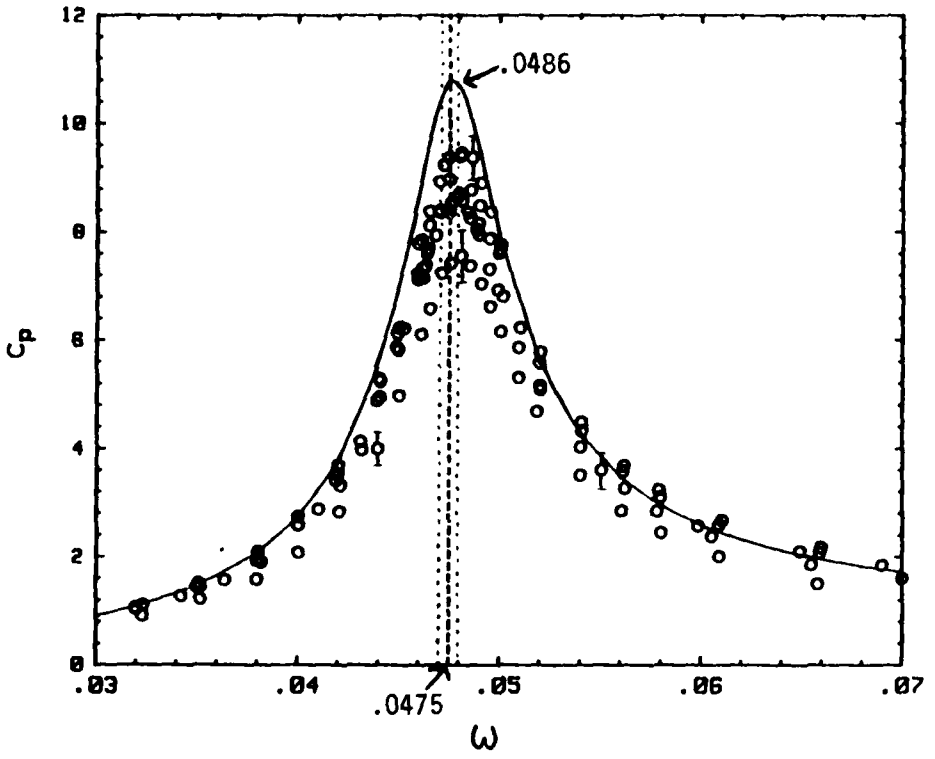

Figure 10d. c/a = 1.0509, f = 1.00, re = 5×10^5

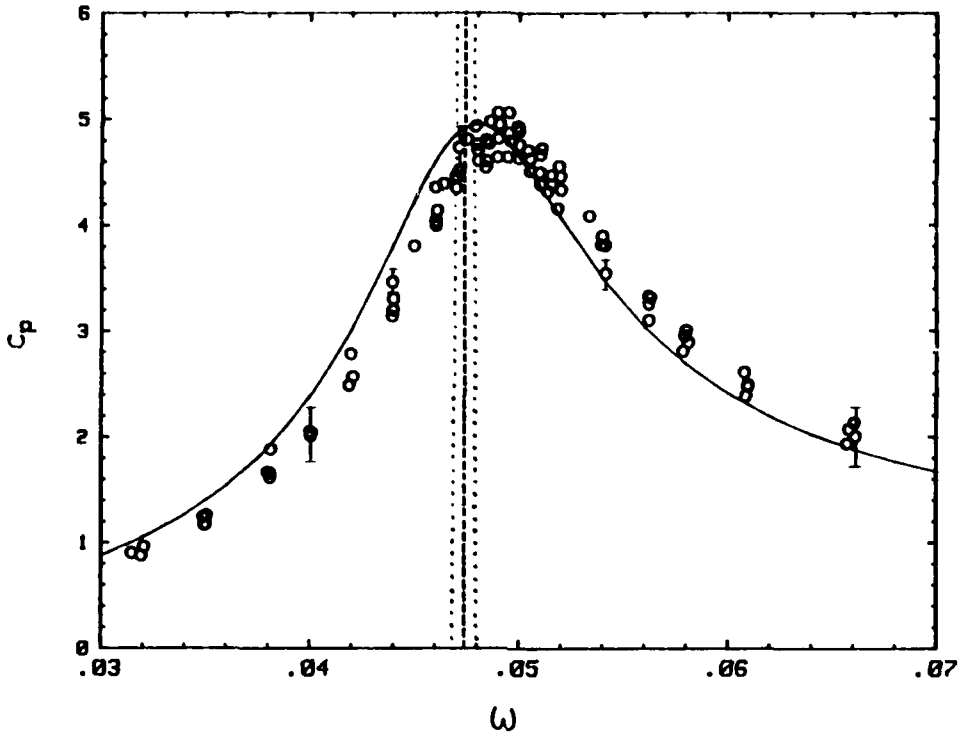

Figure 10e. c/a = 1.0509, f = 1.00, Re = 1×10^5

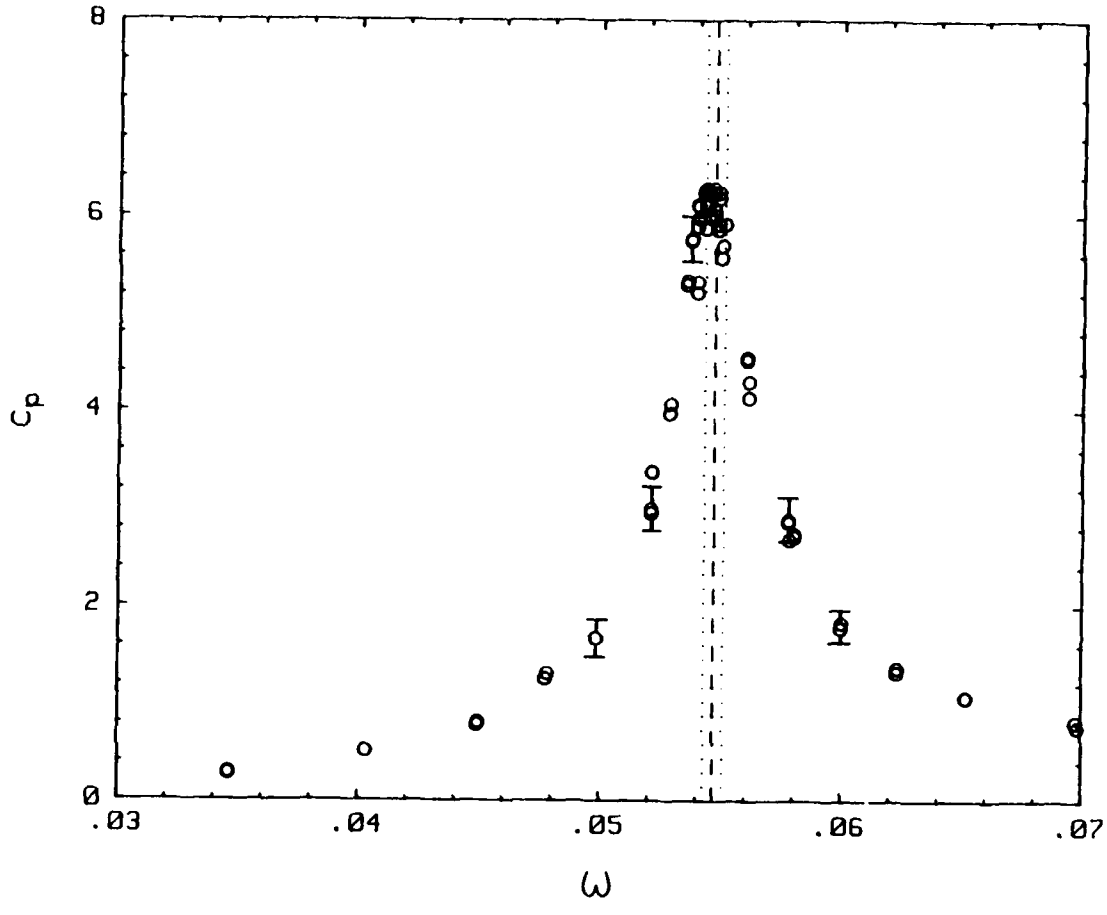

Figure 10f. c/a = 3.1481, f = 0.92, Re = 4 × 10^5.

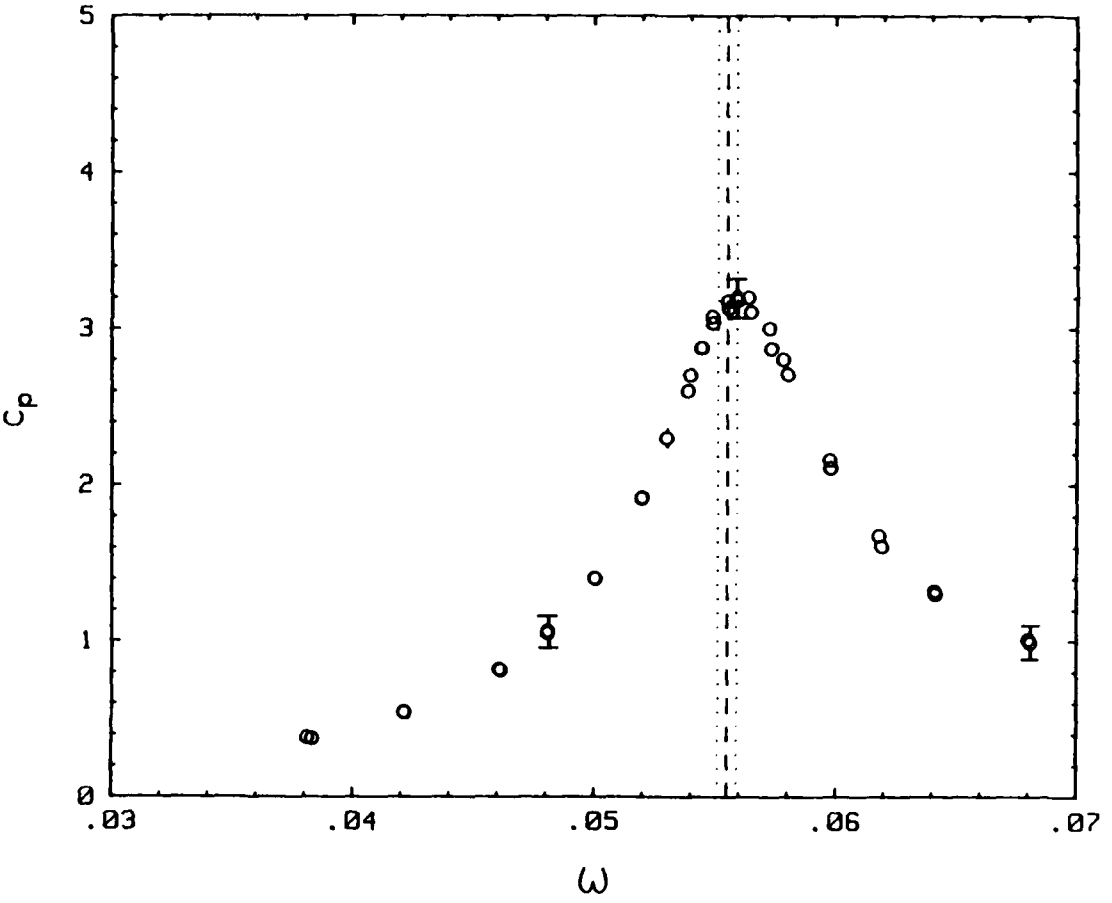

Figure 10g. c/a = 3.1481, f = 0.92, Re = 8×10^4.

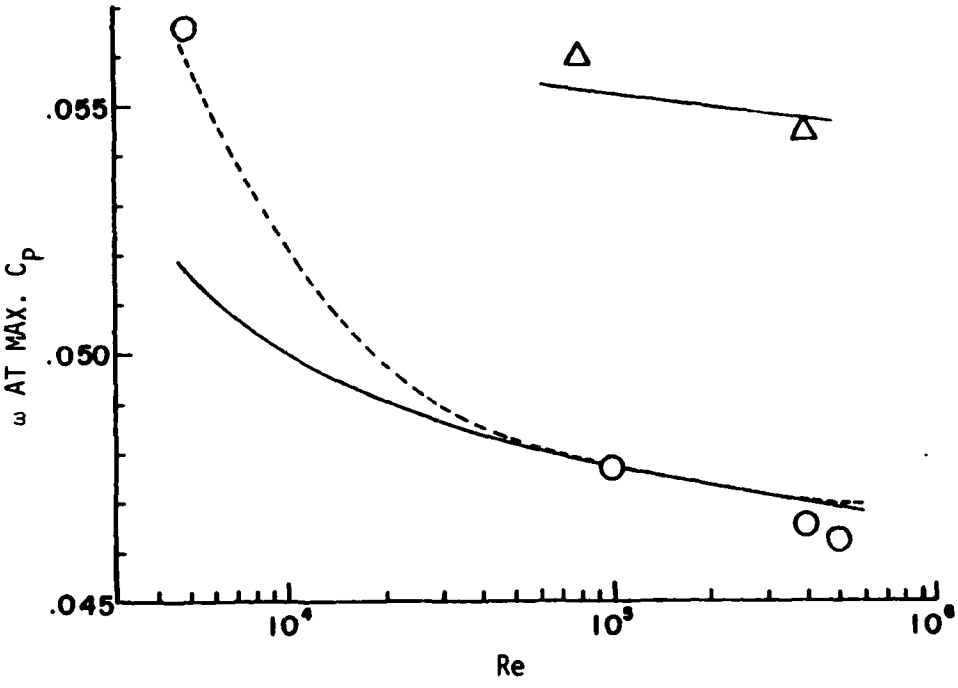

Figure 11. Variation of Frequency of Peak Response with Reynolds Number. Transducer at r/a = 0.668. Solid Lines are Stewartson-Wedemeyer eigenfrequency; dashed lines are Gerber frequency for peak response.

a. c/a = 3.1481, O - f = 1.00; Δ - f = 0.92

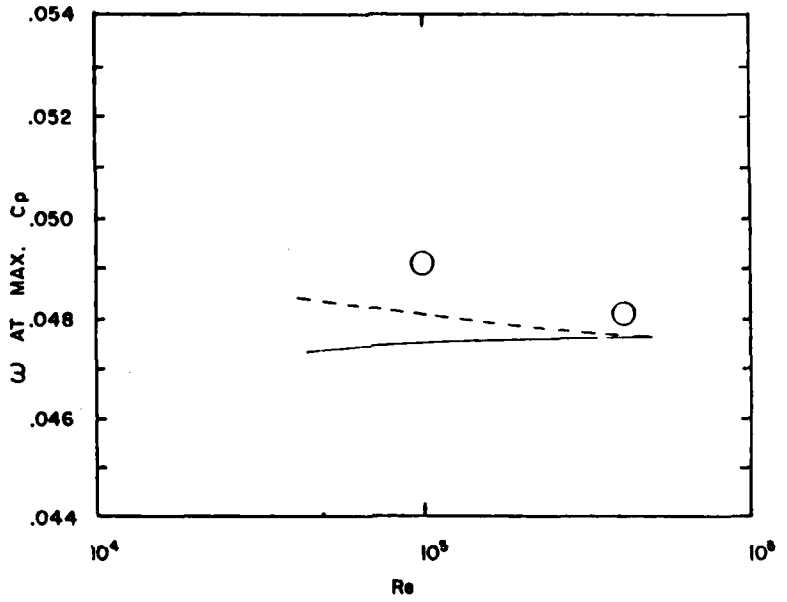

Figure 11b. c/a = 1.0509, f = 1.00

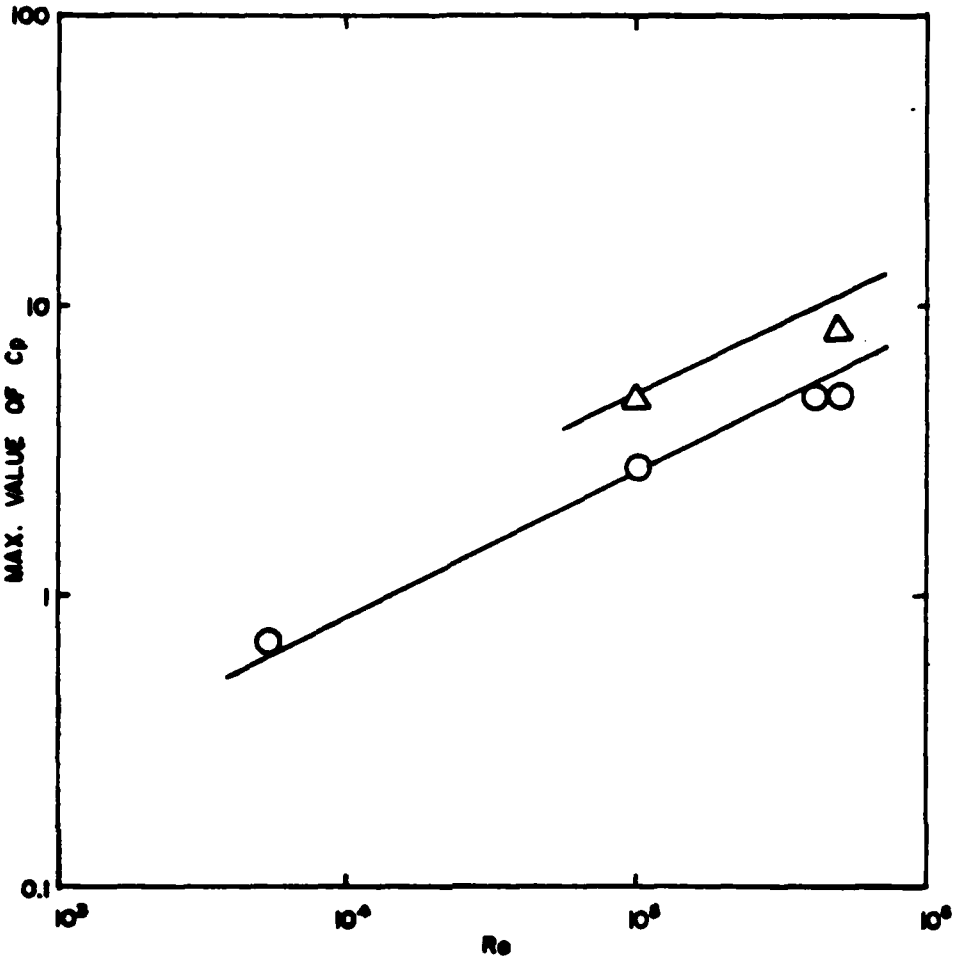

Figure 12. Variation of Amplitude of Peak Response with Reynolds Number. Transducer at 0.668. Solid lines are Gerber peak response. f = 1.00; O - c/a = 3.1481; Δ - c/a = 1.0509.

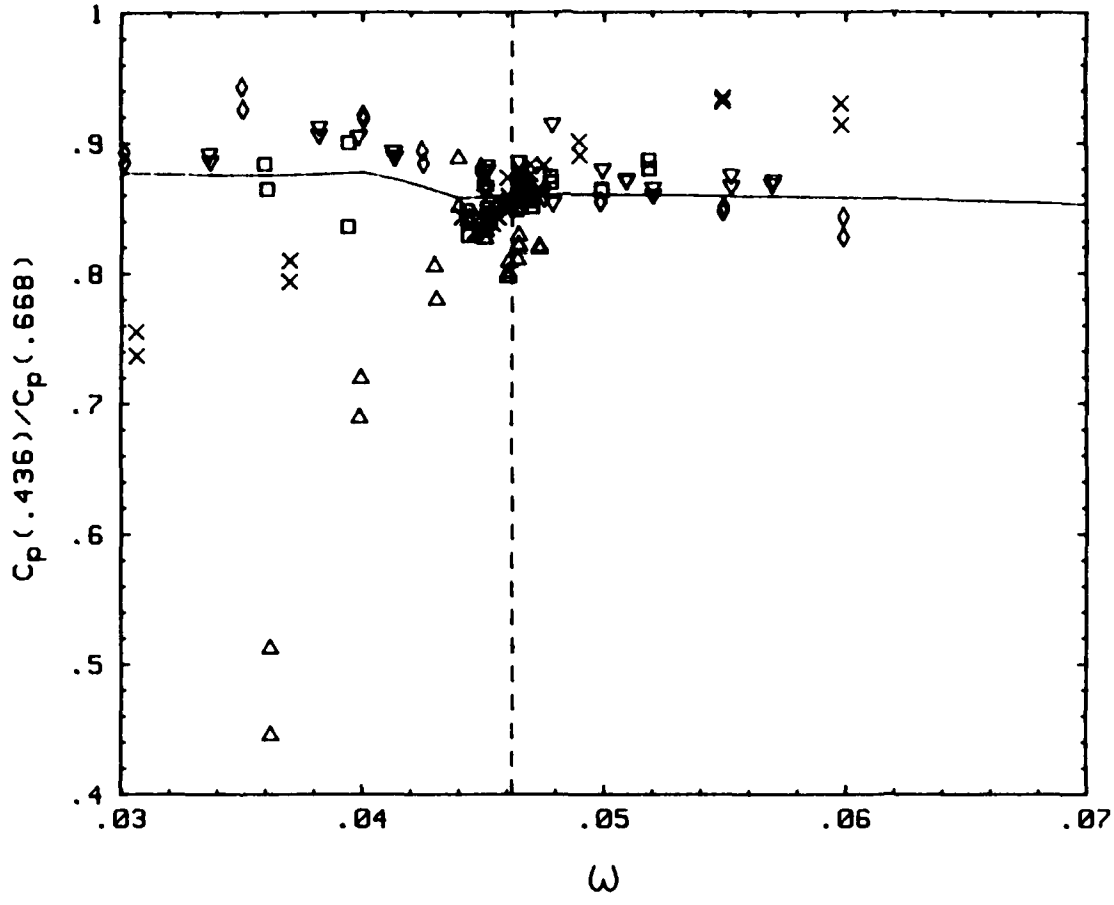

Figure 13. Ratio of Amplitude at r/a = 0.436 to Amplitude at r/a = 0.668. Solid line is Gerber theory.

a. c/a = 3.1481, f = 1.00, Re = 5×10^5

Δ - $\varepsilon = 1.66 \times 10^{-4}$; □ - $\varepsilon = 3.79 \times 10^{-4}$;

× - $\varepsilon = 5.93 \times 10^{-4}$; ◊ - $\varepsilon = 8.17 \times 10^{-4}$;

▽ - $\varepsilon = 3.84 \times 10^{-3}$.

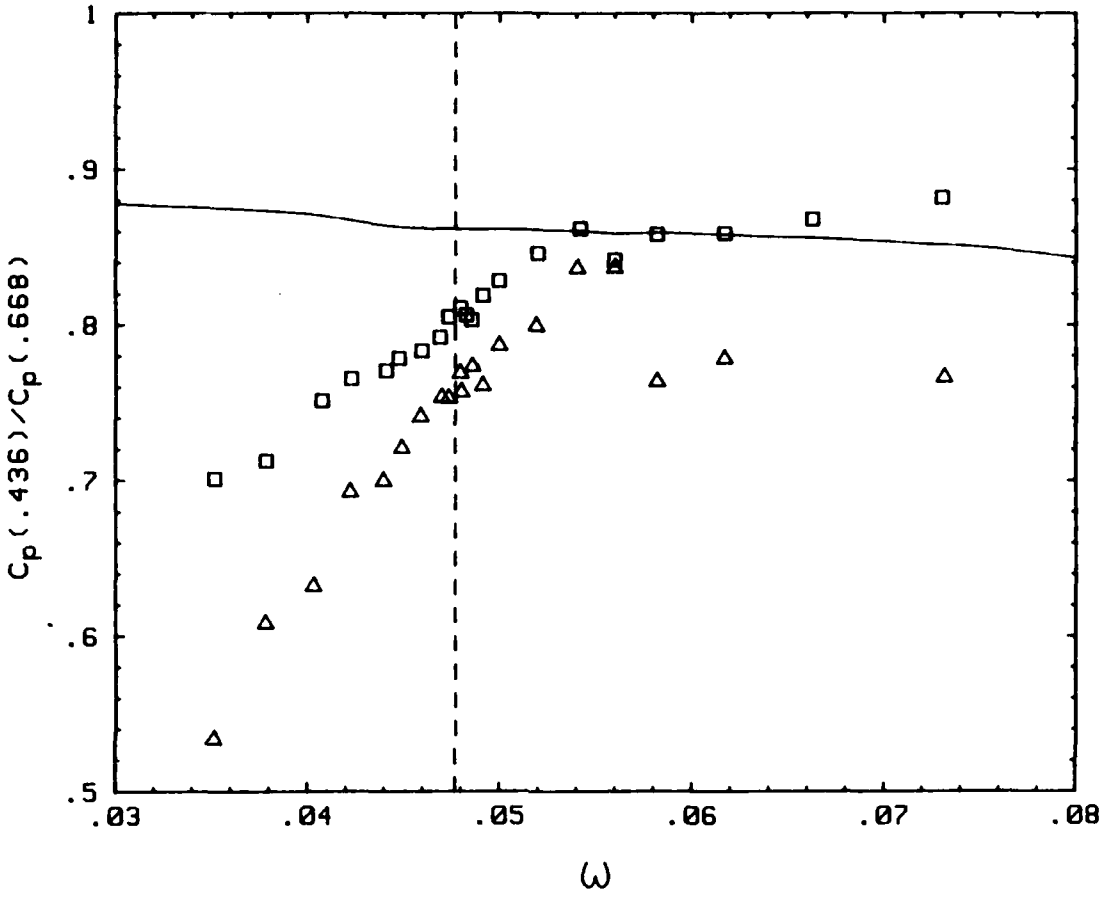

Figure 13b. c/a = 3.1481, f = 1.00, Re = 1×10^5
Δ - $\varepsilon = 1.75 \times 10^{-4}$; □ - $\varepsilon = 3.79 \times 10^{-4}$.

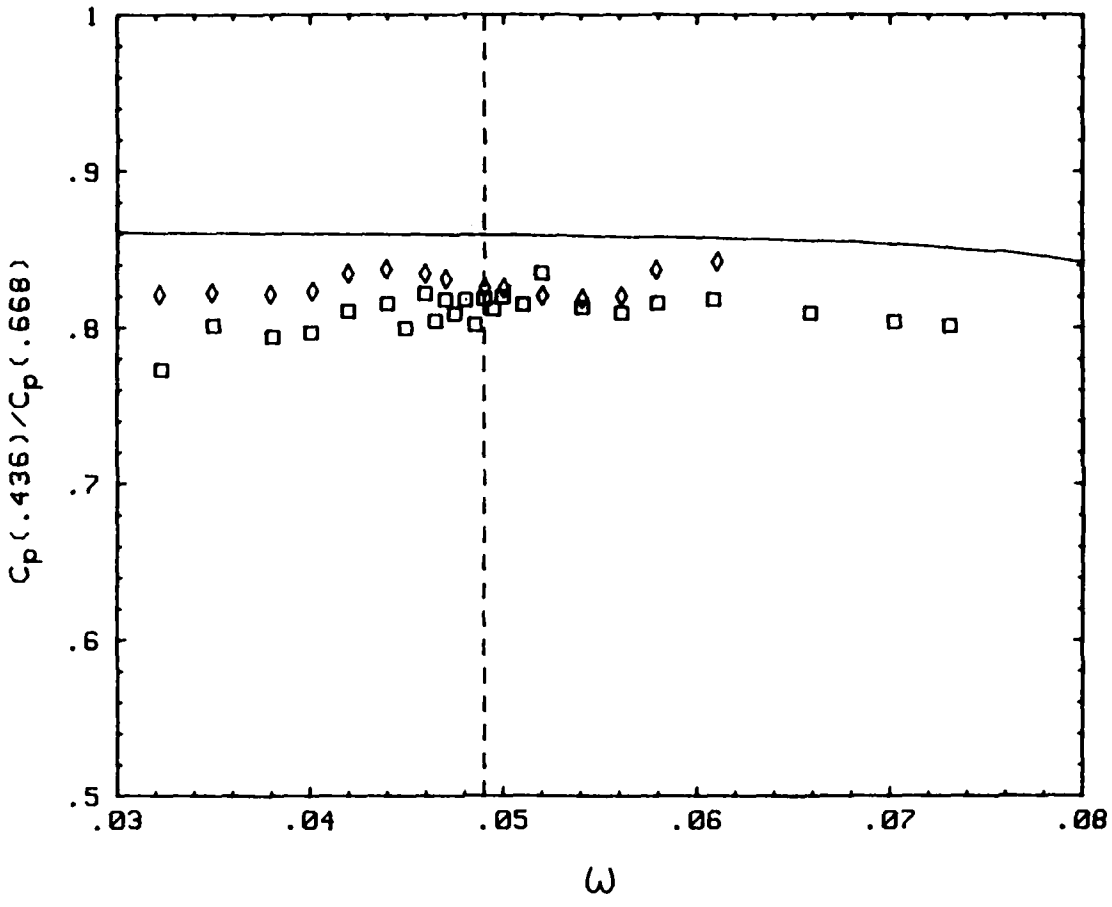

Figure 13c. c/a = 1.0509, f = 1.00, Re = 5×10^5
□ - $\varepsilon = 3.70 \times 10^{-4}$; ◊ - $\varepsilon = 7.30 \times 10^{-4}$.

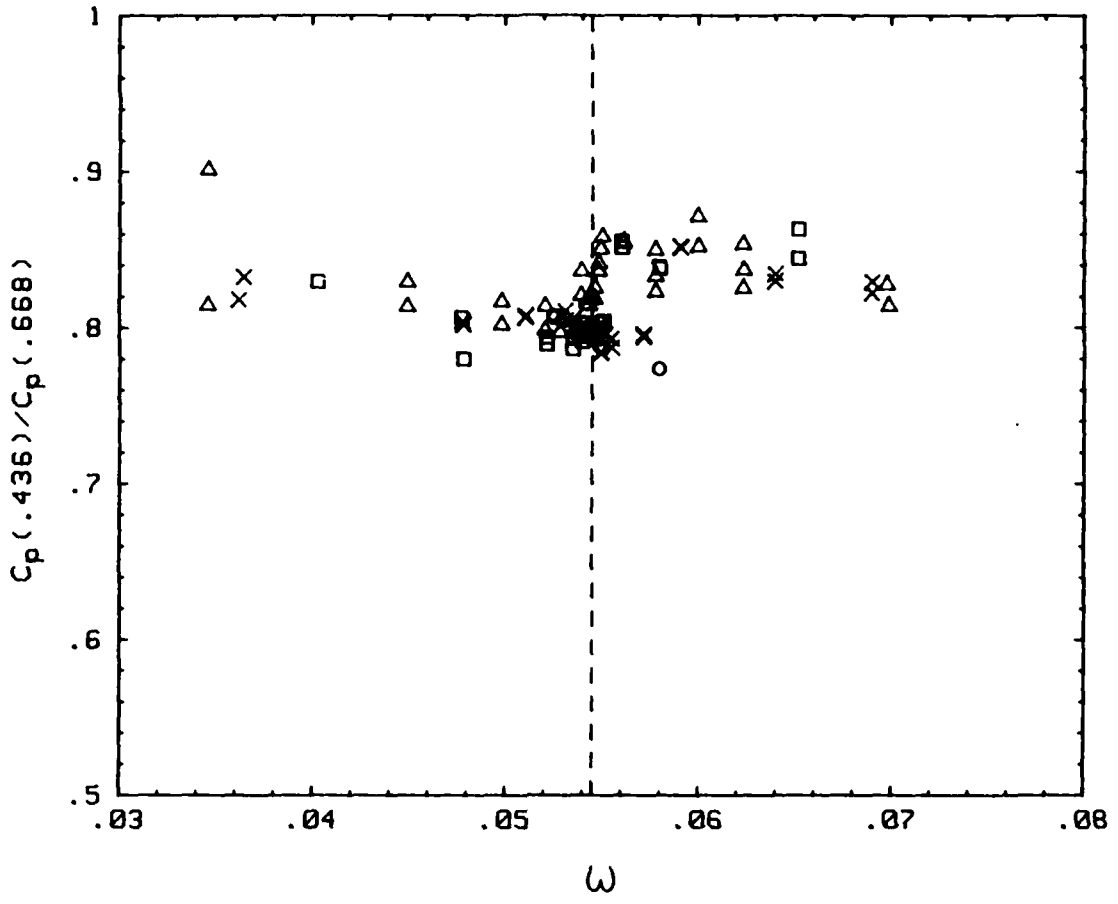

Figure 13d. c/a = 3.1481, f = 0.92, Re = 4×10^5
Δ - $\varepsilon = 1.85 \times 10^{-4}$; □ - $\varepsilon = 3.51 \times 10^{-4}$;
× - $\varepsilon = 7.78 \times 10^{-4}$; ○ - $\varepsilon = 1.97 \times 10^{-3}$.

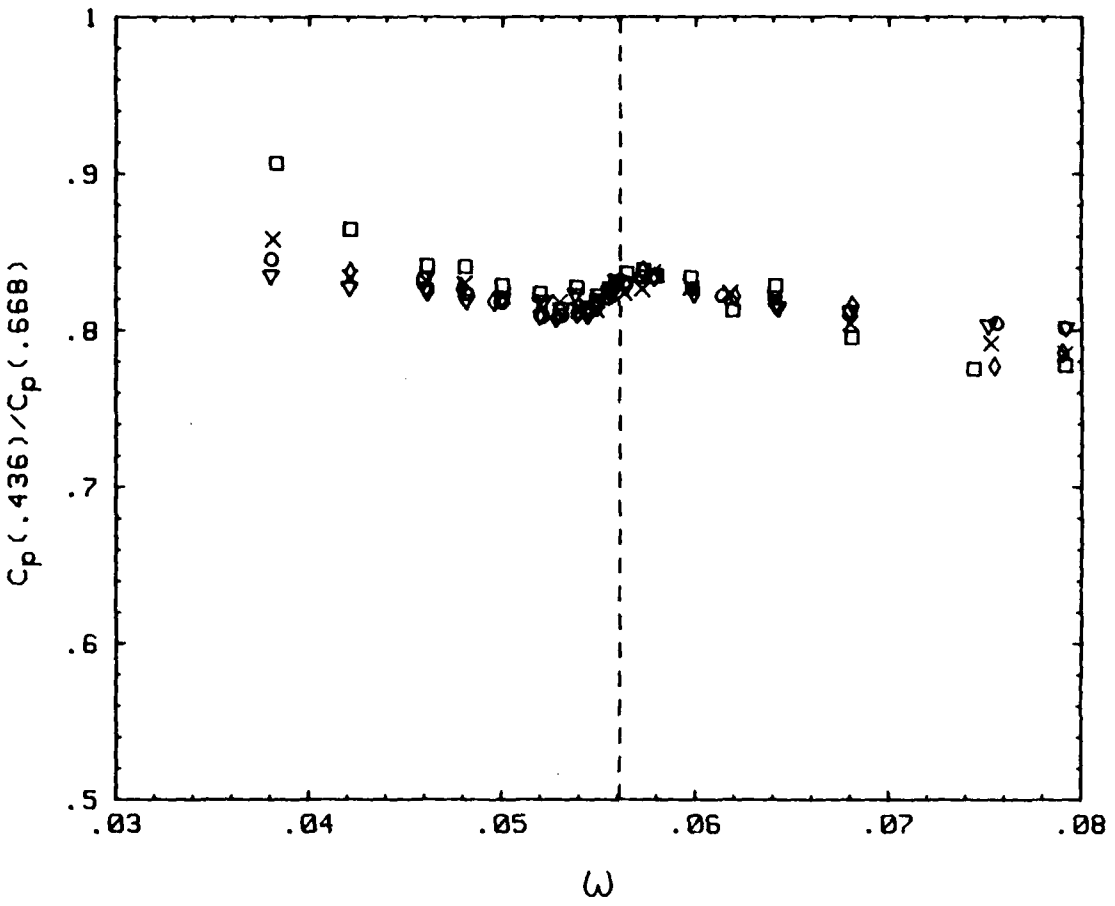

Figure 13e. c/a = 3.1481, f = 0.92, Re = 8×10^4
□ - $\varepsilon = 3.79 \times 10^{-4}$; × - $\varepsilon = 8.95 \times 10^{-4}$;
◇ - $\varepsilon = 1.85 \times 10^{-3}$; ○ - $\varepsilon = 3.78 \times 10^{-3}$;
▽ - $\varepsilon = 8.70 \times 10^{-3}$.

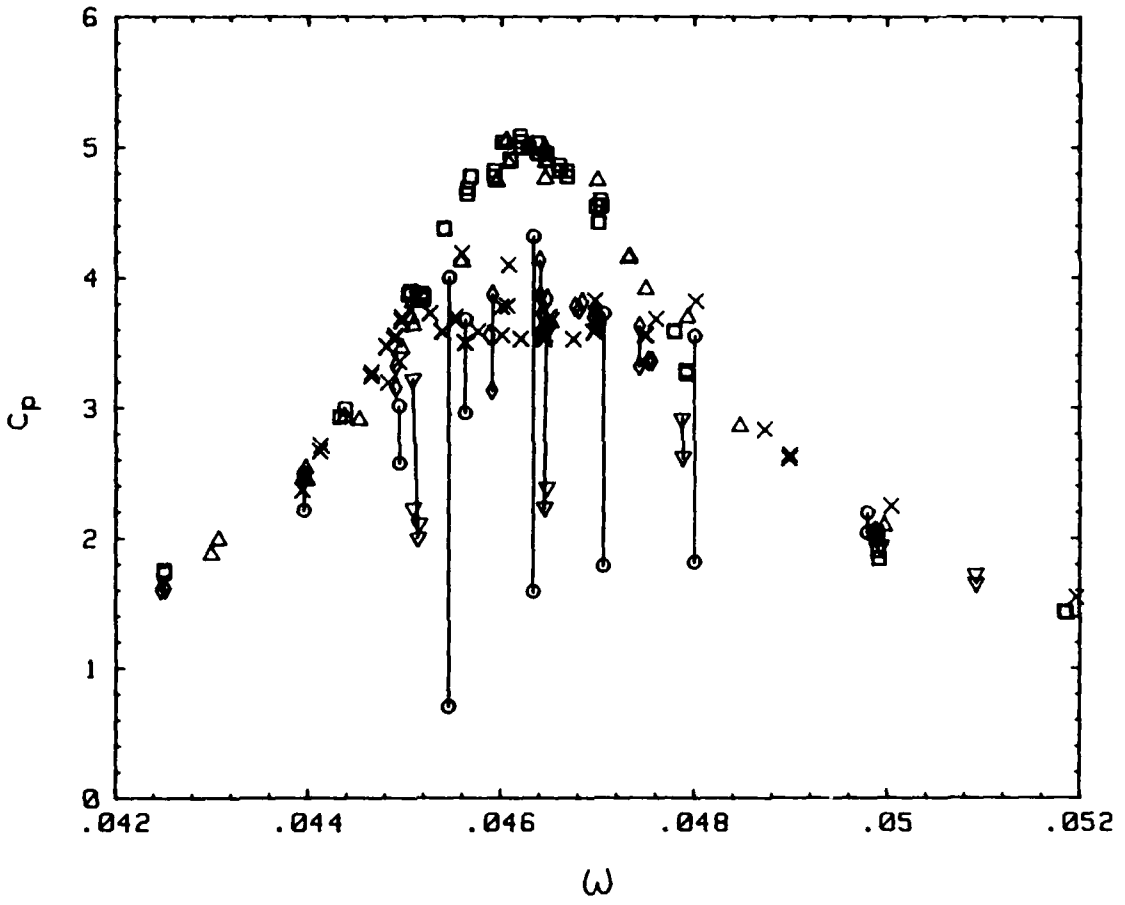

Figure 14. Variation of Pressure Coefficient with Coning Frequency in the Linear/Nonlinear/Nonstationary Regimes Transducer at r/a = 0.668. Symbols connected by vertical lines represent nonstationary behavior.

a. c/a = 3.1481, f = 1.00, Re = 5×10^5

Δ - $\varepsilon = 2 \times 10^{-4}$; □ - $\varepsilon = 3.79 \times 10^{-4}$;

X - $\varepsilon = 6 \times 10^{-4}$; ◊ - $\varepsilon = 8.17 \times 10^{-4}$;

○ - $\varepsilon = 1.85 \times 10^{-3}$; ∇ - $\varepsilon = 3.84 \times 10^{-3}$.

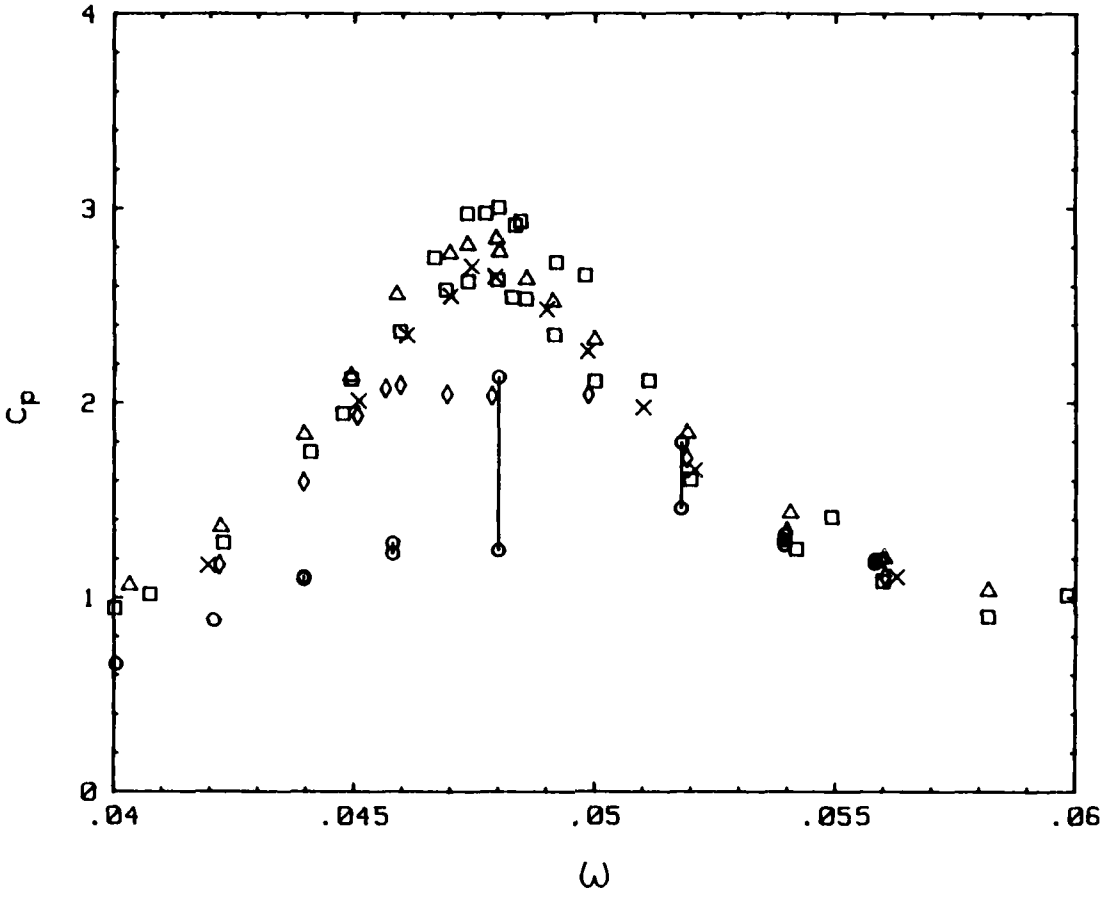

Figure 14b. c/a = 3.1481, f = 1.00, Re = 1×10^5
Δ - $\varepsilon = 1.75 \times 10^{-4}$; □ - $\varepsilon = 4 \times 10^{-4}$;
X - $\varepsilon = 9.23 \times 10^{-4}$; ◊ - $\varepsilon = 3.68 \times 10^{-3}$;
○ - $\varepsilon = 8.70 \times 10^{-3}$.

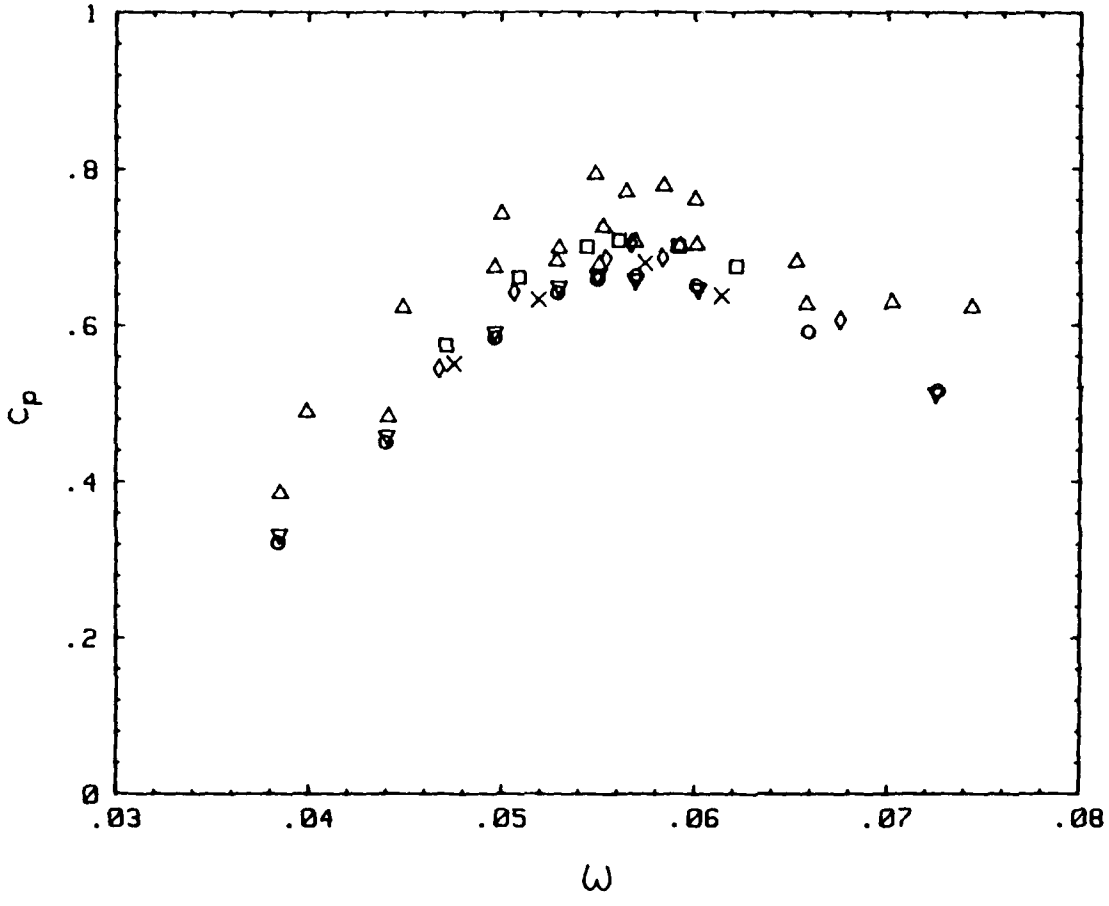

Figure 14c. c/a = 3.1481, f = 1.00, Re = 5×10^3
Δ - $\varepsilon = 4 \times 10^{-4}$; □ - $\varepsilon = 1.90 \times 10^{-3}$;
× - $\varepsilon = 3.75 \times 10^{-3}$; ◊ - $\varepsilon = 6.93 \times 10^{-3}$;
○ - $\varepsilon = 1.74 \times 10^{-2}$; ▽ - $\varepsilon = 3.48 \times 10^{-2}$.

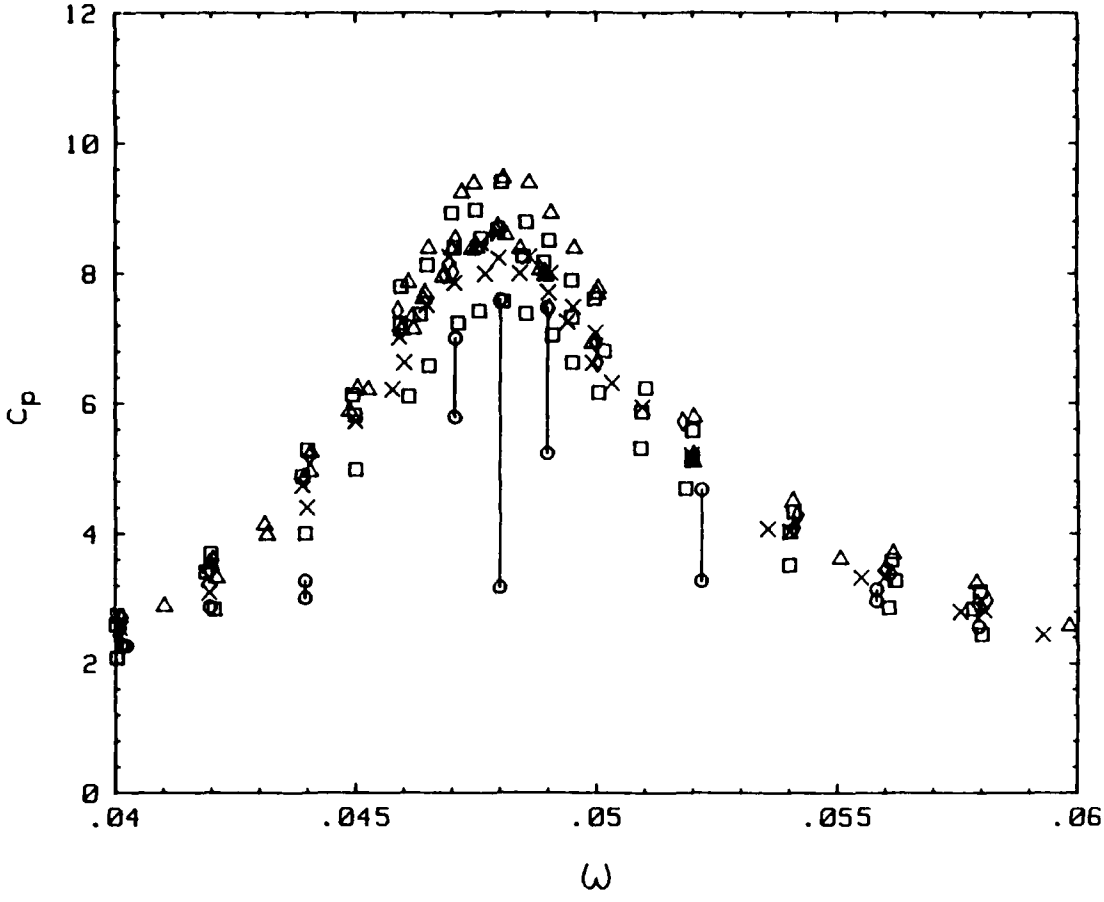

Figure 14d. c/a = 1.0509, f = 1.00, Re = 5×10^5
Δ - $\varepsilon = 2 \times 10^{-4}$; □ - $\varepsilon = 3.70 \times 10^{-4}$;
× - $\varepsilon = 5.64 \times 10^{-4}$; ◊ - $\varepsilon = 7 \times 10^{-4}$;
○ - $\varepsilon = 1.86 \times 10^{-4}$.

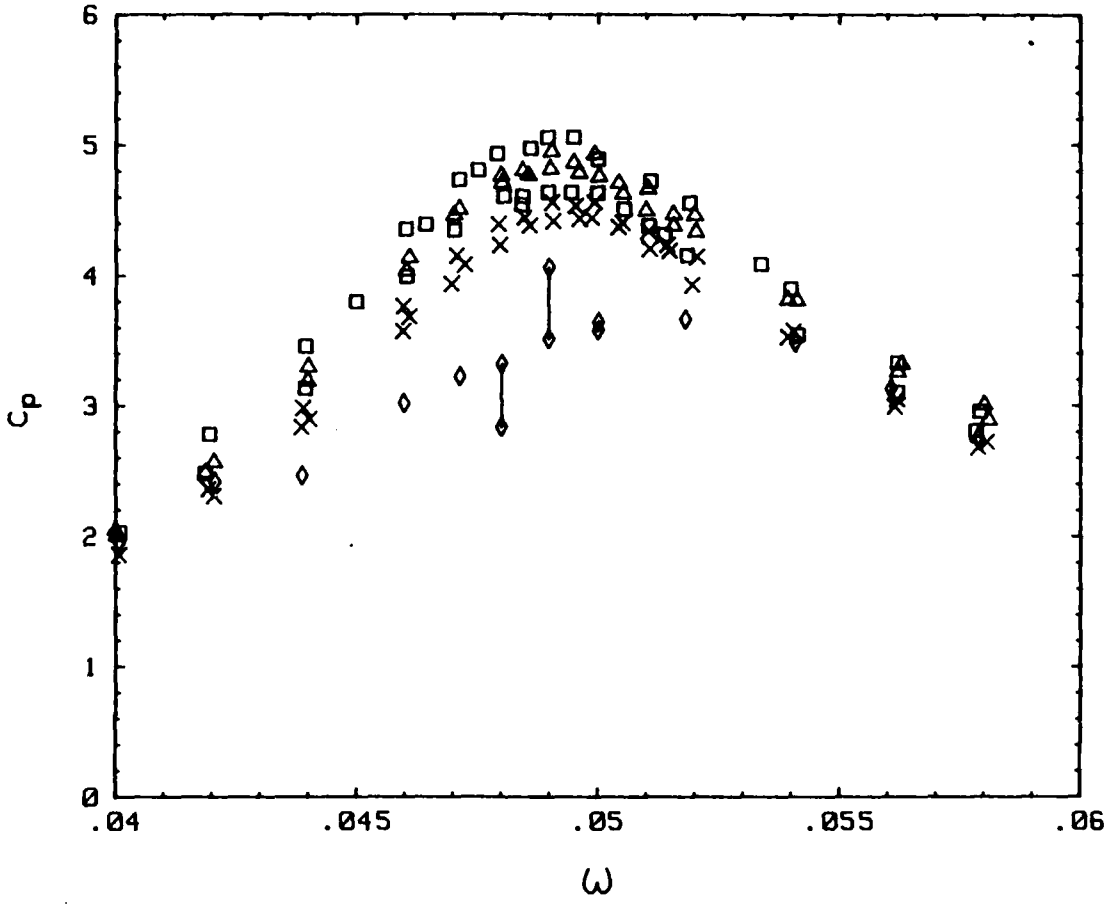

Figure 14e. c/a = 1.0509, f = 1.00, Re = 1×10^5
Δ - $\varepsilon = 1.66 \times 10^{-4}$; □ - $\varepsilon = 3.70 \times 10^{-4}$;
× - $\varepsilon = 9 \times 10^{-4}$; ◊ - $\varepsilon = 3.70 \times 10^{-4}$.

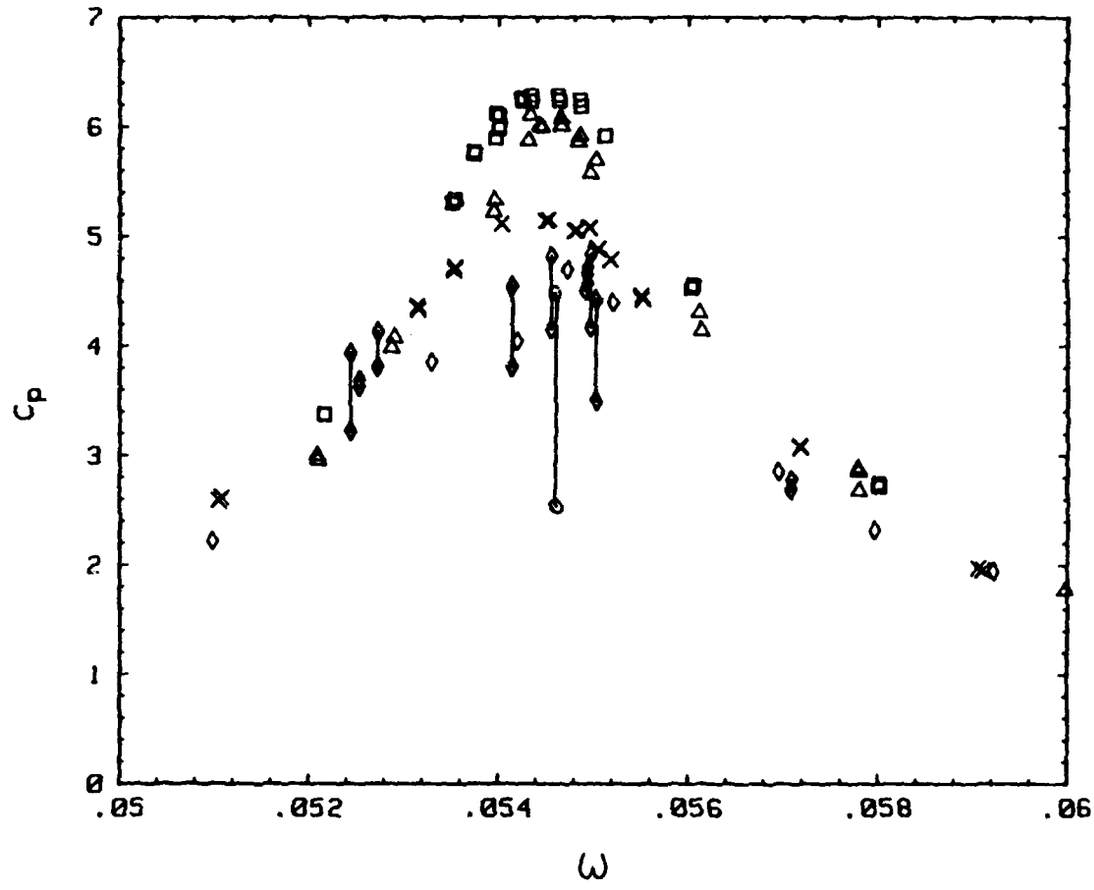

Figure 14f. c/a = 3.1481, f = 0.92, Re = 4×10^5
Δ - $\varepsilon = 1.85 \times 10^{-4}$; $\square$ - $\varepsilon = 3.51 \times 10^{-4}$;
X - $\varepsilon = 7.78 \times 10^{-4}$; $\Diamond$ - $\varepsilon = 1.97 \times 10^{-3}$;
O - $\varepsilon = 3.91 \times 10^{-3}$.

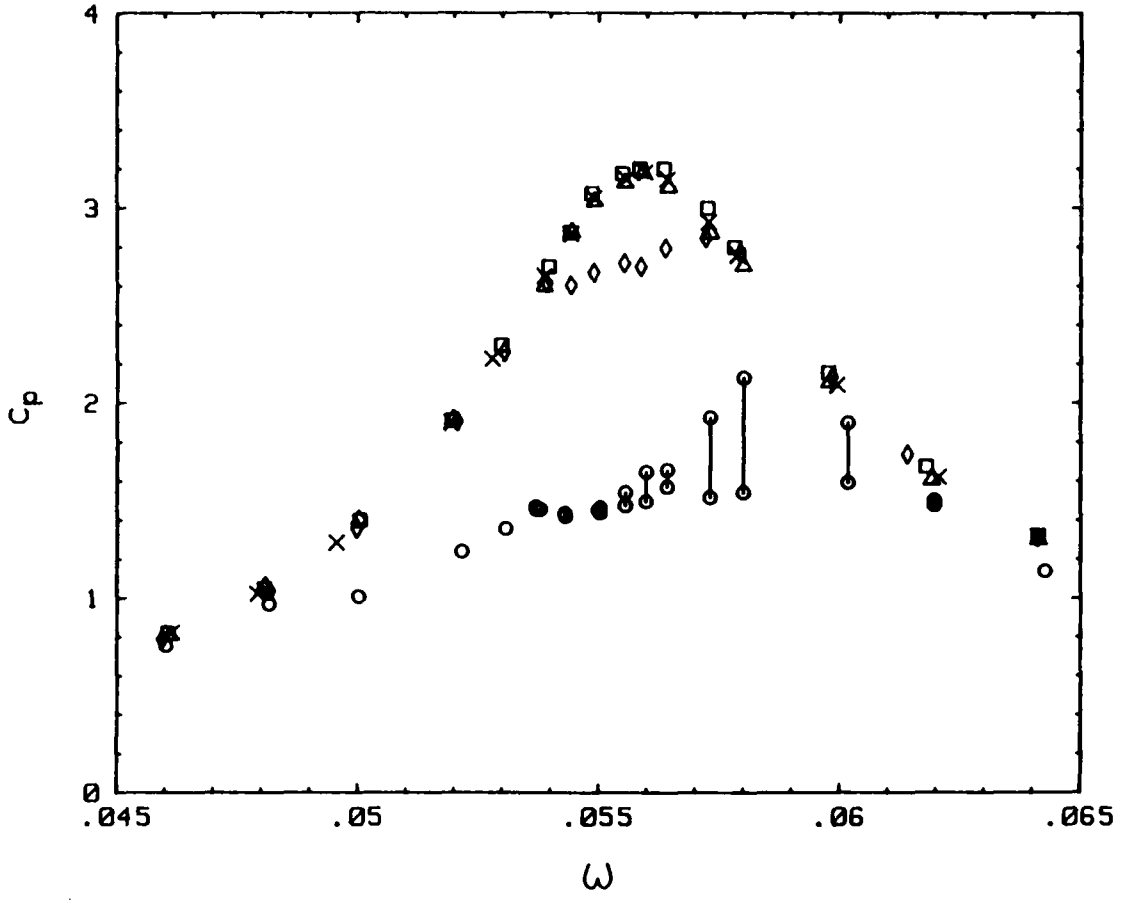

Figure 14g. c/a = 3.1481, f = 0.92, Re = 8×10^4
Δ - $\varepsilon = 3.79 \times 10^{-4}$; □ - $\varepsilon = 8.95 \times 10^{-4}$;
× - $\varepsilon = 1.85 \times 10^{-3}$; ◊ - $\varepsilon = 3.78 \times 10^{-3}$;
○ - $\varepsilon = 8.70 \times 10^{-3}$.

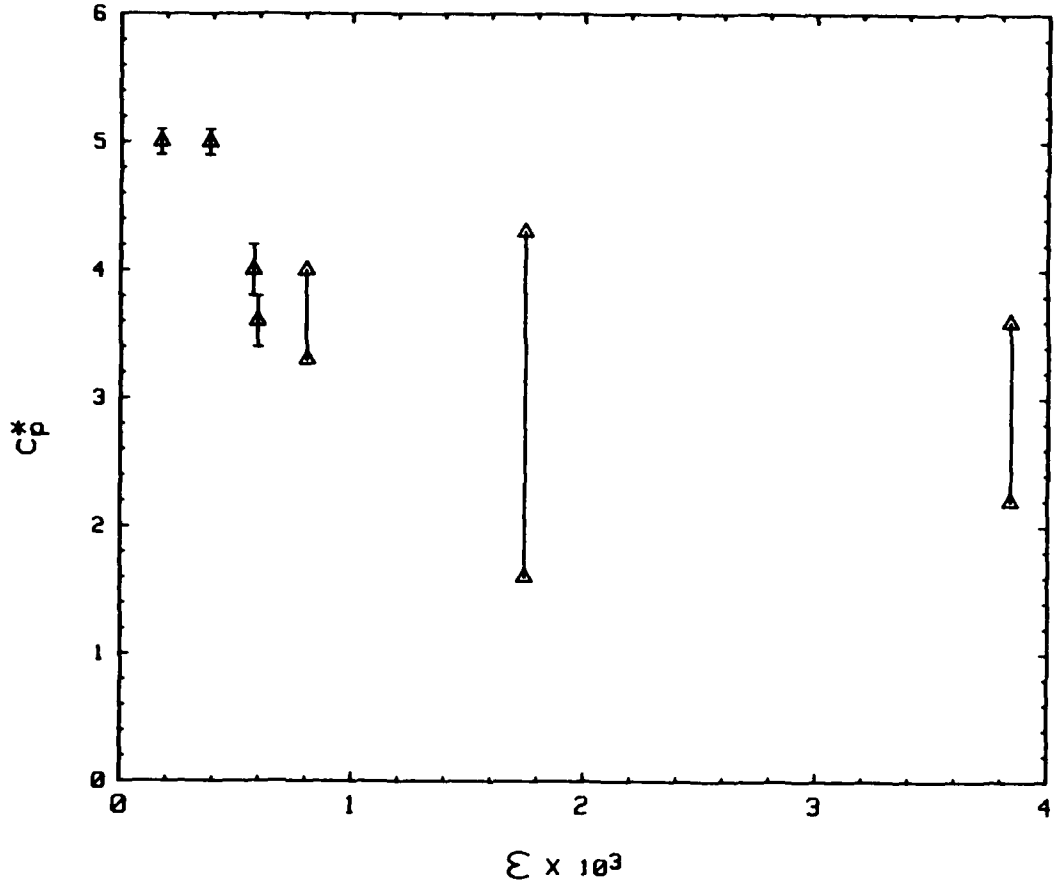

Figure 15. Dependence of Peak Amplitude on Coning Angle. Symbols Connected by Vertical Arrows Represent Nonstationary Behavior. Error bars indicate uncertainty.

a. $c/a = 3.1481$, $f = 1.00$, $Re = 5 \times 10^5$.

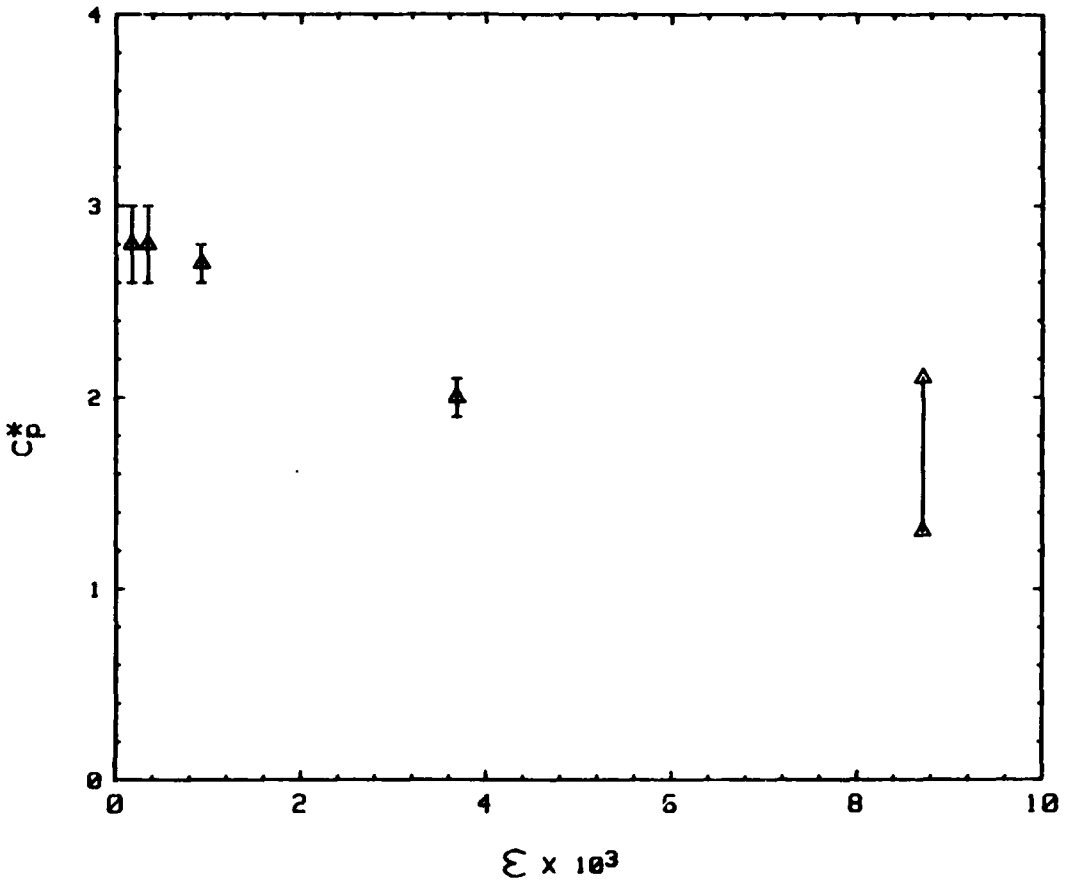

Figure 15b. c/a = 3.1481, f = 1.00, Re = 1 × 10^5.

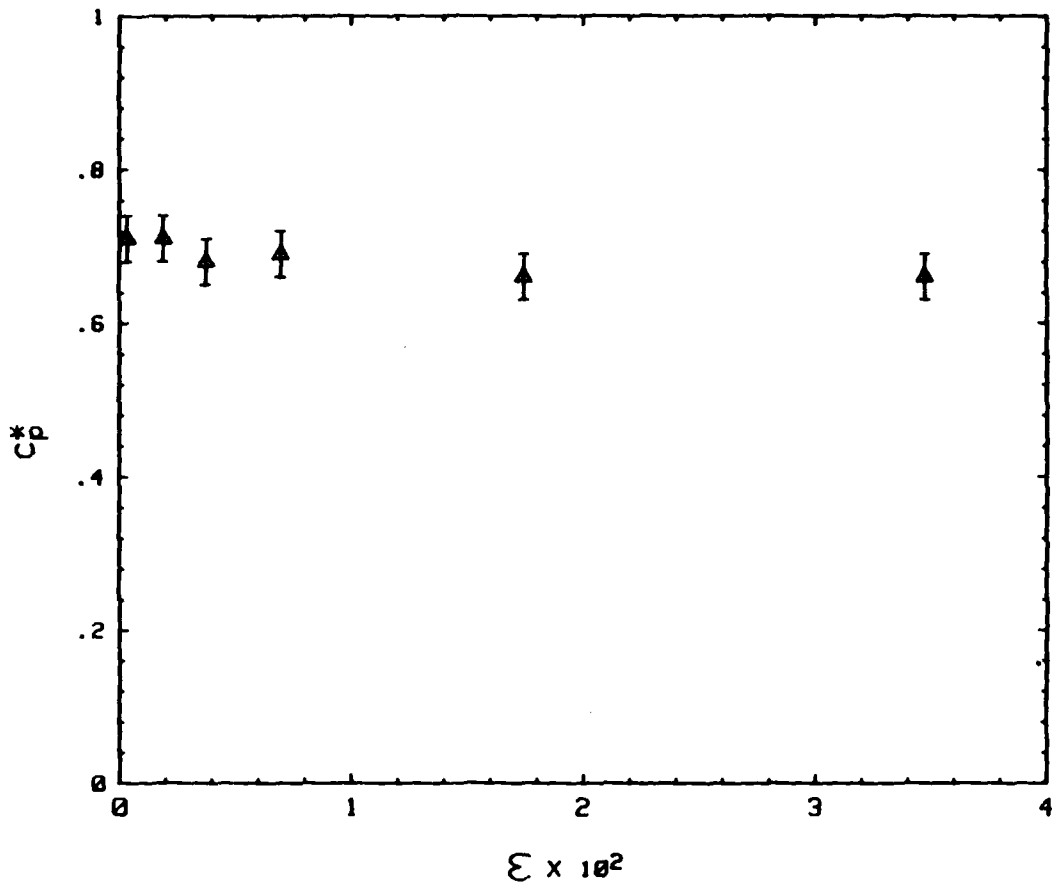

Figure 15c. c/a = 3.1481, f = 1.00, Re = 5×10^3.

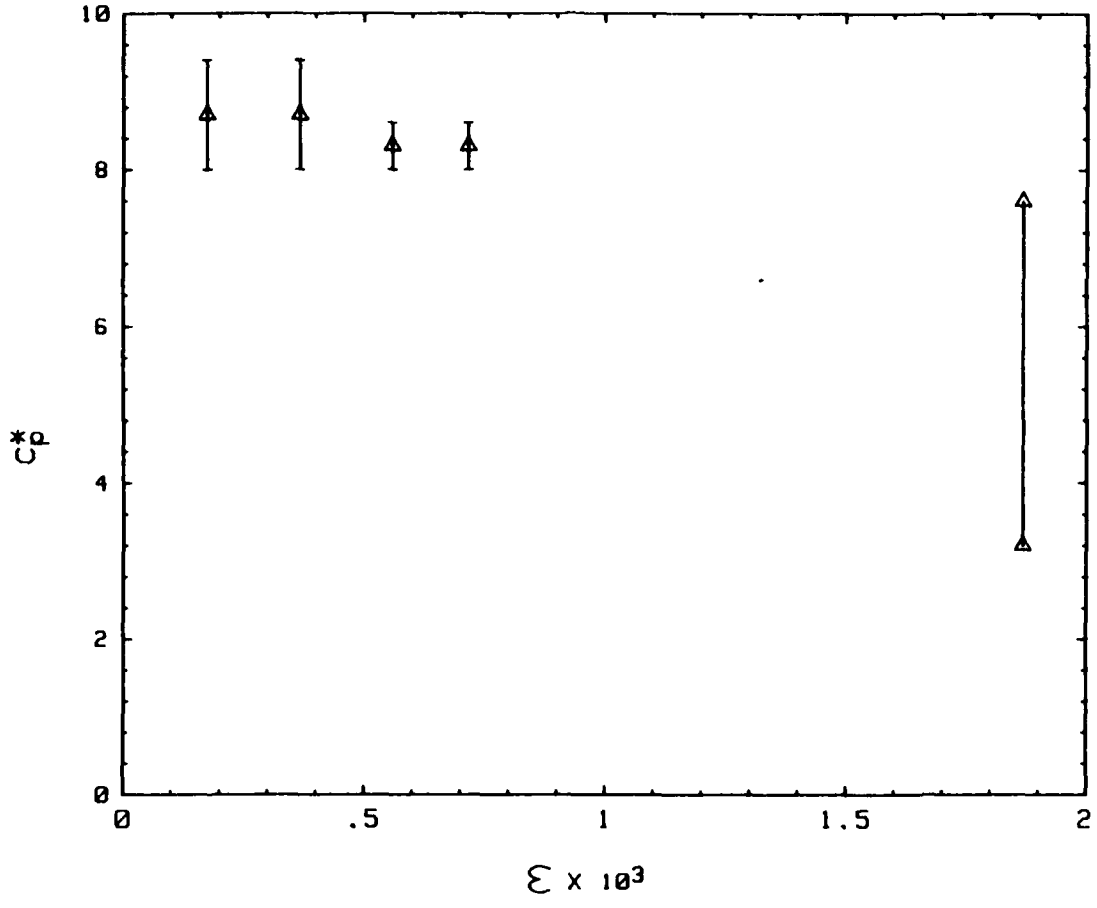

Figure 15d. c/a = 1.0509, f = 1.00, Re = 5×10^5.

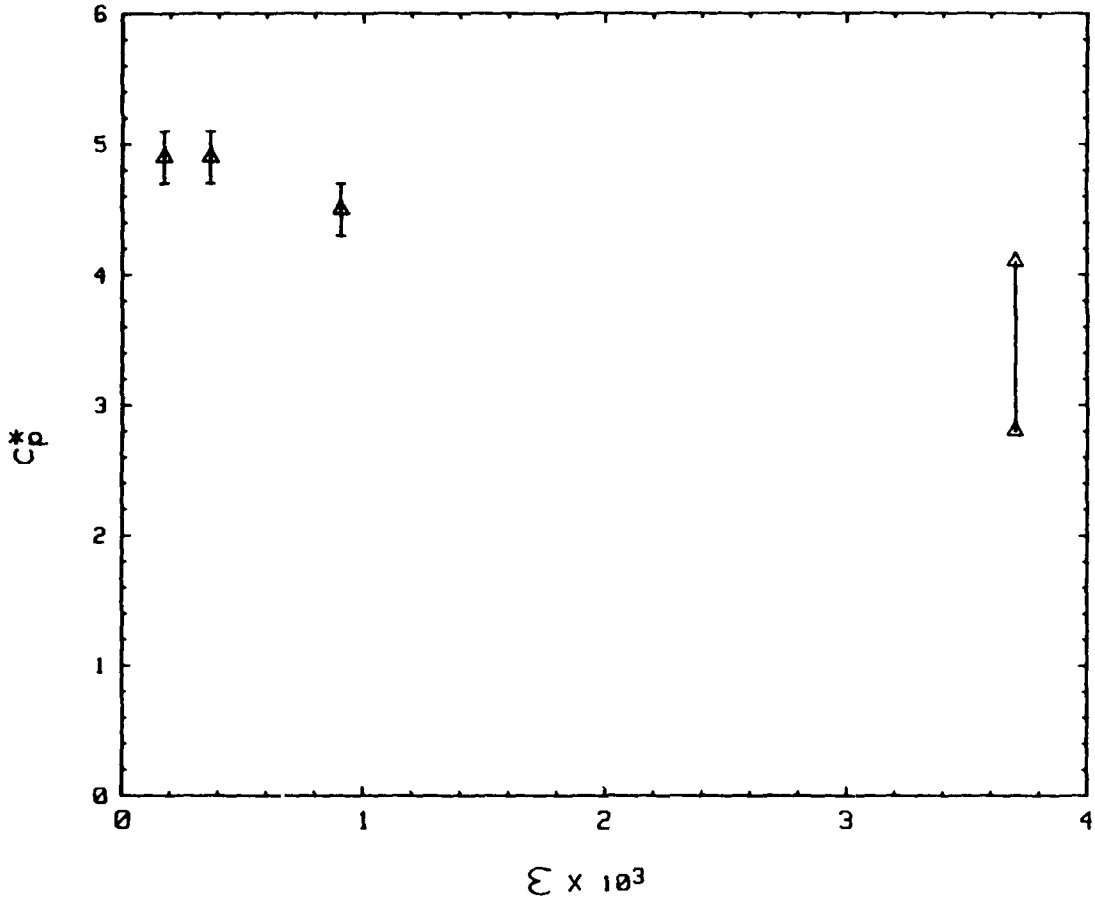

Figure 15e. c/a = 1.0509, f = 1.00, Re = 1 × 10^5.

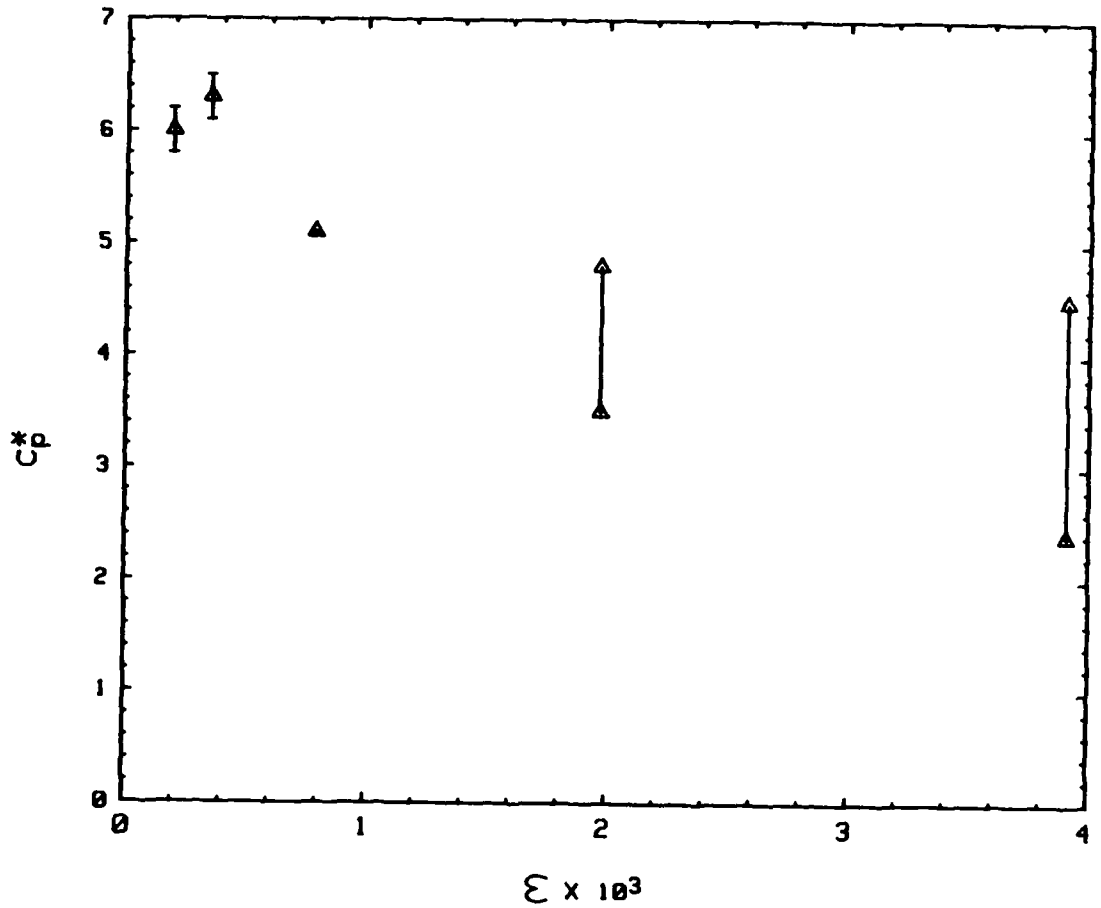

Figure 15f. c/a = 3.1481, f = 0.92, Re = 4 × 10^5.

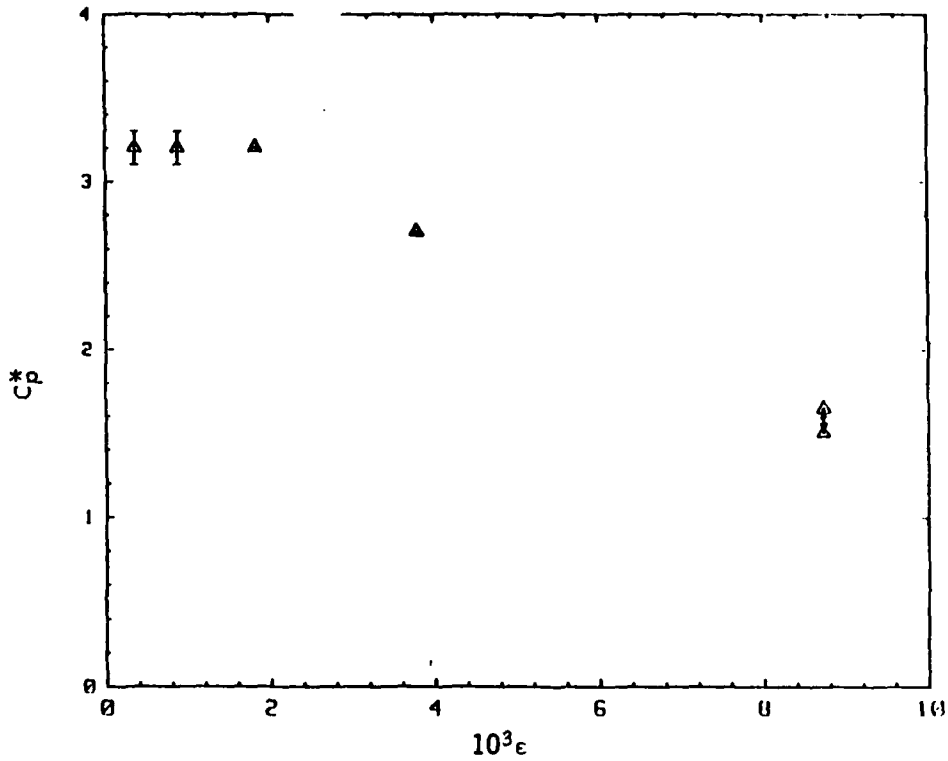

Figure 15g. c/a = 3.1481, f = 0.92, Re = 8×10^4.

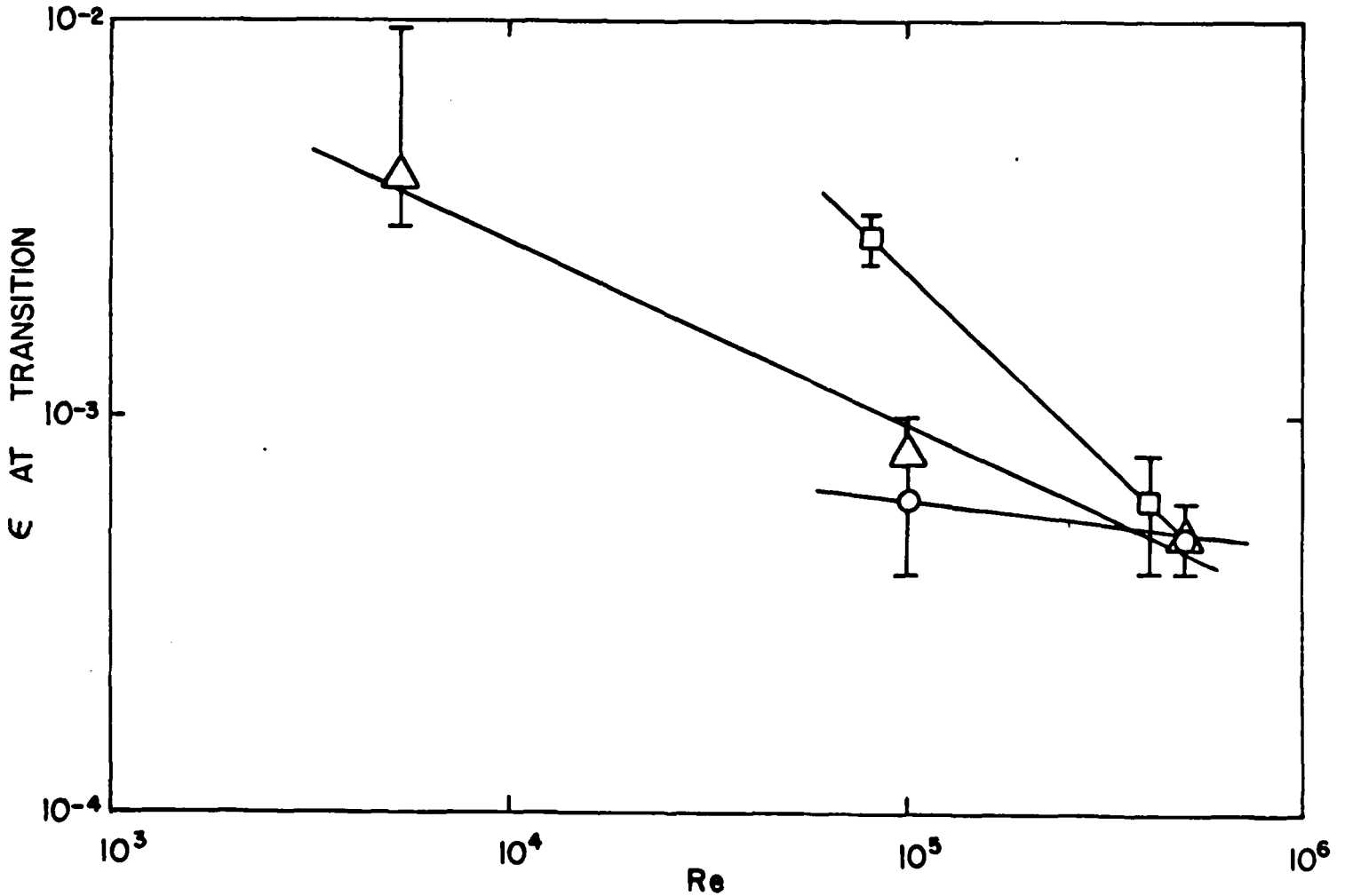

Figure 16. Coning Angle at Which Transition to Nonlinear Behavior Occurred
○ - c/a = 1.0509, f = 1.00; △ - c/a = 3.1481,
f = 1.00; □ - c/a = 3.1481, f = 0.92.

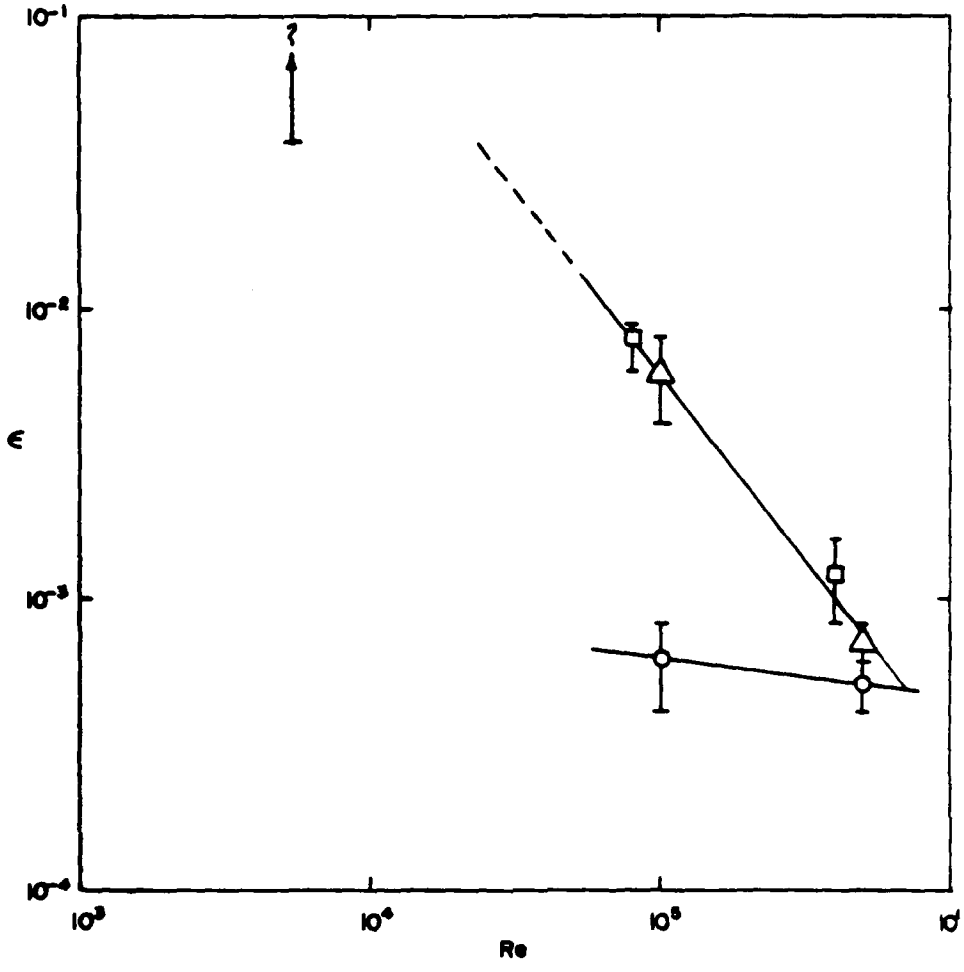

Figure 17. Coning Angle at Which Transition to Nonstationary Behavior Occurred

○ - c/a = 1.0509, f = 1.00; △ - c/a = 3.1481, f = 1.00; □ - c/a = 3.1481, f = 0.92.

LIST OF SYMBOLS

a	radius of cylindrical cavity
b	radius of air core
c	half length of cylindrical cavity
Cp, C_p	pressure coefficient, $\frac{\hat{p}}{\varepsilon\rho\Omega^2 a^2}$
C_p^*	value of C_p at ω of maximum linear C_p
E	Ekman number, $\nu/\Omega c^2$
f	fill ratio, (volume of liquid)/(volume of cavity)
F	Froude number, $\Omega^2 b/g$
g	acceleration of gravity
j	axial mode number of inertial oscillation
K_p	slope (dp/dV) of pressure transducer calibration curve
m	radial mode number of inertial oscillation
p	pressure
$\hat{p}$	amplitude of fluctuations of pressure
r	radial coordinate
Re	Reynolds number, $\Omega a^2/\nu$
t	time
V	voltage
z	axial coordinate
ε	coning angle
λ	a frequency
ν	kinematic viscosity
ρ	density
Ω	cylinder rotation frequency

LIST OF SYMBOLS
(Continued)

ω'	cylinder coning frequency
ω	ω'/Ω

APPENDIX A: PROPERTIES OF LIQUIDS

The liquids used in this experiment were Dow Corning 200 Silicon Fluid, of 1cS, 5cS, and 100cS nominal kinematic viscosities. Relevant properties, extracted from the manufacturer's literature are shown in Table A-1.

Table A-1. Properties of Liquids

Viscosity at 25° C (nominal)	Specific Gravity at 25° C	Coefficient of Thermal Expansion (β) (cc/cc/°C)
1cS	0.818	.00134
5cS	0.940	.00105
100cS	0.960	.00096

Also in the manufacturer's literature are charts showing the variation of viscosity with temperature, for the 5cS and 100cS fluids. For convenience in computer data reduction, a simple function of the form $\nu(T) = \exp(A+BT)$ was fit to several points read from each of the two manufacturer's curves, and was used to determine the viscosity of each liquid as a function of room temperature at the time of each run. For the range of temperature encountered in the experiment (19.6° C - 27.8° C) such a function fit the points read from the charts to within one percent greatest error, which probably is less than the error in reading the chart.

The U.S. Army ARRADCOM Chemical Systems Laboratory measured the viscosity of a sample of the 1cS fluid used in the experiment, finding it to be 1.044 cS at 25° C and 0.932 cS at 35° C. The same simple exponential used above was fit to these points, and was used in the same fashion. The Laboratory also measured the density at 25° C, obtaining 0.8149 g/ml as the result. The coefficients used in the viscosity curves are shown in Table A-2. To estimate the variation of density with temperature, it was assumed that the coefficient of thermal expansion β remained constant with temperature. With this assumption it is easy to show that

$$\rho(T) = \rho(25^0\ C) \cdot [1 - \rho(25^0\ C) \cdot \beta \cdot (T-25^0\ C)]$$

Table A-2. Coefficients in Expression $\nu(T) = \exp(A+BT)$

Fluid (Nominal Viscosity)	A	B
1cS	.35402	-.012339
5cS	2.1832	-.02122
100cS	5.1312	-.020655

APPENDIX B: CALIBRATIONS

1. Pressure Transducers. The pressure transducers were calibrated in two stages:

a. Three transducers, called "calibration" transducers, were calibrated against a Consolidated Electrodynamics Type 6-201 Primary Pressure Standard. This calibration was performed twice, once before and once after the completion of the experiments. The resulting pressure versus voltage data were fit with three straight lines, one for each transducer. The slope of the lines changed about one percent (worst case) between the two calibrations.

b. The two transducers in the cylinder, called "test" transducers, were calibrated against the other three transducers. This calibration was done four times during the experiments. The slopes of the resulting calibration curves changed by no more than 0.4% (worst case) between calibrations of the same transducer.

Including uncertainties in both calibrations, the final calibration constant K_p was probably accurate to about one percent.

2. Tunable Discriminators. The EMR model 4142 tunable discriminators had adjustments for deviation, coarse center frequency, offset (fine center frequency), type of low-pass filter, filter cutoff frequency, and bandedge voltage. The coarse center frequency was always set to the VCO nominal center frequency (40 kHz or 52.5 KHz). The low pass filter used was of constant-delay type, with a cutoff frequency of 1 KHz. The deviation was set to 7.5%, the same as the nominal VCO deviation.

The input of each VCO could be set to the transducer amplifier output (the data signal), to a D.C. reference signal V_D, which was approximately 2.5 volts above VCO reference, or to VCO reference, V_R. The discriminator offset was adjusted so that when the VCO input was set to V_D, the discriminator output was $(V_D - 2.50) \pm .005$ volts. The discriminator bandedge voltage was adjusted so that when the VCO input was set to V_R, the discriminator output was $-2.50 \pm .005$ volts. After these adjustments were performed, the discriminator output was equal to the VCO input minus $2.50 \pm .03$ volts, at any VCO input voltage from zero to five volts.

3. System Transfer Function. The calibration of transducer pressure to discriminator output voltage was conceptually divided into two parts: the conversion of pressure to voltage by the transducer, represented by the transducer calibration coefficient, K_p, and the various voltage level changes, voltage-to-frequency conversions and their inverses accomplished by the transducer amplifiers and the telemetry link, represented by the system transfer function, $H(\lambda)$. The measurement of the transfer function was accomplished with the Hewlett-Packard 3582A spectrum analyzer (which was also used to collect the experimental data). To perform the measurement, a pseudo-random noise source, available as an output from the analyzer, was connected to a

transducer amplifier input, in parallel with the transducer, and also to one input channel of the analyzer (Figure B-1). The output of the corresponding discriminator was connected to the other analyzer input, and the analyzer was adjusted so as to perform exponential averaging over 16 sample spectra, then compute the transfer function from one input signal to the other using the averaged spectra (see the manufacturer's literature[22] for details). This process was repeated for the other channel, and the results were stored in the HP 9845B computer which was connected to the analyzer. Note that the computed transfer function was complex; both magnitude and phase were stored.

4. Determination of Fluctuating Pressure Amplitude. The discriminator output was a mixture of signals of the form $V_d(\lambda,t) = \hat{V}(\lambda) \cos(\lambda t + \theta)$, corresponding to fluctuating pressure signals $p(\lambda,t) = \hat{p}(\lambda) \cos(\lambda t + \phi)$. The spectrum analyzer presented $\hat{V}(\lambda)$; the amplitude of a particular spectral component of the fluctuating pressure was then

$$\hat{p}(\lambda) = K_p \hat{V}(\lambda) / |H(\lambda)|,$$

where $K_p = dp/dV$, the slope of the pressure transducer calibration and $|H(\lambda)|$ is the magnitude of the telemetry system transfer function.

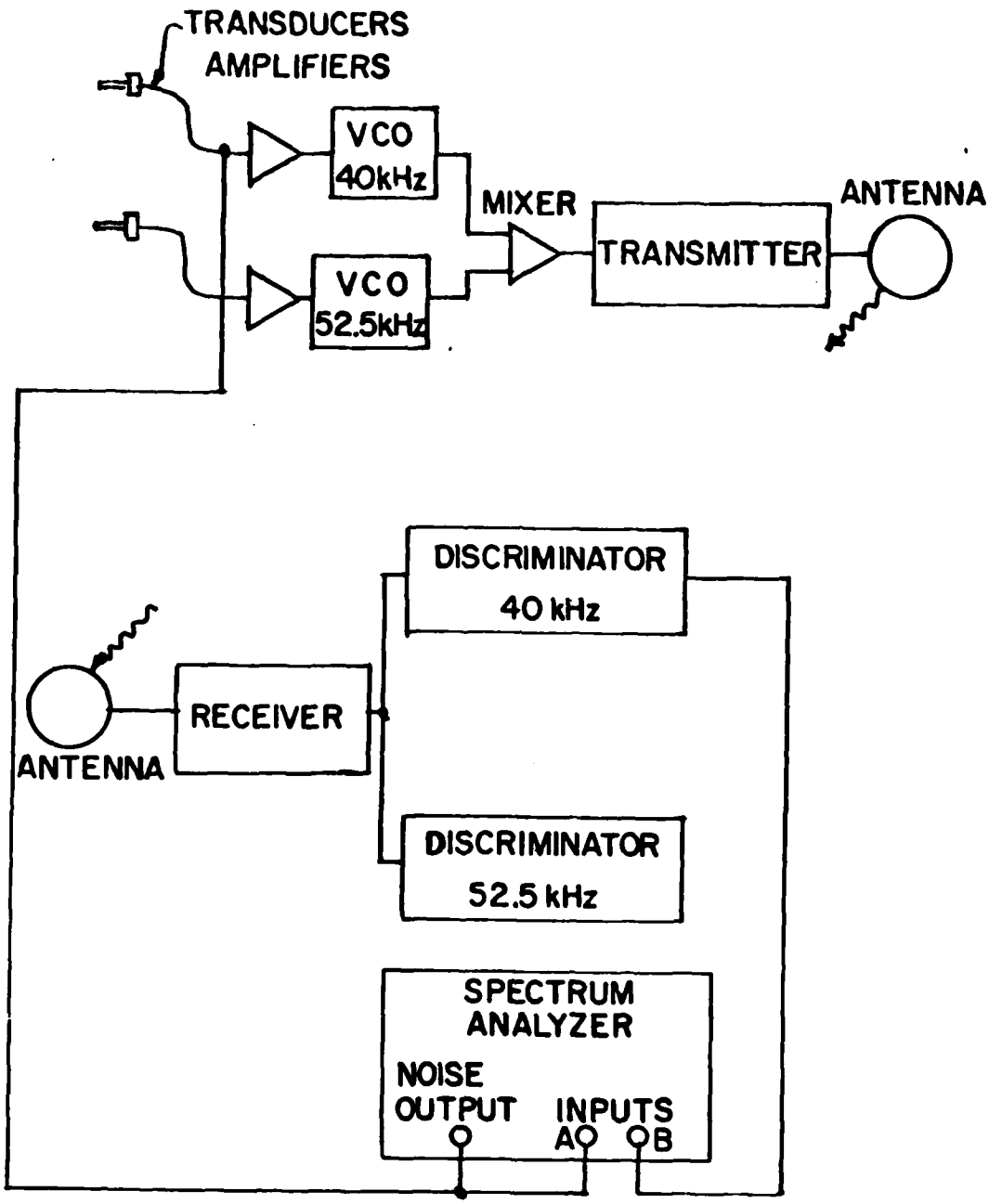

Figure B.1. Setup for Measuring Transfer Function of Telemetry Link.

DISTRIBUTION LIST

No. of Copies	Organization
12	Commander Defense Technical Info Center ATTN: DDC-DDA Cameron Station Alexandria, VA 22314
1	Commander US Army Engineer Waterways Experiment Station ATTN: R.H. Malter Vicksburg, MS 39180
1	Commander US Army Materiel Development and Readiness Command ATTN: DRCDMD-ST 5001 Eisenhower Avenue Alexandria, VA 22333
3	Commander US Army Armament Research and Development Command ATTN: DRDAR-TSS (2 cys) DRDAR-LC, Dr. J.Frasier Dover, NJ 07801
6	Commander US Army Armament Research and Development Command ATTN: DRDAR-LCA-F Mr. D. Mertz Mr. E. Falkowski Mr. A. Loeb Mr. R. Kline Mr. S. Kahn Mr. S. Wasserman Dover, NJ 07801
1	Commander US Army Armament Materiel Readiness Command ATTN: DRSAR-LEP-L, Tech Lib Rock Island, IL 61299
1	Director US Army ARRADCOM Benet Weapons Laboratory ATTN: DRDAR-LCB-TL Watervliet, NY 12189
1	Commander US Army Aviation Research and Development Command ATTN: DRDAV-E 4300 Goodfellow Boulevard St. Louis, MO 63120
1	Director US Army Air Mobility Research and Development Laboratory ATTN: SAVDL-D, W.J. McCroskey Ames Research Center Moffett Field, CA 94035
1	Commander US Army Communications Rsch and Development Command ATTN: DRDCO-PPA-SA Fort Monmouth, NJ 07703
1	Commander US Army Electronics Research and Development Command Technical Support Activity ATTN: DELSD-L Fort Monmouth, NJ 07703
3	Commander US Army Missile Command ATTN: DRSMI-R DRSMI-YDL DRSMI-RDK Mr. R. Deep Redstone Arsenal, AL 35809
1	Commander US Army Tank Automotive Research & Development Cmd ATTN: DRDTA-UL Warren, MI 48090

DISTRIBUTION LIST

No. of Copies	Organization
1	Commander US Army Jefferson Proving Ground ATTN: STEJP-TD-D Madison, IN 47250
1	Commander US Army Research Office ATTN: Dr. R.E. Singleton P.O. Box 12211 Research Triangle Park, NC 27709
1	AGARD-NATO ATTN: R.H. Korkegi APO New York 09777
1	Director US Army TRADOC Systems Analysis Activity ATTN: ATAA-SL, Tech Lib White Sands Missile Range, NM 88002
3	Commander Naval Air Systems Command ATTN: AIR-604 Washington, DC 20360
2	Commander David W. Taylor Naval Ship Research & Development Cmd ATTN: H.J. Lugt, Code 1802 S. de los Santos Head, High Speed Aero Division Bethesda, MD 20084
1	Commander Naval Surface Weapons Center ATTN: DX-21, Lib Br Dahlgren, VA 22448
5	Commander Naval Surface Weapons Center Applied Aerodynamics Division ATTN: K.R. Enkenhus M. Ciment S.M. Hastings A.E. Winklemann W.C. Ragsdale Silver Spring, MD 20910
1	AFATL (DLDL, Dr. D.C.Daniel) Elgin AFB, FL 32542
2	AFFDL (W.L. Hankey; J.S.Shang) Wright-Patterson AFB, OH 45433
4	Director National Aeronautics and Space Administration ATTN: D.R. Chapman J. Rakich W.C. Rose B. Wick Ames Research Center Moffett Field, CA 94035
4	Director National Aeronautics and Space Administration ATTN: E. Price J. South J.R. Sterrett Tech Library Langley Research Center Langley Station Hampton, VA 23365
1	Director National Aeronautics and Space Administration Lewis Research Center ATTN: MS 60-3, Tech Lib 21000 Brookpark Road Cleveland, OH 44135

DISTRIBUTION LIST

No. of Copies	Organization
2	Director National Aeronautics and Space Administration Marshall Space Flight Center ATTN: A.R. Felix, Chief S&E-AERO-AE Dr. W.W. Fowlis Huntsville, AL 35812
2	Director Jet Propulsion Laboratory ATTN: L.M. Mach Tech Library 4800 Oak Grove Drive Pasadena, CA 91103
3	Arnold Research Org., Inc. ATTN: J.D. Whitfield R.K. Matthews J.C. Adams Arnold AFB, TN 37389
3	Aerospace Corporation ATTN: H. Mirels R.L. Varwig Aerophysics Lab. P.O. Box 92957 Los Angeles, CA 90009
1	AVCO Systems Division ATTN: B. Reeves 201 Lowell Street Wilmington, MA 01887
3	Boeing Commerical Airplane Company ATTN: G.M. Bowes M.S. 1W-82, Org B-8120 P.E. Rubbert, MS 3N-29 J.D. McLean, MS 3N-19 Seattle, WA 98124
3	Calspan Corporation ATTN: A. Ritter G. Homicz W. Rae P.O. Box 400 Buffalo, NY 14221
1	General Dynamics ATTN: Research Lib 2246 P.O. Box 748 Fort Worth, TX 76101
1	General Electric Company, RESD ATTN: R.A. Larmour 3198 Chestnut Street Philadelphia, PA 19101
2	Grumman Aerospace Corporation ATTN: R.E. Melnik L.G. Kaufman Bethpage, NY 11714
2	Lockheed-Georgia Company ATTN: B.H. Little, Jr. G.A. Pounds Dept 72074, Zone 403 86 South Cobb Drive Marietta, GA 30062
1	Lockheed Missiles and Space Company ATTN: Tech Info Center 3251 Hanover Street Palo Alto, CA 94304
3	Martin-Marietta Laboratories ATTN: S.H. Maslen S.C. Traugott H. Obremski 1450 S. Rolling Road Baltimore, MD 21227
2	McDonnell Douglas Astronautics Corporation ATTN: J. Xerikos H. Tang 5301 Bolsa Avenue Huntington Beach, CA 92647

DISTRIBUTION LIST

No. of Copies	Organization
2	McDonnell-Douglas Corporation Douglas Aircraft Company ATTN: T. Cebeci K. Stewartson 3855 Lakewood Boulevard Long Beach, CA 90801
2	Sandia Laboratories ATTN: F.G. Blottner Tech Lib Albuquerque, NM 87115
2	United Aircraft Corporation Research Laboratories ATTN: M.J. Werle Library East Hartford, CT 06108
1	Vought Systems Division LTV Aerospace Corporation ATTN: J.M. Cooksey Chief, Gas Dynamics Lab, 2-53700 P.O. Box 5907 Dallas, TX 75222
1	Arizona State University Department of Mechanical and Energy Systems Engineering ATTN: G.P., Neitzel Tempe, AZ 85281
3	California Institute of Technology ATTN: Tech Library H.B. Keller, Mathematics Dept. D. Coles, Aeronautics Dept. Pasadena, CA 91109
1	Cornell University Graduate School of Aero Engr ATTN: Library Ithaca, NY 14850
2	Illinois Institute of Tech ATTN: M.V. Morkovin H.M. Nagib 3300 South Federal Chicago, IL 60616
1	The Johns Hopkins University Department of Mechanics and Materials Science ATTN: S. Corrsin Baltimore, MD 21218
4	The Johns Hopkins University Applied Physics Laboratory ATTN: Dr. R.D. Whiting Dr. D. A. Hurdif Dr. R. S. Hirsh Mr. E. R. Bohn Johns Hopkins Road Laurel, MD 20810
3	Massachusetts Institute of Technology ATTN: E. Covert H. Greenspan Tech Lib 77 Massachusetts Avenue Cambridge, MA 02139
2	North Carolina State Univ Mechanical and Aerospace Engineering Department ATTN: F.F. DeJarnette J.C. Williams Raleigh, NC 27607
1	Notre Dame University Department of Aero Engr ATTN: T.J. Mueller South Bend, IN 46556

DISTRIBUTION LIST

No. of Copies	Organization
2	Ohio State University Dept of Aeronautical and Astronautical Engineering ATTN: S.L. Petrie O.R. Burggraf Columbus, OH 43210
2	Polytechnic Institute of New York ATTN: G. Moretti S.G. Rubin Route 110 Farmingdale, NY 11735
3	Princeton University James Forrestal Research Ctr Gas Dynamics Laboratory ATTN: S.M. Bogdonoff S.I. Cheng Tech Library Princeton, NJ 08540
1	Purdue University Thermal Science & Prop Center ATTN: Tech Library W. Lafayette, IN 47907
1	Rensselaer Polytechnic Institute Department of Math Sciences ATTN: R.C. DiPrima Troy, NY 12181
1	San Diego State University Department of Aerospace Engr and Engr Mechanics College of Engineering ATTN: K.C. Wang San Diego, CA 92182
1	Southern Methodist University Department of Civil and Mechanical Engineering ATTN: R.L. Simpson Dallas, TX 75275
1	Southwest Research Institute Applied Mechanics Reviews 8500 Culebra Road San Antonio, TX 78228
1	Texas A&M University College of Engineering ATTN: R.H. Page College Station, TX 77843
1	University of California-Berkeley Department of Aerospace Engineering ATTN: M. Holt Berkeley, CA 94720
1	University of California-Davis ATTN: H.A. Dwyer Davis, CA 95616
2	University of California-San Diego Department of Aerospace Engineering and Mechanical Engineering Sciences ATTN: P. Libby Tech Library La Jolla, CA 92037
1	University of Cincinnati Department of Aerospace Engineering ATTN: R.T. Davis Cincinnati, OH 45221
1	University of Colorado Department of Astro-Geophysics ATTN: E.R. Benton Boulder, CO 80302
1	University of Hawaii Dept of Ocean Engineering ATTN: G. Venezian Honolulu, HI 96822

DISTRIBUTION LIST

No. of Copies	Organization
2	University of Maryland ATTN: W. Melnik J.D. Anderson College Park, MD 20740
2	University of Michigan Department of Aeronautical Engineering ATTN: W.W. Wilmarth Tech Library East Engineering Building Ann Arbor, MI 48104
1	University of Santa Clara Department of Physics ATTN: R. Greeley Santa Clara, CA 95053
3	University of Southern California Department of Aerospace Engineering ATTN: T. Maxworthy P. Weidman L.G. Redekopp Los Angeles, CA 90007
1	University of Texas Department of Aerospace Engineering ATTN: J.C. Westkaemper Austin, TX 78712
1	University of Virginia Department of Aerospace Engineering & Engineering Physics ATTN: I.D. Jacobson Charlottesville, VA 22904
1	University of Washington Department of Mechanical Engineering ATTN: Tech Library Seattle, WA 98195
1	University of Wyoming ATTN: D.L. Boyer University Station Laramie, WY 82071
1	Virginia Polytechnic Institute and State University Department of Aerospace Engineering ATTN: Tech Library Blacksburg, VA 24061
1	Woods Hole Oceanographic Institute ATTN: J.A. Whitehead Wolds Hole, MA 02543

Aberdeen Proving Ground

Dir, USAMSAA
ATTN: DRXSY-D
DRXSY-MP, H. Cohen

Cdr, USATECOM
ATTN: DRSTE-TO-F

Cdr/Dir, USA CSL
ATTN: Munitions Div, Bldg. E3330
E.A. Jeffers
W.C. Dee
W.J. Pribyl

Dir, USACSL, Bldg. E3516, EA
ATTN: DRDAR-CLB-PA

USER EVALUATION OF REPORT

Please take a few minutes to answer the questions below; tear out this sheet, fold as indicated, staple or tape closed, and place in the mail. Your comments will provide us with information for improving future reports.

1. BRL Report Number _____

2. Does this report satisfy a need? (Comment on purpose, related project, or other area of interest for which report will be used.)

_____

_____

_____

3. How, specifically, is the report being used? (Information source, design data or procedure, management procedure, source of ideas, etc.) _____

_____

_____

4. Has the information in this report led to any quantitative savings as far as man-hours/contract dollars saved, operating costs avoided, efficiencies achieved, etc.? If so, please elaborate.

_____

_____

5. General Comments (Indicate what you think should be changed to make this report and future reports of this type more responsive to your needs, more usable, improve readability, etc.) _____

_____

_____

_____

6. If you would like to be contacted by the personnel who prepared this report to raise specific questions or discuss the topic, please fill in the following information.

Name: _____

Telephone Number: _____

Organization Address: _____

_____

_____

FOLD HERE

Director
US Army Ballistic Research Laboratory
Aberdeen Proving Ground, MD 21005

NO POSTAGE
NECESSARY
IF MAILED
IN THE
UNITED STATES

OFFICIAL BUSINESS
PENALTY FOR PRIVATE USE, $300

BUSINESS REPLY MAIL
FIRST CLASS PERMIT NO 12062 WASHINGTON, DC
POSTAGE WILL BE PAID BY DEPARTMENT OF THE ARMY

Director
US Army Ballistic Research Laboratory
ATTN: DRDAR-TSB
Aberdeen Proving Ground, MD 21005

FOLD HERE

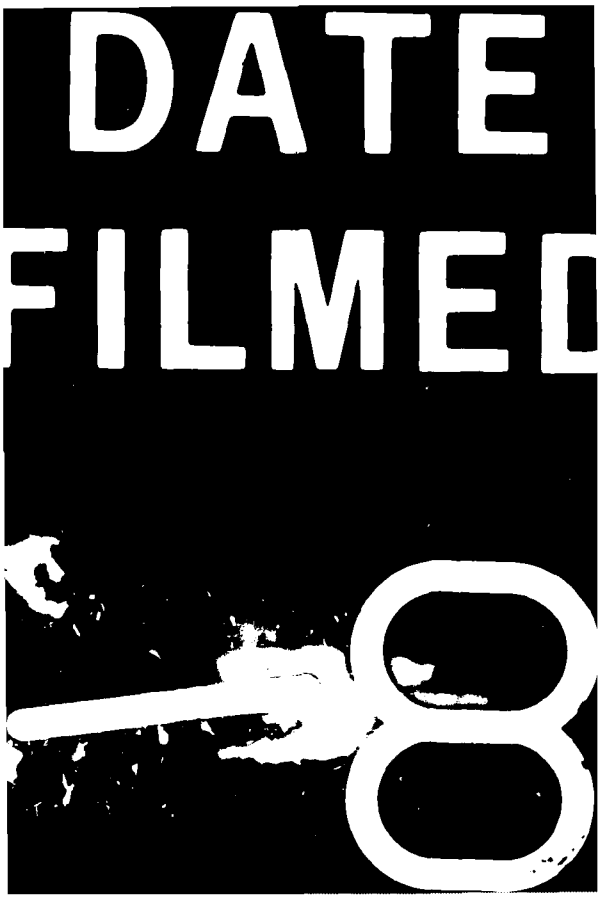
DATE
FILMED